Narrow-width approximation in the Minimal Supersymmetric Standard Model

Diplomarbeit
von
Christoph Uhlemann

vorgelegt bei

Professor Dr. R. Rückl

am
Institut für Theoretische Physik und Astrophysik
der
Bayerischen Julius-Maximilians-Universität
Würzburg

29. November 2007

Zusammenfassung

Die Narrow-Width Approximation (NWA) wird vielfach verwendet, um komplizierte Streu- und Zerfallsprozesse in einfachere Teilprozesse zu faktorisieren, welche dann in Störungsrechnung einfacher und genauer behandelt werden können. In dieser Arbeit untersuchen wir die Anwendbarkeit der im Standardmodell sehr genau getesteten und i.d.R. gut funktionierenden NWA in Erweiterungen des Standardmodells. Da hier häufig neue, schwere Teilchen vorrausgesagt werden, welche über viele Zwischenstufen mit resonanten, instabilen Teilchen zerfallen, ist die NWA besonders wichtig um komplizierte Prozesse genau berechnen zu können. Wir untersuchen im ersten Teil der Arbeit analytische Eigenschaften der NWA. Wir entwickeln zunächst eine Möglichkeit, die NWA formal aus der Formel für den vollen Streuquerschnitt abzuleiten, untersuchen dann das Verhalten bei verschwindender totaler Zerfallsbreite des instabilen Teilchens und geben schließlich, als Hauptresultat dieses Abschnitts, unter ganz allgemeinen Vorraussetzungen einen Beweis dafür, dass der Fehler durch Anwendung der NWA von der Ordnung Γ/m ist, wobei m und Γ die Masse und totale Zerfallsbreite des instabilen Teilchens sind.
Im zweiten Abschnitt untersuchen wir die NWA im Minimalen Supersymmetrischen Standardmodell (MSSM). Diese aus theoretischer Sicht besonders attraktive Erweiterung des Standardmodells ist sehr gut untersucht und könnte am Large Hadron Collider bereits in den ersten Jahren gefunden werden. Für eine systematische Untersuchung erzeugen wir alle resonanten $1 \to 3$ Zerfälle, die im MSSM möglich sind, und untersuchen die Abhängigkeit der Güte der NWA von den auftretenden Massen und Kopplungen. Zunächst bestimmen wir ganz allgemein die Prozesse und Parameterkonfigurationen, für die die NWA keine guten Ergebnisse liefert, und untersuchen, wodurch es zu Problemen kommt, um uns dann speziellen Modellen zuzuwenden. Da der Parameterraum des MSSM mit über einhundert Parametern nicht systematisch nach problematischen Zerfällen durchsucht werden kann, beschränken wir uns auf zehn Benchmarkpunkte (die sogenannten SPS Punkte), die für phänomenologische Studien festgelegt wurden. Wir erzeugen für diese SPS Punkte alle resonanten $1 \to 3$ Zerfälle und diskutieren die Problemfälle.
Im letzten Abschnitt der Arbeit untersuchen wir nochmals die Näherungen, die im ersten Abschnitt nötig waren um die NWA formal abzuleiten, und entwickeln modifizierte NWA Formeln, die bestimmte Aspekte besser berücksichtigen. Dabei entwickeln wir eine Modifikation, die im wesentlichen alle Vorteile der eigentlichen NWA beibehält und die Eigenschaften des Phasenraums besser berücksichtigt. Wir wenden diese modifizierte NWA Formel auf die erzeugten Zerfälle für die SPS Punkte an und finden insgesamt eine leichte Verbesserung des Fehlers.

Contents

1 Introduction

In the past century a powerful model of the fundamental particles and interactions has emerged. The so-called Standard Model (SM) of particle physics was developed to describe three of the four fundamental interactions, namely the electro-magnetic, the weak and the strong interaction. It is tested to an incredible precision hardly found anywhere else in physics and so far there are no experimental results from collider experiments that contradict SM predictions. However, neutrino masses, whose nature in terms of Dirac or Majorana type is still unclear, have to be incorporated and the SM does not provide a suitable dark matter candidate. Furthermore there are clear signs on the theoretical side that the SM is an effective low-energy model, rather than a fundamental theory. First of all, there is the missing description of gravity which can not be incorporated within the SM framework. But despite the lack of a quantum description of gravity, there are other problems, suggesting that there has to be new physics far below the Planck scale. For example the hierarchy problem of why the Higgs mass, which would – unless we accept an extreme fine-tuning – run all the way up to the Planck scale due to loop contributions, is that small compared to the scale of new physics. These theoretical arguments indicate that new physics will play an important role at the TeV scale which will soon become accessible at the Large Hadron Collider (LHC), scheduled to start in 2008. We therefore expect discoveries revealing physics beyond the Standard Model (BSM) and giving insight into more fundamental theories in the near future. A promising extension of the SM is supersymmetry, which solves the hierarchy problem. In particular the Minimal Supersymmetric Standard Model (MSSM) as the supersymmetric extension with minimal additional particle content is of interest and studied very well. The MSSM, although not being a fundamental theory itself, in addition to solving the hierarchy problem allows for a unification of the couplings of strong and electroweak interactions and gives suitable dark matter candidates. A typical phenomenological feature is the production of the superpartners of the SM particles and their subsequent decay through cascade decays into SM particles and the lightest supersymmetric particle (LSP), which leads to many particles in the final states and complex scattering amplitudes. The new particles can only be identified by means of their decay products and therefore, accurate

predictions are required to successfully extract the correct values of additional Lagrangian parameters out of the experimental data. To achieve the desired accuracy, it is necessary to include next-to-leading order (NLO) calculations which are very challenging or not yet feasible for these long decay chains. An approach to avoid these complications is to factorize the (potentially resonant) production and decay of the unstable particles by means of the narrow-width approximation (NWA). The NWA provides a way of consistently neglecting sub- and non-resonant contributions as well as non-factorizable loop contributions. Loop calculations can then be carried out for the simpler subprocesses and considerable simplifications occur already at treelevel. For these reasons, the NWA is used frequently in studies of BSM physics. Based on the involved scales the NWA error is typically assumed to be of $\mathcal{O}(\Gamma/m)$, where m, Γ are the mass and width of the unstable particle, respectively. Although the NWA is well tested in SM scenarios, to our knowledge there exists no proof for the smallness of the NWA error. Therefore, in order to make reliable theoretical predictions, the NWA has to be checked in the context of new physics. In this work we first derive some analytical properties of the NWA and give a proof that the NWA error is of $\mathcal{O}(\Gamma/m)$. We then take the MSSM as specific extension of the SM to do a systematic check of the NWA performance. For that, we first do a general analysis which is not specific to supersymmetric theories and then study specific MSSM scenarios, namely the SPS points.

1.1. The Standard Model

The SM of particle physics gives a very well tested description of all fundamental forces but gravity. However, the gravitational effects in the energy ranges currently accessible are negligibly small and the SM provides an excellent description of collider physics. It consists of an outer symmetry of the Poincaré group of space-time transformations and an inner symmetry group which is the direct product of the symmetry group of strong interactions $SU(3)_C$ with the group of electroweak interactions $SU(2)_L \times U(1)_Y$. We have three generations of spin-$\frac{1}{2}$ fermions in the SM with the corresponding particles of each generation having the same quantum numbers but different masses. The left-handed parts of the fermions transform as $SU(2)_L$ doublets and are built of pairs of charged leptons with the corresponding neutrinos and up- with down-type quarks. The righthanded parts of the quarks and charged leptons transform as $SU(2)_L$ singlets. For each group generator of the inner symmetries we have a massless spin-1 gauge boson which transforms under the adjoint representation of the respective group. This gives eight gluons for $SU(3)_C$, three gauge bosons W^i for $SU(2)_L$ and a single gauge boson B for $U(1)_Y$. Since explicit mass terms would spoil gauge invariance, the particles are assumed to acquire masses due to spontaneous symmetry breaking, namely the Higgs mechanism. Therefore an additional complex scalar field Φ which is a doublet under $SU(2)_L$ is introduced together with a potential that produces a non-gauge-invariant

ground state. In this way the gauge invariance is broken spontaneously, meaning that the Lagrangian is still gauge-invariant while the vacuum state is not. The Higgs field Φ has hypercharge $Y = 1$ and its ground state acquires a vacuum expectation value v such that $SU(2)_L \times U(1)_Y$ is broken down to $U(1)_Q$. The electric charge is $Q = I_3 + \frac{1}{2}Y$ where I_3 is the third component of weak isospin. In order to preserve $U(1)_Q$ only the lower component of the Higgs field is assigned a vacuum expectation value. The breaking of a continuous global symmetry generates one massless Goldstone boson for each broken symmetry generator. In the case of the local symmetry $SU(2)_L \times U(1)_Y$, these Goldstone bosons are no physical particles. By an appropriate gauge choice – the unitary gauge – they can be eliminated. Their degrees of freedom become the longitudinal modes of the gauge bosons which become massive. Of the four degrees of freedom of the Higgs field Φ, three have become the massive modes of the gauge bosons and a scalar neutral Higgs field H is left which is yet to be discovered. After symmetry breaking, the gauge bosons of $SU(2)_L \times U(1)_Y$ mix to give as mass eigenstates the charged massive bosons $W^{\pm}$ consisting of W^1 and W^2, the neutral massive Z boson and the massless photon γ which are mixtures of W^3 and B. The fermions acquire masses proportional to the respective Yukawa couplings and the Higgs vacuum expectation value.

1.2. Narrow-width approximation

The NWA is used to reduce the complexity of scattering amplitudes. The idea is to treat a process consisting of the (potentially resonant) production of an unstable particle and the following decay as two separate processes not depending on each other. The denominator of the unstable-particle propagator generally has a Breit-Wigner form $\frac{1}{q^2 - m^2 + im\Gamma}$, with m, q and Γ being the mass, 4-momentum and width of the intermediate particle, respectively. For small Γ, off-shell effects are strongly suppressed and the intermediate particle is basically on-shell. The Breit-Wigner can then be integrated out, factorizing the cross section into a production cross section times a branching ratio which is the quotient of the partial decay width and the total width of the unstable particle

$$\sigma = \sigma_{prod} \times \frac{\Gamma_{partial}}{\Gamma} = \sigma_{prod} \times \mathrm{BR}. \tag{1.1}$$

This way, the phasespace dimension as well as the number of contributing diagrams is reduced and the calculation of the full process is split into two simpler calculations, which do not take into account spin/polarization correlation effects[1]. Furthermore, it is not possible to calculate interference with non-resonant contributions, or to calculate differential cross sections with respect to q^2. The error of the NWA calculation

[1] The Breit-Wigner can be integrated out without discarding spin/polarization correlations, but the resulting cross section can then not be factorized in the form of Equation 1.1.

compared to the off-shell calculation integrated over the full phasespace is – based on the involved scales – usually believed to be of $\mathcal{O}(\frac{\Gamma}{m})$. In the SM, the NWA works quite well for most of the processes, which seems to rely on the specific mass spectrum and couplings of the SM. That is, the masses of unstable particles are typically much larger than masses of any lighter particles they decay to, and the widths of unstable particles are typically small compared to their mass. Examples with well working NWA are the decays of the heavy top quark (e.g. $t \to bW^+ \to bu\bar{d}$) and the decays of the massive gauge bosons. There are only a few resonant processes that require off-shell calculations (e.g. $e^+e^- \to W^+W^- \to 4f$ [1]). In extensions of the SM there are often nearly degenerate masses of parent and daughter particles and the new particles can only be probed by means of their decay products. It is not clear a priori that the NWA is a good approximation in these scenarios. A detailed understanding of the cascade decays and the approximations in their calculation is necessary to deduce the correct particle properties from the experimental data.

1.3. Supersymmetry

In this section we want to develop the MSSM, which is a very well studied extension of the SM and can actually solve a number of problems. Supersymmetry for example provides a natural explanation of the small Higgs mass. The relation between bosons and fermions adds a quadratically divergent bosonic contribution to the Higgs mass, which – due to supersymmetry – precisely cancels the divergent contribution of the SM fermions. After the breaking of supersymmetry, a logarithmically divergent contribution remains in contrast to the quadratic divergence in the SM. Furthermore, after the introduction of R-parity, the LSP becomes stable and can give a suitable dark-matter candidate. More details of the formalism can be found in [2] and phenomenological aspects are discussed in [3].

1.3.1. Supersymmetry algebra

After Coleman and Mandula had shown in 1967 [4] that any Lie group containing the Poincaré group P and some internal symmetry group G must be the direct product $P \otimes G$, it was clear that internal symmetries can only be combined with space-time symmetry in a trivial way. As the proof uses only very general assumptions such as Lorentz invariance of the S-matrix or analyticity of the scattering amplitudes, the only way to bypass this limitation is to not use Lie algebras defined by commutator relations but rather use so-called superalgebras, which also contain anticommutators. We can then define operators Q and $\bar{Q}$ with the following properties:

$$\begin{aligned} \left\{Q_\alpha{}^A, \bar{Q}_{\dot{\beta}B}\right\} &= 2\sigma^\mu_{\alpha\dot{\beta}} P_\mu \delta^A_B, \\ \left\{Q_\alpha{}^A, Q_\beta{}^B\right\} &= \epsilon_{\alpha\beta} X^{AB}, \end{aligned} \tag{1.2}$$

$$\begin{aligned}\left\{\bar{Q}_{\dot{\alpha}A}, \bar{Q}_{\dot{\beta}B}\right\} &= -\epsilon_{\dot{\alpha}\dot{\beta}} X^{\star}_{AB}, \\ \left[P_\mu, Q_\alpha{}^A\right] &= \left[P_\mu, \bar{Q}_{\dot{\alpha}A}\right] = 0.\end{aligned}$$

These supersymmetry generators Q and $\bar{Q}$ carry Weyl spinor indices $\alpha, \dot{\alpha}$ and $\beta, \dot{\beta}$ each running from 1 to 2. The undotted indices transform under the $(0, \frac{1}{2})$ spinor representation of the Poincaré group and the dotted ones under the $(\frac{1}{2}, 0)$ representation. The indices A and B refer to an internal space and run from 1 to some $\mathcal{N} \geq 1$. P_μ denotes the energy-momentum operator which generates the Lorentz translations, while $\sigma^\mu_{\alpha\dot{\beta}} = (1, \sigma^i_{\alpha\dot{\beta}})$ is a four-dimensional generalization of the Pauli matrices. As chiral fermions, which are needed to construct the observed parity violation via $SU(2)_L$, are not allowed for $\mathcal{N} > 1$, only the $\mathcal{N} = 1$ case is of interest for the currently accessible energy ranges and will be discussed now. The algebra for $\mathcal{N} = 1$ becomes

$$\begin{aligned}\left\{Q_\alpha, \bar{Q}_{\dot{\beta}}\right\} &= 2\sigma^\mu_{\alpha\dot{\beta}} P_\mu, \\ \{Q_\alpha, Q_\beta\} &= \left\{\bar{Q}_{\dot{\alpha}}, \bar{Q}_{\dot{\beta}}\right\} = 0, \\ [P_\mu, Q_\alpha] &= \left[P_\mu, \bar{Q}_{\dot{\alpha}}\right] = 0.\end{aligned} \tag{1.3}$$

The first line of (1.3) shows the connection of the space-time symmetry and the internal symmetry. According to the spin-statistics theorem, the second line shows that the $Q, \bar{Q}$ are fermionic operators, i.e. they transform as half-integer-spin objects. By calculation one finds that their spin is $\frac{1}{2}$. The third line ensures the invariance of supersymmetry under Lorentz transformations. The action of Q on one-particle states is to convert a boson into a fermion and vice versa. The one-particle states belong to the irreducible representations of the supersymmetry algebra, the so-called supermultiplets. Each supermultiplet contains fermionic and bosonic states which are called superpartners of each other and by applying Q and $\bar{Q}$ they are transformed into one another. The simplest supermultiplet is the so-called chiral supermultiplet consisting of a single Weyl fermion with two helicity states and one complex scalar field. Additionally, we can construct a gauge or vector supermultiplet out of a massless spin-1 vector boson and a massless spin-$\frac{1}{2}$ Weyl fermion. From Equation (1.3) we have

$$[P_\mu P^\mu, Q_\alpha] = [P_\mu P^\mu, \bar{Q}_{\dot{\alpha}}] = 0 \tag{1.4}$$

and thus, application of the supersymmetry generators does not change M^2, the squared mass of the particles inside a supermultiplet. In unbroken supersymmetry, the fermions and bosons inside a supermultiplet therefore have the same mass.

1.3.2. Superfield formalism

Considerable simplification of the notation in supersymmetric theories can be achieved by using the superfield formalism. In this formalism, the usual four-dimensional space-time is extended to the so-called superspace by introducing additional Grassmann

variables. With these anticommuting variables, the superalgebra can be written in terms of commutators

$$\begin{aligned} \left[\theta^\alpha Q_\alpha, \bar{Q}_{\dot{\beta}}\bar{\theta}^{\dot{\beta}}\right] &= 2\theta^\alpha \sigma^\mu_{\alpha\dot{\beta}} \bar{\theta}^{\dot{\beta}} P_\mu, \\ \left[\theta^\alpha Q_\alpha, \theta^\beta Q_\beta\right] &= [\bar{Q}_{\dot{\alpha}}\bar{\theta}^{\dot{\alpha}}, \bar{Q}_{\dot{\beta}}\bar{\theta}^{\dot{\beta}}] = 0, \\ [P^\mu, \theta^\alpha Q_\alpha] &= \left[P^\mu, \bar{\theta}^{\dot{\alpha}}\bar{Q}_{\dot{\alpha}}\right] = 0. \end{aligned} \tag{1.5}$$

A finite supersymmetric transformation can be written as

$$G(x_\mu, \theta^\alpha, \bar{\theta}_{\dot{\alpha}}) = e^{i(\theta^\alpha Q_\alpha + \bar{\theta}_{\dot{\alpha}}\bar{Q}^{\dot{\alpha}} - x_\mu P^\mu)}$$

with the supersymmetry generators Q_α, $\bar{Q}^{\dot{\alpha}}$ and the generator of translation P^μ. The coordinates can be combined into a tuple and a point in superspace is then given by $X = (x_\mu, \theta^\alpha, \bar{\theta}_{\dot{\alpha}})$. The superspace itself is the set of all these tuples. The fields become functions of X, i.e. they are functions of the usual space-time coordinate x_μ as well as of θ^α and $\bar{\theta}_{\dot{\alpha}}$ and are called superfields, e.g. $\Phi(x_\mu, \theta^\alpha, \bar{\theta}_{\dot{\alpha}})$. The infinitesimal form of a supersymmetry transformation is

$$\delta_G(0, \xi, \bar{\xi})\Phi(x_\mu, \theta, \bar{\theta}) = \left[\xi\frac{\partial}{\partial\theta} + \bar{\xi}\frac{\partial}{\partial\bar{\theta}} - i(\xi\sigma_\mu\bar{\theta} - \theta\sigma_\mu\bar{\xi})\frac{\partial}{\partial x_\mu}\right]\Phi(x_\mu, \theta, \bar{\theta})$$

and the supersymmetry generators can be given as differential operators in superspace by

$$Q_\alpha = \frac{\partial}{\partial\theta^\alpha} - i\sigma^\mu_{\alpha\dot{\beta}}\bar{\theta}^{\dot{\beta}}\frac{\partial}{\partial x^\mu}, \tag{1.6}$$

$$\bar{Q}_{\dot{\alpha}} = -\frac{\partial}{\partial\bar{\theta}^{\dot{\alpha}}} + i\theta^\beta\sigma^\mu_{\beta\dot{\alpha}}\frac{\partial}{\partial x^\mu}. \tag{1.7}$$

Analogously to covariant derivatives in gauge theory, we now introduce the covariant derivatives D_α and $\bar{D}_{\dot{\alpha}}$ with respect to the supersymmetry generators. These are constructed to be invariant under Q and $\bar{Q}$, i.e.

$$\{D_\alpha, Q_\alpha\} = \{\bar{D}_{\dot{\alpha}}, Q_\alpha\} = \{D_\alpha, \bar{Q}_{\dot{\alpha}}\} = \{\bar{D}_{\dot{\alpha}}, \bar{Q}_{\dot{\alpha}}\} = 0.$$

These covariant derivatives are

$$D_\alpha = \frac{\partial}{\partial\theta^\alpha} + i\sigma^\mu_{\alpha\dot{\beta}}\bar{\theta}^{\dot{\beta}}\frac{\partial}{\partial x^\mu}, \tag{1.8}$$

$$\bar{D}_{\dot{\alpha}} = -\frac{\partial}{\partial\bar{\theta}^{\dot{\alpha}}} - i\theta^\beta\sigma^\mu_{\beta\dot{\alpha}}\frac{\partial}{\partial x^\mu}. \tag{1.9}$$

The superfields can be expanded into component fields and due to the anticommuting properties of the Grassman variables, this expansion terminates with the second order in θ and $\bar{\theta}$. The general expansion is given by

$$\Phi(x_\mu, \theta^\alpha, \bar{\theta}_{\dot{\alpha}}) = f(x) + \theta\varphi(x) + \bar{\theta}\bar{\chi}(x)$$

$$
\begin{aligned}
&+\theta\theta m(x) + \bar{\theta}\bar{\theta} n(x) + \theta\sigma^{\mu}\bar{\theta} v_{\mu}(x) \\
&+\theta\theta\bar{\theta}\bar{\lambda}(x) + \bar{\theta}\bar{\theta}\theta\psi(x) + \theta\theta\bar{\theta}\bar{\theta} d(x)
\end{aligned}
\tag{1.10}
$$

where the spinor indices are not written explicitly. This expansion is valid for arbitrary superfields. However, in the MSSM we only need two types of superfields, which can be obtained by imposing covariant constraints on the general superfield.

Chiral and vector superfields

The first kind of field we need in the MSSM is the chiral superfield defined by the constraint

$$
\bar{D}_{\dot{\alpha}}\Phi(x_{\mu}, \theta^{\alpha}, \bar{\theta}_{\dot{\alpha}}) = 0 \tag{1.11}
$$

which leads to the chiral superfield

$$
\begin{aligned}
\Phi \;=\; & \phi(x) + i\theta\sigma^{\mu}\bar{\theta}\partial_{\mu}\phi(x) + \frac{1}{4}\theta\theta\bar{\theta}\bar{\theta}\partial_{\mu}\partial^{\mu}\phi(x) \\
& + \sqrt{2}\theta\psi(x) - \frac{i}{\sqrt{2}}\theta\theta\partial_{\mu}\psi(x)\sigma^{\mu}\bar{\theta} + \theta\theta F(x)
\end{aligned}
$$

with a complex scalar field ϕ, a complex Weyl spinor ψ and an auxiliary complex field F with mass dimension two. This auxiliary field balances the fermionic and bosonic degrees of freedom off-shell and under supersymmetry transformations it transforms into a total space-time derivative. Therefore, it does not represent a physical degree of freedom and can be written in terms of the other, physical fields. The product of chiral superfields again is a chiral superfield, which can be shown via $\bar{D}_{\dot{\alpha}}(\Phi_1\Phi_2) = (\bar{D}_{\dot{\alpha}}\Phi_1)\Phi_2 + \Phi_1(\bar{D}_{\dot{\alpha}}\Phi_2) = 0$. An antichiral superfield can analogously be defined by demanding $D_{\alpha}\Psi(x_{\mu}, \theta^{\alpha}, \bar{\theta}_{\dot{\alpha}}) = 0$. The hermitian conjugate of a chiral superfield $\Phi^{\dagger}$ is an antichiral superfield.
Vector superfields on the other hand can be defined by demanding

$$
\overline{V}(x, \theta, \bar{\theta}) = V(x, \theta, \bar{\theta}). \tag{1.12}
$$

The complete expansion of a vector superfield is given by

$$
\begin{aligned}
V(x, \theta, \bar{\theta}) \;=\; & C(x) + i\theta\chi(x) - i\bar{\theta}\bar{\chi}(x) + \frac{i}{2}\theta\theta[M(x) + iN(x)] - \frac{i}{2}\bar{\theta}\bar{\theta}[M(x) - iN(x)] \\
& - \theta\sigma^{\mu}\bar{\theta}A_{\mu}(x) + i\theta\theta\bar{\theta}\left[\bar{\lambda}(x) + \frac{i}{2}\bar{\sigma}^{\mu}\partial_{\mu}\chi(x)\right] - i\bar{\theta}\bar{\theta}\theta\left[\lambda(x) + \frac{i}{2}\sigma^{\mu}\partial_{\mu}\bar{\chi}(x)\right] \\
& + \frac{1}{2}\theta\theta\bar{\theta}\bar{\theta}\left[D(x) + \frac{1}{2}\partial_{\mu}\partial^{\mu}C(x)\right]
\end{aligned}
$$

where C, D, M and N are scalar fields, λ and χ are Weyl spinors and A_{μ} is the vector field giving the name to this kind of superfield. All the fields are real in order to fulfill

(1.12). With the vector superfields generalizing the gauge fields we can now define a supersymmetric gauge transformation which in the non-Abelian case is given by

$$\Phi \rightarrow e^{-i\Lambda}\Phi, \tag{1.13}$$

$$e^V \rightarrow e^{-i\Lambda^\dagger} e^V e^{i\Lambda} \tag{1.14}$$

with chiral superfields Λ_a, vector superfields V_a and $\Lambda = T^a\Lambda_a$, $V = T^a V_a$ with T^a being the generators of the gauge group. In the Abelian case the transformation of the vector superfield reduces to

$$V \rightarrow V + i(\Lambda - \Lambda^\dagger).$$

Using part of the supersymmetric gauge freedom, the gauge can be fixed by

$$\chi(x) \equiv C(x) \equiv M(x) \equiv N(x) \equiv 0$$

which removes unphysical degrees of freedom, breaks supersymmetry and leaves the 'ordinary' gauge freedom. This gauge is called Wess-Zumino gauge [5] and the expansion of the vector superfield simplifies to

$$V = -\theta\sigma^\mu\bar{\theta}A_\mu(x) + i\theta\theta\bar{\theta}\bar{\lambda}(x) - i\bar{\theta}\bar{\theta}\theta\lambda(x) + \frac{1}{2}\theta\theta\bar{\theta}\bar{\theta}D(x) \tag{1.15}$$

from which we have $V^3 = 0$. The expansion contains the auxiliary scalar field D with mass dimension two and as was the case for the chiral superfield, this auxiliary field again transforms into a total derivative under supersymmetry transformations and therefore does not represent physical, propagating degrees of freedom.

1.3.3. The Lagrangian

For a supersymmetric theory, the action must be invariant under supersymmetry transformations and therefore the Lagrangian is required to change only by a total space-time derivative. To achieve this, we only use the F and D terms in the Lagrangian which can then be written as

$$\mathcal{L} = \int d^2\theta\mathcal{L}_F + \int d^2\theta d^2\bar{\theta}\mathcal{L}_D. \tag{1.16}$$

As was already noted, the product of chiral superfields again is a chiral superfield and since the product of four or more chiral superfields produces terms with mass dimension larger than four, the most general form of a renormalizable, holomorphic superpotential to appear in $\mathcal{L}_F$ is

$$W(\Phi) = \lambda_i\Phi_i + \frac{1}{2}m_{ij}\Phi_i\Phi_j + \frac{1}{3}g_{ijk}\Phi_i\Phi_j\Phi_k. \tag{1.17}$$

The product of two chiral superfields produces fermion mass terms $\propto \psi_i\psi_j$ and the product of three chiral superfields produces Yukawa terms $\propto \psi_i\psi_j\phi_k$. With the product $\Phi^\dagger\Phi$ of a chiral field and its hermitian conjugate, we can introduce the kinetic terms. The product is self-conjugate and therefore a vector superfield with the possible contribution to the Lagrangian

$$\int d^2\theta d^2\bar{\theta}\ \mathcal{L}_D = \int d^2\theta d^2\bar{\theta}\ \Phi^\dagger\Phi = FF^\star + \phi\partial_\mu\partial^\mu\phi^\star + i\partial^\mu\bar{\psi}\bar{\sigma}_\mu\psi.$$

This expression contains kinetic terms for the scalar and the fermionic component but no kinetic term for the auxiliary field F and thus, the auxiliary field can be integrated out. Gauge interactions can be introduced by the supersymmetric generalization of the minimal coupling $\Phi^\dagger\Phi \to \Phi^\dagger e^{2gV}\Phi$ with vector superfields V_a, $V = T^aV_a$ and the generators of the gauge group T^a. In the component fields the ordinary derivatives are replaced by the covariant derivatives $D_\mu = \partial_\mu + igA^a_\mu T_a$. We need to introduce kinetic terms for the gauge fields as well. These can be expressed in terms of a superpotential by using the supersymmetric field strength

$$W_\alpha = -\frac{1}{4}(\bar{D}\bar{D})e^{-2gV}D_\alpha e^{2gV} \tag{1.18}$$

which transforms as $W_\alpha \to e^{-i\Lambda}W_\alpha e^{i\Lambda}$ under the non-Abelian gauge transformation. The product $W_\alpha W^\alpha$ is a chiral superfield and its trace gauge invariant, so it can appear in the supersymmetric Lagrangian. Again, the auxiliary fields do not acquire kinetic terms and can be integrated out. The Lagrangian now reads

$$\begin{aligned}\mathcal{L}_{SUSY} &= \int d^2\theta \left[\frac{1}{16g^2}\,\mathrm{tr}(W_\alpha W^\alpha + \bar{W}_{\dot{\alpha}}\bar{W}^{\dot{\alpha}}) + W(\Phi) + \mathrm{h.c.}\right] \\ &\quad + \int d^2\theta d^2\bar{\theta}(\Phi^\dagger e^{2gV}\Phi)\end{aligned} \tag{1.19}$$

and with m_{ij} and g_{ijk} totally symmetric it is invariant under the gauge transformation $\Phi \to e^{-i\Lambda}\Phi$, $e^{2gV} \to e^{-i\Lambda^\dagger}e^{2gV}e^{i\Lambda}$. The auxiliary fields F and D can be eliminated by using their equations of motion, which – as the Lagrangian does not contain kinetic terms – have the simple form

$$\frac{\partial\mathcal{L}}{\partial F_i} = F_i^\star + \lambda_i + m_{ki}\phi_k + g_{kli}\phi_k\phi_l = 0, \tag{1.20}$$

$$\frac{\partial\mathcal{L}}{\partial F_i^\star} = F_i + \lambda_i^\star + m^\star_{ki}\phi^\star_k + g^\star_{kli}\phi^\star_k\phi^\star_l = 0, \tag{1.21}$$

$$\frac{\partial\mathcal{L}}{\partial D_a} = D^a + g\phi^\star_i T^a_{ij}\phi_j = 0. \tag{1.22}$$

Using these expressions, the Lagrangian can be rewritten completely in terms of the physical fields.

1.3.4. Supersymmetry breaking

As seen in the previous section, supersymmetry forces all members of a supermultiplet to have the same mass. This means, that if supersymmetry were unbroken, there would be a superpartner of the same mass for each SM particle and since these superpartners of SM particles have not been found, supersymmetry has to be spontaneously broken. To achieve spontaneous symmetry breaking inside the supersymmetric Lagrangian, it must be impossible for the F and D terms to simultaneously vanish. There are two possibilities, one of them is the Fayet-Iliopoulos or D-term mechanism [6] of adding a D term linear in the auxiliary field to the Lagrangian. The other one is O'Raifeartaigh or F-term supersymmetry breaking [7] where chiral supermultiplets are used with a superpotential such that not all F-terms can be zero simultaneously. Both mechanisms are phenomenologically insufficient because they do not generate an acceptable spectrum (see [3] for details) and thus, the breaking of supersymmetry has to occur indirectly or radiatively. Basically, there are three scenarios of breaking supersymmetry in a 'hidden sector'. In gravity-mediated supersymmetry breaking (mSUGRA) [8, 9] the two sectors interact essentially by gravitational interactions which mediate the breaking to the 'visible sector' which we observe. The minimal version of this scenario is characterized by four parameters and a sign, these are the universal scalar mass parameter m_0, the gaugino mass parameter $m_{1/2} = M_i$, where M_i are the gluino-, wino- and bino-masses, the trilinear coupling parameter A_0, the ratio of the Higgs vacuum expectation values $\tan\beta$ and the sign of the supersymmetric Higgs mass parameter μ. Another possibility is gauge-mediated supersymmetry breaking (GMSB) [10, 11, 12] in which the supersymmetry breaking is mediated by gauge interactions involving so-called messenger chiral supermultiplets that couple to the MSSM particles through gauge boson and gaugino interactions. In the minimal version of GMSB there are four parameters and a sign, the messenger mass M_{mess}, the messenger index N_{mess}, the universal soft supersymmetry breaking mass scale felt by the low energy sector Λ, $\tan\beta$ and the sign of μ. In the third scenario the breaking is mediated via the super-Weyl anomaly and it is therefore called 'anomaly mediated supersymmetry breaking' (AMSB) [13]. The parameters are m_{aux} setting the overall scale of the supersymmetric-particle (sparticle) masses, $\tan\beta$, the sign of μ and a phenomenological parameter m_0 which is introduced to keep the squared slepton masses positive. From a phenomenological point of view it is not that important how exactly supersymmetry is broken, but rather which additional terms are generated in the Lagrangian. We want to keep the cancellation of the quadratically divergent contributions to the Higgs mass in order to not lose the solution of the hierarchy problem of the SM. The allowed terms which do not alter the cancellation are called 'soft supersymmetry breaking terms' and it was shown [14] that only the following terms are allowed:

- scalar mass terms $m_{ij}^2 \phi_i^\star \phi_j$

- trilinear scalar interactions $t_{ijk}\phi_i\phi_j\phi_k + \text{h.c.}$
- gaugino masses $\frac{1}{2}m_l\bar{\lambda}_l\lambda_l$
- bilinear terms $b_{ij}\phi_i\phi_j + \text{h.c.}$
- linear terms $l_i\phi_i$

1.3.5. The Minimal Supersymmetric Standard Model

The minimal phenomenologically viable extension of the SM is a $\mathcal{N} = 1$ supersymmetry with soft supersymmetry breaking. As the SM, the MSSM has the gauge group $SU(3)_C \times SU(2)_L \times U(1)_Y$ which describes the strong and electro-weak interactions, and the particle content of the MSSM is obtained by replacing all fields by the corresponding superfields. The matter fields are replaced by chiral superfields, with the fermionic part describing the ordinary SM fermions and the scalar part describing the superpartners, the so-called 'sfermions'. For each gauge field a vector superfield is introduced, which – besides the SM vector bosons – contains their fermionic superpartners, the gauginos. In the Higgs sector some care is needed since it is not sufficient to just replace the scalar Higgs field by a superfield. In order to give masses to the up-type and down-type quarks, the Higgs field H as well as its hermitian conjugate $H^\star$ would be needed. This spoils analyticity of the superpotential and thus we need a second Higgs doublet with negative hypercharge. Another reason for the introduction of two Higgs fields is that the fermionic part of a single Higgs field with negative hypercharge would contribute to the chiral anomaly [15, 16]. In order to compensate this, the second Higgs superfield with oppositely hypercharged fermion is needed. The particle content of the MSSM is given in Table 1.1. For the gauge superfields we have the field strengths

$$\begin{aligned} W^a_{C_\alpha} &= -\frac{1}{4}(\bar{D}\bar{D})e^{-2g_s\hat{G}}D_\alpha e^{2g_s\hat{G}}, \\ W^i_{L_\alpha} &= -\frac{1}{4}(\bar{D}\bar{D})e^{-2g_w\hat{W}}D_\alpha e^{2g_w\hat{W}}, \\ W_{Y_\alpha} &= -\frac{1}{4}(\bar{D}\bar{D})e^{-2g_y\hat{B}}D_\alpha e^{2g_y\hat{B}} = -\frac{g_y}{4}\bar{D}\bar{D}D_\alpha\hat{B}. \end{aligned} \tag{1.23}$$

The superpotential of the MSSM is defined as

$$W_{MSSM} = \varepsilon_{ij}\left(Y_e^{IJ}\hat{H}_1^i\hat{L}^{jI}\hat{E}^J - Y_u^{IJ}\hat{H}_2^i\hat{Q}^{jI}\hat{U}^J + Y_d^{IJ}\hat{H}_1^i\hat{Q}^{jI}\hat{D}^J - \mu\hat{H}_1^i\hat{H}_2^j\right) \tag{1.24}$$

where the 3×3 matrices Y_e, Y_u and Y_d denote the Yukawa couplings and I, J are generation indices that are summed over. Inserting the field strengths and the superpotential together with the F-terms into Equation (1.19), we get the supersymmetric part of the Lagrangian

$$\mathcal{L}_{SUSY} = \int d^2\theta\big[\big(\frac{1}{16g_s^2}W^a_{C\alpha}W_C^{a\alpha} + \frac{1}{16g_w^2}W^a_{L\alpha}W_L^{a\alpha}$$

	fields			group representation		
	superfield	fermion field	boson field	$SU(3)_C$	$SU(2)_L$	$U(1)_Y$
matter sector						
Quarks	$\hat{Q}_I$	$\begin{pmatrix} u_{L,I} \\ d_{L,I} \end{pmatrix}$	$\begin{pmatrix} \tilde{u}_{L,I} \\ \tilde{d}_{L,I} \end{pmatrix}$	**3**	**2**	$\frac{1}{3}$
	$\hat{U}_I$	$u^c_{R,I}$	$\tilde{u}^\star_{R,I}$	$\bar{\mathbf{3}}$	**1**	$-\frac{4}{3}$
	$\hat{D}_I$	$d^c_{R,I}$	$\tilde{d}^\star_{R,I}$	$\bar{\mathbf{3}}$	**1**	$\frac{2}{3}$
Leptons	$\hat{L}_I$	$\begin{pmatrix} \nu_{L,I} \\ e_{L,I} \end{pmatrix}$	$\begin{pmatrix} \tilde{\nu}_{L,I} \\ \tilde{e}_{L,I} \end{pmatrix}$	**1**	**2**	-1
	$\hat{E}_I$	$e^c_{R,I}$	$\tilde{e}^\star_{R,I}$	**1**	**1**	2
gauge sector						
$SU(3)_C$	$\hat{G}^a$	$\tilde{\lambda}^a_G$	G^a_μ	**8**	**1**	0
$SU(2)_L$	$\hat{W}^i$	$\tilde{\lambda}^i_W$	W^i_μ	**1**	**3**	0
$U(1)_Y$	$\hat{B}$	$\tilde{\lambda}_B$	B_μ	**1**	**1**	0
Higgs sector						
	$\hat{H}_1$	$\begin{pmatrix} \tilde{H}^1_1 \\ \tilde{H}^2_1 \end{pmatrix}$	$\begin{pmatrix} H^1_1 \\ H^2_1 \end{pmatrix}$	**1**	**2**	-1
	$\hat{H}_2$	$\begin{pmatrix} \tilde{H}^1_2 \\ \tilde{H}^2_2 \end{pmatrix}$	$\begin{pmatrix} H^1_2 \\ H^2_2 \end{pmatrix}$	**1**	**2**	1

Table 1.1.: Superfields and particles of the MSSM in interaction basis. Superfields are denoted by a hat, superpartners by a tilde.

$$
\begin{aligned}
&+\frac{1}{16g_y^2}W_{Y\alpha}W_Y{}^{\alpha}+W_{MSSM}\big)+\text{h.c.}\big]\\
&+\int d^2\theta d^2\bar{\theta}\big[\hat{L}^\dagger e^{2g_w\hat{W}+2g_y\hat{B}}\hat{L}+\hat{E}^\dagger e^{2g_y\hat{B}}\hat{E}\\
&+\hat{Q}^\dagger e^{2g_s\hat{G}+2g_w\hat{W}+2g_y\hat{B}}\hat{Q}+\hat{U}^\dagger e^{-2g_s\hat{G}^T+2g_y\hat{B}}\hat{U}+\hat{D}^\dagger e^{-2g_s\hat{G}^T+2g_y\hat{B}}\hat{D}\\
&+\hat{H}_1^\dagger e^{2g_w\hat{W}+2g_y\hat{B}}\hat{H}_1+\hat{H}_2^\dagger e^{2g_w\hat{W}+2g_y\hat{B}}\hat{H}_2\big].
\end{aligned}
\tag{1.25}
$$

The soft supersymmetry breaking terms are Majorana mass terms for the gauginos, mass terms for the scalar superpartners and the scalar Higgs, a bilinear term coupling the two scalar Higgs fields and trilinear interaction terms for the scalar superpartners

$$
\begin{aligned}
\mathcal{L}^{soft}_{Majorana} &= -\frac{1}{2}\left(M_1\bar{\tilde{\lambda}}_B\tilde{\lambda}_B+M_2\bar{\tilde{\lambda}}^i_W\tilde{\lambda}^i_W+M_3\bar{\tilde{\lambda}}^a_G\tilde{\lambda}^a_G\right)+\text{h.c.},\\
\mathcal{L}^{soft}_{scalarmass} &= -\tilde{L}^\star M^2_{\tilde{L}}\tilde{L}-\tilde{E}^\star M^2_{\tilde{E}}\tilde{E}-\tilde{Q}^\star M^2_{\tilde{Q}}\tilde{Q}-\tilde{U}^\star M^2_{\tilde{U}}\tilde{U}-\tilde{D}^\star M^2_{\tilde{D}}\tilde{D}\\
&\quad -m_1^2|H_1|^2-m_2^2|H_2|^2,\\
\mathcal{L}^{soft}_{bilinear} &= m_{12}^2(\epsilon_{ij}H_1^iH_2^j+\text{h.c.}),\\
\mathcal{L}^{soft}_{trilinear} &= \epsilon_{ij}\left(A_u^{IJ}H_2^i\tilde{Q}^{jI}\tilde{U}^J-A_d^{IJ}H_1^i\tilde{Q}^{jI}\tilde{D}^J-A_e^{IJ}H_1^i\tilde{L}^{jI}\tilde{E}^J\right)+\text{h.c.}
\end{aligned}
\tag{1.26}
$$

Most of the free parameters of the MSSM appear in the soft breaking sector. There are the trilinear couplings A_u, A_d, A_e which in general are complex 3×3 matrices, the complex mass parameters $M_{\tilde{L}}$, $M_{\tilde{E}}$, $M_{\tilde{Q}}$, $M_{\tilde{U}}$, $M_{\tilde{D}}$ which are hermitian 3×3 matrices, the real Higgs mass parameters m_1, m_2, the gaugino mass parameters M_1, M_2, M_3 and the bilinear Higgs coupling m_{12}. As this huge parameter space is hard to handle, we do the analysis in this work for ten benchmark points described in Section 1.3.6. In order to protect the proton from decay and to get a suitable dark matter candidate, we introduce an additional global symmetry called R-parity [17]. Each particle is assigned the new quantum number R-parity $P_R=(-1)^{2s+3(B-L)}$, where s, B and L are spin, baryon number and lepton number, respectively. From this definition we have $P_R=-1$ for all superpartners and $P_R=1$ for all other particles, i.e. the Standard Model particles and the Higgs fields. We demand that R-parity is conserved multiplicatively. With this additional symmetry the proton decays are forbidden and since each vertex must have an even number of supersymmetric particles, the lightest supersymmetric particle (LSP) is stable.

Particle content

We now make the conversion from interaction eigenstates to mass eigenstates and give the additional particle content of the MSSM. First, we consider the Higgs sector. We reparameterize the Higgs fields as

$$
H_1=\begin{pmatrix}v_1+\frac{1}{\sqrt{2}}(\phi_1^0-i\chi_1^0)\\ -\phi_1^-\end{pmatrix}\qquad H_2=\begin{pmatrix}\phi_2^+\\ v_2+\frac{1}{\sqrt{2}}(\phi_2^0+i\chi_2^0)\end{pmatrix}
\tag{1.27}
$$

with the vacuum expectation values v_1, v_2, real scalar fields ϕ_i^0, χ_i^0 and complex scalar fields ϕ_1^+, ϕ_2^-. Using this in the Higgs potential

$$\begin{aligned} V_{Higgs} &= |\mu|^2(|H_1|^2+|H_2|^2)+\frac{1}{8}(g_w^2+g_y^2)(|H_1|^2-|H_2|^2)^2 \\ &\quad +\frac{1}{2}g_w^2|H_1^\dagger H_2|^2+m_1^2|H_1|^2+m_2^2|H_2|^2-m_3^2(\epsilon_{ij}H_1^iH_2^j+\text{h.c.}) \end{aligned} \tag{1.28}$$

we get the mass matrices by differentiating twice with respect to ϕ and χ. This way we obtain four real 2×2 matrices which can be diagonalized by the rotations

$$\begin{aligned} \begin{pmatrix} G^\pm \\ H^\pm \end{pmatrix} &= \begin{pmatrix} \cos\beta & \sin\beta \\ -\sin\beta & \cos\beta \end{pmatrix}\begin{pmatrix} \phi_1^\pm \\ \phi_2^\pm \end{pmatrix}, \\ \begin{pmatrix} G^0 \\ A^0 \end{pmatrix} &= \begin{pmatrix} \cos\beta & \sin\beta \\ -\sin\beta & \cos\beta \end{pmatrix}\begin{pmatrix} \chi_1^0 \\ \chi_2^0 \end{pmatrix}, \\ \begin{pmatrix} H^0 \\ h^0 \end{pmatrix} &= \begin{pmatrix} \cos\alpha & \sin\alpha \\ -\sin\alpha & \cos\alpha \end{pmatrix}\begin{pmatrix} \phi_1^0 \\ \phi_2^0 \end{pmatrix} \end{aligned} \tag{1.29}$$

where $\tan\beta=\frac{v_2}{v_1}$ with $0<\beta<\frac{\pi}{2}$ and $\tan 2\alpha=\tan 2\beta\frac{m_A^2+m_Z^2}{m_A^2-m_Z^2}$ with $-\frac{\pi}{2}<\alpha<0$. Analogously to the SM we get three would-be Goldstone bosons $G^\pm$, G^0 which become the massive modes of the gauge bosons. The remaining physical Higgs bosons are two neutral CP-even Higgs bosons h^0 and H^0, a CP-odd one A^0 and two charged ones $H^\pm$. As in the SM, the gauge bosons are turned into the mass eigenstates $W^\pm$, Z and γ with the single vacuum expectation value replaced by $v=\sqrt{v_1^2+v_2^2}$. The mass eigenstates of the eight $SU(3)_C$ gauge bosons are identical to the interaction eigenstates, giving eight massless gluons.

Next, we consider the supersymmetric partners – the Higgsinos and Gauginos. After breaking of $SU(2)_L\times U(1)_Y$, all particles with the same $SU(3)_C$ and $U(1)_Q$ quantum numbers can mix. The neutral Higgsinos $\tilde{H}_1^0$, $\tilde{H}_2^0$ and the neutral gauginos $\tilde{B}$, $\tilde{W}^0$ combine to form four mass eigenstates called neutralinos $\tilde{\chi}_i^0$ with $i=1,\ldots,4$ which are Majorana fermions. The charged Higgsinos $\tilde{H}_1^-$, $\tilde{H}_2^+$ combine with the charged gauginos $\tilde{W}^\pm$ to form two charged mass eigenstates called charginos $\tilde{\chi}_i^\pm$ with $i=1,2$ which are Dirac fermions. The gluinos, the gauginos of $SU(3)_C$, do not mix with any other particles since they are the only fermions interacting exclusively via the strong interaction. They give eight Majorana fermions, the gluinos with mass $m_{\tilde{g}}=|M_3|$.

Now, we come to the sleptons and squarks. In principle, any scalar particles with the same electric charge and R-parity can mix. This would imply mixing of the six up-type squarks $\tilde{u}_L$, $\tilde{c}_L$, $\tilde{t}_L$, $\tilde{u}_R$, $\tilde{c}_R$, $\tilde{t}_R$, the same for down-type squarks and selectrons and mixing of the three sneutrinos. However, this general mixing would lead to additional contributions to flavor changing neutral currents which are experimentally constrained to be small. Also, the interactions mediating the soft supersymmetry breaking are assumed to be flavor blind (e.g. gravity) and thus, we end up with 7

nearly degenerate pairs of the first and second generation squarks and sleptons which are $(\tilde{e}_L, \tilde{\mu}_L)$, $(\tilde{e}_R, \tilde{\mu}_R)$, $(\tilde{u}_L, \tilde{c}_L)$, $(\tilde{u}_R, \tilde{c}_R)$, $(\tilde{d}_L, \tilde{s}_L)$, $(\tilde{d}_R, \tilde{s}_R)$ and $(\tilde{\nu}_e, \tilde{\nu}_\mu)$. Due to the large Yukawa and soft couplings of the third generation there is substantial mixing of the left- and righthanded parts, giving mass eigenstates $(\tilde{\tau}_1, \tilde{\tau}_2)$, $(\tilde{t}_1, \tilde{t}_2)$ and $(\tilde{b}_1, \tilde{b}_2)$. The neutrinos are assumed to be massless in the MSSM and therefore, in the sneutrino sector there are only left-handed fields and the interaction eigenstates are identical to the mass eigenstates.

1.3.6. Snowmass points and slopes

In the unconstrained version of the MSSM with no particular SUSY breaking mechanism assumed, i.e. when all possible SUSY breaking terms are used, there are more than one hundred (105) parameters in addition to the parameters of the SM. But even the four- or five-dimensional parameter space of the three SUSY breaking mechanisms mentioned in Section 1.3.4 is too large to be scanned thoroughly and so, 10 specific points with attached model lines, the 'Snowmass Points and Slopes', were defined, each of them with different aim and motivation. See [18] and [19] for a detailed discussion. The SPS points 1-5 (where SPS 1 consists of two points) are mSUGRA points, SPS 6 is mSUGRA-like, points 7 and 8 are GMSB scenarios and the final point 9 is an AMSB scenario.

- SPS 1 is a 'typical' mSUGRA SPS point and consists of two scenarios - SPS 1a with intermediate $\tan\beta$ and SPS 1b with a relatively large value of $\tan\beta$. The points are defined as
  SPS 1a: $m_0 = 100\,\text{GeV}$, $m_{1/2} = 250\,\text{GeV}$, $A_0 = -100\,\text{GeV}$, $\tan\beta = 10$.
  SPS 1b: $m_0 = 200\,\text{GeV}$, $m_{1/2} = 400\,\text{GeV}$, $A_0 = 0$, $\tan\beta = 30$.
  with $\mu > 0$ for both points. SPS 1a was found to be slightly outside the allowed region to produce an acceptable amount of dark matter density [20, 21]. But only a slight modification of the low energy spectrum is needed to compensate this.

- The point SPS 2 lies in the 'focus point' region with large m_0 and small $|\mu|$, where the LSP $\tilde{\chi}_1^0$ has a sizable higgsino component, thus enhancing its annihilation cross section. This avoids too large relic abundance. The scenario produces relatively heavy squarks and sleptons, while neutralinos and charginos are relatively light. The gluino is lighter than the squarks in this scenario, which is defined by
  SPS 2: $m_0 = 1450\,\text{GeV}$, $m_{1/2} = 300\,\text{GeV}$, $A_0 = 0$, $\tan\beta = 10$ and $\mu > 0$.

- SPS 3. In this scenario, the LSP and the next-to-lightest supersymmetric particle (NLSP) are nearly mass degenerate and there can be rapid coannihilation between them. This can produce sufficiently low relic abundance. Another fea-

ture is the very small slepton-neutralino mass difference.
SPS 3: $m_0 = 90\,\text{GeV}$, $m_{1/2} = 400\,\text{GeV}$, $A_0 = 0$, $\tan\beta = 10$ and $\mu > 0$.

- For SPS 4 we have a large value of $\tan\beta$, which significantly enhances the couplings of A and H to $b\bar{b}$ and $\tau^+\tau^-$ as well as the $H^\pm t\bar{b}$ couplings.
  SPS 4: $m_0 = 400\,\text{GeV}$, $m_{1/2} = 300\,\text{GeV}$, $A_0 = 0$, $\tan\beta = 50$ and $\mu > 0$.

- SPS 5 is characterized by a large negative A_0, which allows a relatively low value for $\tan\beta$ while being consistent with the constraints from the Higgs search at LEP.
  SPS 5: $m_0 = 150\,\text{GeV}$, $m_{1/2} = 300\,\text{GeV}$, $A_0 = -1000$, $\tan\beta = 5$ and $\mu > 0$.

- At SPS 6, the bino mass parameter M_1 is larger than in usual mSUGRA scenarios, reducing the mass difference between the lightest chargino and χ_1^0, χ_2^0 and the sleptons.
  SPS 6: $m_0 = 150\,\text{GeV}$, $m_{1/2} = 300\,\text{GeV}$, $A_0 = 0$, $\tan\beta = 10$ and $\mu > 0$
  at GUT scale $M_1 = 480\,\text{GeV}$, $M_2 = M_3 = 300\,\text{GeV}$.

- SPS 7 is a GMSB scenario with the gravitino (the superpartner of the graviton) as the LSP and the NLSP being the lighter stau. The interactions of the gravitino are of gravitational strength and therefore it does not play a role in collider physics.
  SPS 7: $\Lambda = 40\,\text{TeV}$, $M_{mess} = 80\,\text{TeV}$, $N_{mess} = 3$, $\tan\beta = 15$, $\mu > 0$.

- For SPS 8 the lightest neutralino is the NLSP and the gravitino is the LSP.
  SPS 8: $\Lambda = 100\,\text{TeV}$, $M_{mess} = 200\,\text{TeV}$, $N_{mess} = 1$, $\tan\beta = 15$, $\mu > 0$.

- SPS 9 is an AMSB scenario which has a very small neutralino-chargino mass difference as a typical feature of AMSB scenarios. The LSP is a wino-like neutralino and the NLSP is a nearly mass degenerate wino-like chargino.
  SPS 9: $m_0 = 450\,\text{GeV}$, $m_{aux} = 60\,\text{TeV}$, $\tan\beta = 10$, $\mu > 0$.

1.4. Feynman rules for Majorana fermions

Majorana fermions are of interest in the SM as possible facilitators for neutrinoless double beta decay. The MSSM, however, contains Majorana fermions from the very beginning. For example the gluinos and the neutralinos are Majorana fermions and as we want to study the MSSM as a specific extension, some care is needed when applying Feynman rules to these particles. Since the Majorana particles are self-conjugate, the direction of fermion-number flow is not determined a priori, which results for example in ambiguities in the external spinor assignments and the relative signs of coherent amplitudes. In [22], a set of Majorana Feynman rules is proposed, where a continuous

fermion flow is introduced and which uses only the usual fermion propagator together with two sets of vertices. The relative signs of interfering diagrams are determined in the same way as for Dirac fermions. The continuous fermion flow can be chosen with arbitrary direction as long as this is done consistently for all diagrams, one just has to use special 'reversed' vertex functions and propagators for reversed Dirac lines. Since the propagator depends on the relative orientation of fermion flow and momentum flow, the reversed propagator is the usual one with the replacement $p \to -p$, or $S_R(p) = S(-p)$. In the reversed vertex functions, terms proportional to γ_μ pick up a -1, while the terms proportional to 1, γ_5, $\gamma_\mu\gamma_5$ stay the same. As long as we choose the directions of Majorana lines in such a way, that the Dirac lines keep their usual directions, no differences occur.

1.5. Finite-width effects and gauge invariance

The NWA provides a way to simplify the calculation of processes with unstable intermediate states and in the following, we discuss how the width of an unstable particle enters the calculation and to what extend gauge invariance is concerned. The width of an unstable particle enters its propagator – and this way the Feynman amplitude – through the resummation of self-energy contributions. Consider the resummation of one-particle-irreducible (1PI) self-energy contributions to the scalar propagator shown in Figure 1.1, where 1PI means diagrams which can not be cut into two by just removing a single line.

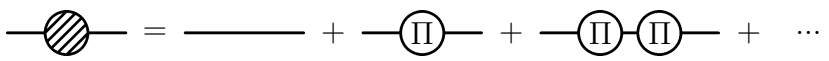

Figure 1.1.: Dyson resummation of 1PI self energy contributions.

Let $D_\Phi(p^2)$ and $D^0_\Phi(p^2)$ denote the resummed and unresummed propagator respectively. With $i\Pi_\Phi(p^2)$ denoting the 1PI self-energy contributions, we get

$$\begin{aligned} D_\Phi(p^2) &= D^0_\Phi(p^2) + D^0_\Phi(p^2) i\Pi_\Phi(p^2) D^0_\Phi(p^2) + \cdots \\ &= D^0_\Phi(p^2) \sum_{n=0}^{\infty} \left(i\Pi_\Phi(p^2) D^0_\Phi(p^2) \right)^n . \end{aligned} \tag{1.30}$$

This implies for the inverse propagator the relation

$$D_\Phi(p^2)^{-1} = \left[D^0_\Phi(p^2) \sum_{n=0}^{\infty} \left(i\Pi_\Phi(p^2) D^0_\Phi(p^2) \right)^n \right]^{-1} \tag{1.31}$$

$$= \left[\sum_{n=0}^{\infty} \left(i\Pi_\Phi(p^2) D^0_\Phi(p^2)\right)^n\right]^{-1} D^0_\Phi(p^2)^{-1} \tag{1.32}$$

$$= \left(1 - i\Pi_\Phi(p^2) D^0_\Phi(p^2)\right) D^0_\Phi(p^2)^{-1} \tag{1.33}$$

$$= D^0_\Phi(p^2)^{-1} - i\Pi_\Phi(p^2). \tag{1.34}$$

This so-called Dyson equation is solved by

$$D_\Phi(p^2) = \frac{D^0_\Phi(p^2)}{1 - i\Pi_\Phi(p^2) D^0_\Phi(p^2)}. \tag{1.35}$$

For scalar particles, the resummed propagator is given by

$$D_\Phi(p^2) = \frac{i}{p^2 - m_0^2 + \Pi_\Phi(p^2)} \tag{1.36}$$

and with the physical mass defined as the real part of the pole of the propagator $m^2 = m_0^2 - \mathrm{Re}\Pi_\Phi(m^2)$ and the width $\Gamma = \frac{1}{m}\mathrm{Im}\Pi_\Phi(m^2)$, the propagator reads

$$D_\Phi(p^2) = \frac{i}{p^2 - m_0^2 + \Pi(p^2)} \approx \frac{i}{p^2 - m^2 + im\Gamma}. \tag{1.37}$$

For massive vector bosons things are a bit more complicated due to the Lorentz tensor structure of the propagator and the self energy. With the decomposition of $\Pi^{\mu\nu}_W$ into a transverse and a longitudinal part

$$\Pi^{\mu\nu}_W(q^2) = \Pi^T_W(q^2)(g^{\mu\nu} - \frac{q^\mu q^\nu}{q^2}) + \Pi^L_W(q^2)\frac{q^\mu q^\nu}{q^2} \tag{1.38}$$

the resulting propagator in unitary gauge is given by (see [23])

$$D_W(q^2) = \frac{-i}{q^2 - m^2 - \Pi^T_W(q^2)} \left[g^{\mu\nu} - \frac{q^\mu q^\nu}{q^2} \frac{q^2 + \Pi^L_W(q^2) - \Pi^T_W(q^2)}{m^2 + \Pi^L_W(q^2)}\right]. \tag{1.39}$$

This resummation of self energies takes into account a specific part of a Feynman diagram to all orders in perturbation theory, while other loop contributions are ignored. This mixing of different orders in the perturbation expansion threatens to violate gauge invariance. Another problem is, that the self energy contribution does not develop an imaginary part for $q^2 < 0$, i.e. the decay threshold for the unstable particle. As a simple solution, one could introduce a step function $m\Gamma \to m\Gamma\Theta(q^2)$, but this was found to make things even worse [23]. However, in our analyses we always have $q^2 \geq 0$ and therefore we concentrate on gauge invariance issues.

There are several schemes for introducing finite-width effects in tree-level calculations and a few of them are discussed now. In the overall factor scheme [24] the amplitude without finite-width effects, which is gauge invariant, is multiplied by

$$\frac{p^2 - m^2}{p^2 - m^2 + im\Gamma}$$

for each resonant propagator. This generates the Breit-Wigner propagators for the resonant intermediate states while gauge invariance is preserved. However, the overall factor has no physical sense or meaning for the non-resonant diagrams. The complex mass scheme [25] is a more sophisticated version of the simple fixed width scheme [26] and it ensures full gauge invariance. The Feynman rules are changed by the replacement $m^2 \to m^2 - im\Gamma$ everywhere the mass m appears. For the W and Z bosons this implies the use of a complex Weinberg angle

$$\cos^2 \Theta_W = \frac{M_W^2 - iM_W\Gamma_W}{M_Z^2 - iM_Z\Gamma_Z}.$$

This scheme is manifestly gauge invariant again but the physical content of the complex Feynman rules is not clear. Loop schemes are another possibility to ensure gauge invariance by including subsets or even all diagrams up to a given number of loops and using strictly resummed propagators. The fermion loop scheme [27] proposes to include all fermionic one-loop diagrams and has been successfully applied to 4 fermion final states, but fails for a six fermion final state [28].

1.6. Monte Carlo integration

In order to check our off-shell calculations, we use automatically generated matrix elements and for their integration we implement the Monte Carlo method (see [29] for details). The general idea of Monte Carlo integration is to generate a sufficiently large number N of random points in the integration region V and then approximate the integral of a function f over this region by

$$\int_V f dV = V \langle f \rangle = \frac{V}{N} \sum_{i=1}^{N} f(x_i) \tag{1.40}$$

where $\langle f \rangle$ is the arithmetic mean of f over the N sample points. An estimate for the result with the one-standard-deviation error is

$$\int_V f dV = V \langle f \rangle \pm V \sqrt{\frac{\langle f^2 \rangle - \langle f \rangle^2}{N}}. \tag{1.41}$$

Note that the Monte Carlo result is not generally distributed as a Gaussian and therefore the estimate can underestimate the real error. If the integration region V is too

complex to be used for the random number generation directly, one could choose a larger region $W \subseteq V$ and set f to zero for all x in $W \setminus V$. These zero-values increase the error estimate (1.41) and therefore W should be chosen as close to V as possible. If the integrand varies very strongly in the integration region, a change of the integration variables can be very useful. If, for example, we want to integrate $f(x) = e^{5x}$ on the interval $[-5, 5]$, the Monte Carlo integration works, but as the integrand becomes very small for large negative x-values, a lot of the sample points contribute almost nothing to $\sum f(x_i)$ and $\sum f^2(x_i)$. A better way to calculate the integral is to substitute $y = \frac{1}{5}e^{5x}$ with $dy = e^{5x}dx$. Then we have

$$\int_{x_0}^{x_1} f(x)dx = \int_{y_0}^{y_1} dy$$

with $y_0 = \frac{1}{5}e^{5x_0}$ and $y_1 = \frac{1}{5}e^{5x_1}$. What is left then is to Monte Carlo integrate a constant function $\tilde{f}(y) \equiv 1$, which is exact after the first sampled point. Of course this is not possible in general, since the substitution only works because we already know the antiderivative of $f(x)$ and it can be inverted. But it is a good idea to extract all analytically integrable dominant factors out of the integrand and make an accordant substitution to make the remaining integrand as close as possible to a constant function and this way speed up the Monte Carlo integration. This technique is known as 'reduction of variance'. More details on the method used here are in Section 3.6.

Analytical NWA properties

2

In this chapter we examine general properties of the NWA, in particular its behavior in the limit of vanishing width of the intermediate particle and ways of formally obtaining the NWA formula. We then examine the impact of spin/polarization correlation effects and prove that the relative NWA error is of $\mathcal{O}(\Gamma/m)$, which is often assumed but to the best of our knowledge no proof has been given in the literature. First, we develop the factorization of the phasespace and of the matrix element in order to obtain the NWA factorization.

2.1. Phasespace factorization

We want to factorize an n-particle phasespace into an m-particle phasespace which will later be the production part of the process and an $(n-m+1)$-particle phasespace which will become the decay part. For this purpose, an additional variable q is introduced, which will be interpreted as the momentum of an intermediate particle. The phasespace can be factorized exactly, i.e. there are no approximations or assumptions necessary. To obtain the factorized form we insert an additional integral over d^4q and an appropriate $\delta^{(4)}$ factor compensating this integration. The d^3q part of the integration will then be reinterpreted as additional particle in the production part, the $\delta^{(4)}$ factor will give energy-momentum conservation in the decay part and we are left with the production and decay phasespaces with an additional q^2-integration. The general n-particle phasespace with P denoting the momentum of the decaying particle or the sum of the momenta of the scattering particles is then factorized as follows:

$$
\begin{aligned}
d\Phi_n &= (2\pi)^4\delta^{(4)}(P-\sum_{i=1}^{n}p_i)\prod_{i=1}^{n}\frac{d^3p_i}{(2\pi)^3 2E_i} && (2.1)\\
&= (2\pi)^4\delta^{(4)}(P-\sum_{i=1}^{m-1}p_i-q)\prod_{i=1}^{m-1}\frac{d^3p_i}{(2\pi)^3 2E_i}\times d^4q\times && (2.2)\\
&\quad \delta^{(4)}(q-\sum_{i=m}^{n}p_i)\prod_{i=m}^{n}\frac{d^3p_i}{(2\pi)^3 2E_i} && (2.3)
\end{aligned}
$$

$$= (2\pi)^4\delta^{(4)}(P-\sum_{i=1}^{m-1}p_i-q)\frac{d^3q}{(2\pi)^3 2E_q}\prod_{i=1}^{m-1}\frac{d^3p_i}{(2\pi)^3 2E_i}\times\frac{2E_q dq^0}{2\pi}\times \quad (2.4)$$

$$(2\pi)^4\delta^{(4)}(q-\sum_{i=m}^{n}p_i)\prod_{i=m}^{n}\frac{d^3p_i}{(2\pi)^3 2E_i} \quad (2.5)$$

$$= (2\pi)^4\delta^{(4)}(P-\sum_{i=1}^{m-1}p_i-q)\frac{d^3q}{(2\pi)^3 2E_q}\prod_{i=1}^{m-1}\frac{d^3p_i}{(2\pi)^3 2E_i}\times\frac{dq^2}{2\pi}\times \quad (2.6)$$

$$(2\pi)^4\delta^{(4)}(q-\sum_{i=m}^{n}p_i)\prod_{i=m}^{n}\frac{d^3p_i}{(2\pi)^3 2E_i} \quad (2.7)$$

$$= d\Phi_m\frac{dq^2}{2\pi}d\Phi_{n-m+1}. \quad (2.8)$$

As we need the factorization of a 3-particle phasespace for the $1\to 3$ process shown

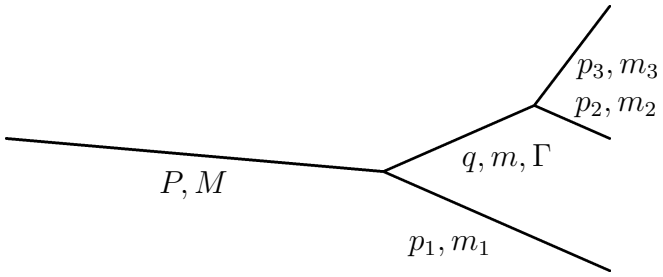

Figure 2.1.: Kinematics of the $1\to 3$ decay.

in Figure 2.1, we give the explicit form here

$$\begin{aligned} d\Phi_3 &= (2\pi)^4\delta^{(4)}(P-\sum_{i=1}^{3}p_i)\prod_{i=1}^{3}\frac{d^3p_i}{(2\pi)^3 2E_i} \\ &= (2\pi)^4\delta^{(4)}(P-q-p_1)\frac{d^3p_1}{(2\pi)^3 2E_1}\frac{d^3q}{(2\pi)^3 2E_q}\times\frac{dq^2}{2\pi}\times \\ &\quad (2\pi)^4\delta^{(4)}(q-p_2-p_3)\frac{d^3p_2}{(2\pi)^3 2E_2}\frac{d^3p_3}{(2\pi)^3 2E_3} \\ &= d\Phi_p\times\frac{dq^2}{2\pi}\times d\Phi_d \end{aligned}$$

where $d\Phi_p$ and $d\Phi_d$ are two-particle phasespaces and the intermediate particle can be treated as on-shell with squared mass q^2. For this process, the explicit forms of $d\Phi_p$ in the restframe of the parent particle and $d\Phi_d$ in the restframe of the intermediate particle are (see [30], where a different convention concerning the $(2\pi)^4$ factors is used)

$$d\Phi_p = (2\pi)^4\delta^{(4)}(P-q-p_1)\frac{d^3p_1}{(2\pi)^3 2E_1}\frac{d^3q}{(2\pi)^3 2E_q}$$

$$= \frac{1}{16\pi^2}\frac{|\vec{p}_1|}{M}d\Omega_p \tag{2.9}$$

and

$$\begin{aligned} d\Phi_d &= (2\pi)^4\delta^{(4)}(q-p_2-p_3)\frac{d^3p_2}{(2\pi)^3 2E_2}\frac{d^3p_3}{(2\pi)^3 2E_3} \\ &= \frac{1}{16\pi^2}\frac{|\vec{p}_2|}{\sqrt{q^2}}d\Omega_d \end{aligned} \tag{2.10}$$

with

$$|\vec{p}_1| = \frac{\sqrt{\left(M^2-(\sqrt{q^2}+m_1)^2\right)\left(M^2-(\sqrt{q^2}-m_1)^2\right)}}{2M}, \tag{2.11}$$

$$|\vec{p}_2| = \frac{\sqrt{\left(q^2-(m_2+m_3)^2\right)\left(q^2-(m_2-m_3)^2\right)}}{2\sqrt{q^2}}. \tag{2.12}$$

2.2. Factorization of the Feynman amplitude

Depending on the type of the intermediate particle, the amplitude for a general process consisting of its production and subsequent decay has one of the following forms in R_ξ gauge

$$\begin{aligned} \mathcal{M}^S_{full} &= \mathcal{M}_p\frac{i}{q^2-m^2+im\Gamma}\mathcal{M}_d, \\ \mathcal{M}^V_{full} &= \mathcal{M}^\mu_p\frac{i(-g_{\mu\nu}+(1-\xi)\frac{q_\mu q_\nu}{q^2-\xi m^2})}{q^2-m^2+im\Gamma}\mathcal{M}^\nu_d, \\ \mathcal{M}^F_{full} &= \mathcal{M}_p\frac{i(\not{q}+m)}{q^2-m^2+im\Gamma}\mathcal{M}_d \end{aligned} \tag{2.13}$$

for scalars, vector bosons and fermions as intermediate particle respectively, where $\mathcal{M}_p$ denotes the production-part amplitude and $\mathcal{M}_d$ the decay-part amplitude. For scalar intermediate particles the squared amplitude is already factorized:

$$|\mathcal{M}_{full}|^2 = |\mathcal{M}_p|^2\frac{1}{(q^2-m^2)^2+(m\Gamma)^2}|\mathcal{M}_d|^2 \tag{2.14}$$

with no need of a spin or polarization sum. In order to get an analog factorization for fermions and vector bosons, the propagators are rewritten as

$$\frac{i(-g_{\mu\nu}+(1-\xi)\frac{q_\mu q_\nu}{q^2-\xi m^2})}{q^2-m^2+im\Gamma} = \sum_\lambda \epsilon^{\star\lambda}_\mu(q)\frac{i}{q^2-m^2+im\Gamma}\epsilon^\lambda_\nu(q), \tag{2.15}$$

$$\frac{i(\not{q}+m)}{q^2-m^2+im\Gamma} = \sum_s u_s(q)\frac{i}{q^2-m^2+im\Gamma}\bar{u}_s(q). \tag{2.16}$$

Using this in the squared amplitudes and suppressing the explicit notion of the q-dependence of the respective spinors and polarization vectors, we get

$$\begin{aligned}
|\mathcal{M}^V_{full}|^2 &= |\sum_\lambda \mathcal{M}^\mu_p \epsilon^{\star\lambda}_\mu \frac{i}{q^2-m^2+im\Gamma}\epsilon^\lambda_\nu \mathcal{M}^\nu_d|^2 && (2.17)\\
&= \sum_{\lambda_1,\lambda_2}\left(\mathcal{M}^\mu_p \epsilon^{\star\lambda_1}_\mu \epsilon^{\lambda_1}_\nu \mathcal{M}^\nu_d\right)\frac{1}{(q^2-m^2)^2+m^2\Gamma^2}\left(\mathcal{M}^\rho_p \epsilon^{\star\lambda_2}_\rho \epsilon^{\lambda_2}_\sigma \mathcal{M}^\sigma_d\right)^\dagger && (2.18)\\
&= \sum_{\lambda_1,\lambda_2}\mathcal{M}^\mu_p \epsilon^{\star\lambda_1}_\mu \epsilon^{\lambda_1}_\nu \mathcal{M}^\nu_d \frac{1}{(q^2-m^2)^2+m^2\Gamma^2}\mathcal{M}^{\sigma\dagger}_d \epsilon^{\star\lambda_2}_\sigma \epsilon^{\lambda_2}_\rho \mathcal{M}^{\rho\dagger}_p && (2.19)\\
&\to \frac{1}{3}\sum_{\lambda_1,\lambda_2}\mathcal{M}^\mu_p \epsilon^{\star\lambda_1}_\mu \epsilon^{\lambda_2}_\nu \mathcal{M}^\nu_d \frac{1}{(q^2-m^2)^2+m^2\Gamma^2}\mathcal{M}^{\sigma\dagger}_d \epsilon^{\star\lambda_2}_\sigma \epsilon^{\lambda_1}_\rho \mathcal{M}^{\rho\dagger}_p && (2.20)\\
&= \sum_{\lambda_1}|\mathcal{M}^\mu_p \epsilon^{\star\lambda_1}_\mu|^2 \frac{1}{(q^2-m^2)^2+m^2\Gamma^2}\frac{1}{3}\sum_{\lambda_2}|\epsilon^{\lambda_2}_\nu \mathcal{M}^\nu_d|^2 && (2.21)
\end{aligned}$$

and

$$\begin{aligned}
|\mathcal{M}^F_{full}|^2 &= |\sum_s \mathcal{M}_p u_s \frac{i}{q^2-m^2+im\Gamma}\bar{u}_s \mathcal{M}_d|^2 && (2.22)\\
&= \sum_{s_1,s_2}\left(\mathcal{M}_p u_{s_1}\bar{u}_{s_1}\mathcal{M}_d\right)\frac{1}{(q^2-m^2)^2+m^2\Gamma^2}\left(\mathcal{M}_p u_{s_2}\bar{u}_{s_2}\mathcal{M}_d\right)^\dagger && (2.23)\\
&= \sum_{s_1,s_2}\mathcal{M}_p u_{s_1}\bar{u}_{s_1}\mathcal{M}_d \frac{1}{(q^2-m^2)^2+m^2\Gamma^2}\mathcal{M}^\dagger_d \bar{u}^\dagger_{s_2} u^\dagger_{s_2}\mathcal{M}^\dagger_p && (2.24)\\
&\to \frac{1}{2}\sum_{s_1,s_2}\mathcal{M}_p u_{s_1}\bar{u}_{s_2}\mathcal{M}_d \frac{1}{(q^2-m^2)^2+m^2\Gamma^2}\mathcal{M}^\dagger_d \bar{u}^\dagger_{s_2} u^\dagger_{s_1}\mathcal{M}^\dagger_p && (2.25)\\
&= \sum_{s_1}|\mathcal{M}_p u_{s_1}|^2 \frac{1}{(q^2-m^2)^2+m^2\Gamma^2}\frac{1}{2}\sum_{s_2}|\bar{u}_{s_2}\mathcal{M}_d|^2. && (2.26)
\end{aligned}$$

In lines (2.20) and (2.25), we have rearranged the spin/polarization sums as follows. In the full amplitude the unstable particle, once it is produced with a certain polarization, also decays with this polarization. We drop this correlation and instead treat both parts as independent of each other and average over the polarization in the decay part to fully factorize the process. We will later see that for total decay rates this rearrangement is exact for on-shell intermediate states. However, generally there are correlation effects due to the rearrangement.

2.3. A formal derivation

We now want to gain insight into the approximations that are necessary to obtain the NWA for unstable particles with finite Γ and for that, we give a formal way to obtain the factorized NWA cross section. It is not meant to be a rigorous derivation in the mathematical sense. To factorize the cross section we use the phasespace-factorization

$$d\Phi = d\Phi_p \frac{dq^2}{2\pi} d\Phi_d$$

where q^2 ('virtuality') is treated like an intermediate mass, i.e. it gives the 'off-shellness' of the intermediate particle. $d\Phi_p$ and $d\Phi_d$ are the phasespaces of the production and decay processes. With the factorization of the spin/polarization-summed and averaged Feynman-amplitude $\overline{\sum}|\mathcal{M}|^2$

$$\overline{\sum}|\mathcal{M}|^2 = (\overline{\sum_p}|\mathcal{M}_p|^2)\frac{1}{(q^2-m^2)^2+(m\Gamma)^2}(\overline{\sum_d}|\mathcal{M}_d|^2)$$

and thus neglecting correlation effects, the formula for the overall calculation becomes

$$\sigma = \int \frac{dq^2}{2\pi}(\int d\Phi_p \overline{\sum_p}|\mathcal{M}_p|^2)\frac{1}{(q^2-m^2)^2+(m\Gamma)^2}(\int d\Phi_d \overline{\sum_d}|\mathcal{M}_d|^2). \tag{2.27}$$

Now the intermediate particle is set on-shell, i.e. instead of integrating the full integrand, q^2 is fixed to m^2 in $\int d\Phi_p \bar{\sum}_p |\mathcal{M}_p|^2$ and $\int d\Phi_d \bar{\sum}_d |\mathcal{M}_d|^2$. For this step to make sense we would need the limit $\Gamma \to 0$ (see Section 2.4). However, we do not want to apply this limit to the whole formula, but rather assume that Γ is small but finite and the production and decay cross sections vary only weakly with q^2 in the small resonance region $[(m-\Gamma)^2, (m+\Gamma)^2]$. For $\Gamma \to 0$ this is exact and for sufficiently small Γ we accept it as an approximation. What is left then is

$$\begin{aligned}
\sigma_{NWA} &= \sigma_p \times \int_{q^2_{min}}^{q^2_{max}} \frac{dq^2}{2\pi} \frac{2m}{(q^2-m^2)^2+(m\Gamma)^2} \times \Gamma_d && (2.28)\\
&= \sigma_p \times \int_{q^2_{min}-m^2}^{q^2_{max}-m^2} \frac{dx}{2\pi} \frac{2m}{x^2+(m\Gamma)^2} \times \Gamma_d && (2.29)\\
&\simeq \sigma_p \times \int_{-\infty}^{\infty} \frac{dx}{2\pi} \frac{2m}{x^2+(m\Gamma)^2} \times \Gamma_d && (2.30)\\
&= \sigma_p \times 2\int_{0}^{\infty} \frac{dx}{2\pi} \frac{2m}{x^2+(m\Gamma)^2} \times \Gamma_d && (2.31)\\
&= \sigma_p \times \frac{\Gamma_d}{\Gamma} =: \sigma_p \times \mathrm{BR} && (2.32)
\end{aligned}$$

where σ_p is the production cross section and Γ_d the partial width of the decay part. With the assumption $q^2_{max} - m^2 \gg m\Gamma$ and $m^2 - q^2_{min} \gg m\Gamma$ the integration bounds

can be shifted to $\pm\infty$ and the integration can be carried out with the simple result $1/\Gamma$. For a particle of mass M decaying into a particle of mass m_1 and the unstable particle of mass m, which then further decays into two particles of masses m_2, m_3 we have $q^2_{min} = (m_2 + m_3)^2$ and $q^2_{max} = (M - m_1)^2$. The assumptions $(M - m_1)^2 - m^2 \gg m\Gamma$ and $m^2 - (m_2 + m_3)^2 \gg m\Gamma$ are fulfilled for most of the SM processes – e.g. the massive gauge bosons which often occur as resonant intermediate states are light compared to the top quark and have a small ratio Γ/m of less than 3%. Additionally, the final state fermions are very light in comparison to the heavy, promptly decaying particles in the SM and there are only the massless photon and gluon as stable final state vector bosons. Consider for example the top decay $t \to bW^+ \to bu\bar{d}$ where from [30] $m_t = 174\,\text{GeV}$, $m_W = 80.4\,\text{GeV}$, $\Gamma_W/m_W = 0.0266$, $m_b = 4.20\,\text{GeV}$ and the up- and down-quark masses are a few MeV. We then have $\frac{(m_t - m_b)^2 - m_W^2}{m_W \Gamma_W} \approx 130 \gg 1$ and $\frac{m_W^2 - (m_u + m_d)^2}{m_W \Gamma_W} \approx \frac{m_W}{\Gamma_W} \approx 37 \gg 1$.
Some of the q^2-values in the integration are unphysical, e.g. $q^2 > P^2$, but for these values the integrand is sufficiently small, making the effect negligible unless parts of the resonance around $q^2 = m^2$ are kinematically cut out. The resulting formula is production cross section times branching ratio (BR), the latter being the quotient of partial decay width and total decay width of the intermediate particle. We can now summarize the assumptions and approximations being made in the NWA. First, we drop spin/polarization correlations and then the off-shell effects in the amplitudes. These two steps could be performed in opposite order, i.e. one could first neglect the off-shell effects due to the matrix elements and then drop spin/polarization correlations. As will be shown later, the last step of dropping the on-shell correlations[1] would then be exact for decay processes. The correlation effects in this case are implicitly dropped in the first step. We then assume that the intermediate particle's mass is sufficiently far away from the kinematical bounds to be able to shift the integration bounds to infinity without producing a large error. If m approaches the kinematical bounds, we find vanishing phasespace factors in the NWA calculation and considerable parts of the Breit-Wigner peak shifting out of the integration region, which is not incorporated in the NWA formula.

2.4. NWA in the limit $\Gamma \longrightarrow 0$

In this section we use the representation of the Dirac delta function as limit of the Cauchy distribution

$$\delta(x) = \lim_{a \to 0} \frac{1}{\pi} \frac{a}{a^2 + x^2} \tag{2.33}$$

[1] When referring to spin correlation or just correlation effects, we always mean spin/polarization correlation effects.

to argue that the NWA formula becomes – up to spin correlation effects – exact as we take the limit $\Gamma \to 0$, which suggests that it is a good approximation for small Γ. Consider the formula for the total cross section and the NWA formula

$$\sigma_{ofs} = \int \frac{dq^2}{2\pi} d\Phi_p(q^2) d\Phi_d(q^2) \frac{|\mathcal{M}'_f(q^2)|^2}{(q^2-m^2)^2+m^2\Gamma^2}, \tag{2.34}$$

$$\sigma_{NWA} = \sigma_p(m^2) \times \frac{1}{\Gamma} \times \Gamma_d(m^2) \tag{2.35}$$

$$= \int d\Phi_p(m^2) |\mathcal{M}_p(m^2)|^2 \times \frac{1}{\Gamma} \times \frac{1}{2m} \int d\Phi_d(m^2) |\mathcal{M}_d(m^2)|^2 \tag{2.36}$$

where we denote the full matrix element up to the denominator of the propagator by $\mathcal{M}'_f$ and the matrix elements for the production and decay part by $\mathcal{M}_p$ and $\mathcal{M}_d$, respectively. In the limit $\Gamma \to 0$ with the factorization of phasespace and matrix element developed in the previous sections, we get

$$\lim_{\Gamma\to 0} \frac{\sigma_{ofs}}{\sigma_{NWA}} = \lim_{\Gamma\to 0} \frac{\Gamma}{\sigma_p(m^2)\Gamma_d(m^2)} \int \frac{dq^2}{2\pi} d\Phi_p(q^2) d\Phi_d(q^2) \frac{|\mathcal{M}'_f(q^2)|^2}{(q^2-m^2)^2+m^2\Gamma^2} \tag{2.37}$$

$$= \int dq^2 d\Phi_p(q^2) d\Phi_d(q^2) \frac{1}{2m} \frac{|\mathcal{M}'_f(q^2)|^2}{\sigma_p(m^2)\Gamma_d(m^2)} \times \tag{2.38}$$

$$\lim_{\Gamma\to 0} \frac{1}{\pi} \frac{m\Gamma}{(q^2-m^2)^2+m^2\Gamma^2} \tag{2.39}$$

$$= \int dq^2 d\Phi_p(q^2) d\Phi_d(q^2) \frac{|\mathcal{M}'_f(q^2)|^2}{\sigma_p(m^2) 2m \Gamma_d(m^2)} \delta(q^2-m^2) \tag{2.40}$$

$$= \int d\Phi_p(m^2) d\Phi_d(m^2) \frac{|\mathcal{M}'_f(m^2)|^2}{\sigma_p(m^2) 2m \Gamma_d(m^2)} \tag{2.41}$$

$$= \int \frac{\left(d\Phi_p(m^2)|\mathcal{M}_p(m^2)|^2\right)\left(d\Phi_d(m^2)|\mathcal{M}_d(m^2)|^2\right)}{\sigma_p(m^2) 2m \Gamma_d(m^2)} \tag{2.42}$$

$$= 1. \tag{2.43}$$

This way, we see that the NWA result is asymptotically equal to the off-shell result ($\sigma_{NWA} \simeq \sigma_{ofs}$), which is obtained very fast, but contains no information about the NWA performance for finite Γ.

2.5. Correlation effects

In this section we argue that there are no spin/polarization correlation effects when the intermediate particle is assumed to be on the mass-shell. We numerically check this result in Section 3.2.4. This absence of correlation effects when the unstable particle is produced on-shell is also needed in the next section where we prove that the NWA error is of $\mathcal{O}(\Gamma/m)$. As seen before, the factorization of the squared amplitude is

exact for scalar intermediate particles and here we consider vector bosons. A similar argument can be used for unstable fermionic particles. For an arbitrary decay process where we produce a vector boson, which then decays, the full amplitude is given by

$$\mathcal{M}_f = \mathcal{M}_p^\mu \frac{-g_{\mu\nu} + (1-\xi)\frac{q_\mu q_\nu}{q^2-\xi m^2}}{q^2 - m^2 + im\Gamma} \mathcal{M}_d^\nu. \tag{2.44}$$

We now consider the case where the intermediate particle is on-shell, i.e. $q^2 = m^2$. Then we have the squared matrix element with the denominator of the propagator suppressed given by

$$|\mathcal{M}'_f|^2 = |\mathcal{M}_p^\mu(-g_{\mu\nu} + \frac{q_\mu q_\nu}{m^2})\mathcal{M}_d^\nu|^2 \tag{2.45}$$

which should be compared to the squared NWA matrix element

$$|\mathcal{M}_{NWA}|^2 = \sum_{\lambda_1} |\mathcal{M}_p^\mu \epsilon_\mu^{\lambda_1}|^2 \times \frac{1}{3}\sum_{\lambda_2} |\mathcal{M}_d^\nu \epsilon_\nu^{\lambda_2}|^2 \tag{2.46}$$

$$= \left[\mathcal{M}_p^\mu(-g_{\mu\nu} + \frac{q_\mu q_\nu}{m^2})\mathcal{M}_p^{\nu\star}\right] \times \frac{1}{3}\left[\mathcal{M}_d^\mu(-g_{\mu\nu} + \frac{q_\mu q_\nu}{m^2})\mathcal{M}_d^{\nu\star}\right]. \tag{2.47}$$

In order to get the total decay rate for a given process, these matrix elements have to be integrated over the full phasespace. In the following we consider the $1 \to 3$ decay shown in Figure 2.1. The result can be generalized by factorizing the phasespace recursively as explained in Section 2.1. We perform the integration in the so-called Gottfried-Jackson frame where $\vec{p}_2 + \vec{p}_3 = 0$ implying $q = (m, \vec{0})$ (see [31]). In this frame we have $P = (P^0, \vec{p}_1)$, $p_1 = (p_1^0, \vec{p}_1)$ and $p_2 = (p_2^0, \vec{p}_2)$, $p_3 = (p_3^0, -\vec{p}_2)$ and the only free variable to integrate over is the cosine of the angle between $\vec{p}_1$ and $\vec{p}_2$ denoted by $\cos\theta$. Since the matrix elements $\mathcal{M}_p^\mu \epsilon_\mu$ and $\mathcal{M}_d^\nu \epsilon_\nu$ are Lorentz invariant, the production and decay amplitudes are Lorentz vectors and because there are no vectors but $\vec{p}_1$ and $\vec{p}_2$ in the production and decay parts respectively, the 3-vector parts of $\mathcal{M}_p = (\mathcal{M}_p^0, \vec{\mathcal{M}}_p)$ and $\mathcal{M}_d = (\mathcal{M}_d^0, \vec{\mathcal{M}}_d)$ have to be proportional to the respective $\vec{p}_1$ and $\vec{p}_2$ as well. In particular, this means that the angle between $\vec{\mathcal{M}}_p$ and $\vec{\mathcal{M}}_d$ also is θ. In the restframe $q = (m, \vec{0})$, we have

$$-g_{\mu\nu} + \frac{q_\mu q_\nu}{m^2} = \begin{pmatrix} 0 & 0 & 0 & 0 \\ 0 & 1 & 0 & 0 \\ 0 & 0 & 1 & 0 \\ 0 & 0 & 0 & 1 \end{pmatrix} \tag{2.48}$$

and thus, with $\tilde{\sigma}$ denoting the on-shell cross section with correlations kept, we get

$$\sigma_{NWA} - \tilde{\sigma} \propto \int_0^1 d(\cos\theta)\left(|\mathcal{M}_{NWA}|^2 - |\mathcal{M}'_f|^2\right) \tag{2.49}$$

$$= \int_0^1 d(\cos\theta)\left[\mathcal{M}_p^\mu(-g_{\mu\nu} + \frac{q_\mu q_\nu}{m^2})\mathcal{M}_p^\nu\right] \tag{2.50}$$

$$\times\frac{1}{3}\left[\mathcal{M}_d^\mu(-g_{\mu\nu}+\frac{q_\mu q_\nu}{m^2})\mathcal{M}_d^\nu\right] \tag{2.51}$$

$$-\int_0^1 d(\cos\theta)|\mathcal{M}_p^\mu(-g_{\mu\nu}+\frac{q_\mu q_\nu}{m^2})\mathcal{M}_d^\nu|^2 \tag{2.52}$$

$$= \int_0^1 d(\cos\theta)\big((\vec{\mathcal{M}}_p\cdot\vec{\mathcal{M}}_p)\ \frac{1}{3}(\vec{\mathcal{M}}_d\cdot\vec{\mathcal{M}}_d)-(\vec{\mathcal{M}}_p\cdot\vec{\mathcal{M}}_d)^2\big) \tag{2.53}$$

$$= \int_0^1 d(\cos\theta)|\vec{\mathcal{M}}_p|^2|\vec{\mathcal{M}}_d|^2\left(\frac{1}{3}-\cos^2\theta\right) \tag{2.54}$$

$$= 0 \tag{2.55}$$

implying that there are no on-shell correlation effects for the $1\to 3$ decay.
To generalize this result to a broader class of processes we consider the case where the parent particle with momentum P is produced by an arbitrary process and the daughter particles with momenta p_i may decay further into particles p_{ij} with $j=1,\ldots,n_j$. We now use the phasespace factorization

$$d\Phi_n = d\Phi_{n-n_3+1}\frac{dp_3^2}{2\pi}d\Phi_{n_3} \tag{2.56}$$

$$= d\Phi_{n-m}\prod_{i=1}^3\frac{dp_i^2}{2\pi}d\Phi_{n_i} \quad \text{with } m=\sum_{i=1}^3(n_i-1) \tag{2.57}$$

$$= d\Phi_{n-m-2}\frac{dP^2}{2\pi}d\Phi_3(p_1,p_2,p_3)\prod_{i=1}^3\frac{dp_i^2}{2\pi}d\Phi_{n_i} \tag{2.58}$$

and integrate everything but $d\Phi_3(p_1,p_2,p_3)$. We can then again go to the frame where $\vec{p}_2+\vec{p}_3=0$ and as the integrand does not depend on other variables except of P, p_1, p_2, p_3 anymore, again apply the above argument.

2.6. Proof that the NWA error is of $\mathcal{O}(\frac{\Gamma}{m})$

Now, we prove that the relative error $R=(\sigma_{ofs}-\sigma_{NWA})/\sigma_{NWA}$ is of $\mathcal{O}(\frac{\Gamma}{m})$. As seen in Section 2.4, the NWA becomes exact with $\Gamma\to 0$ and now we want to prove that the first off-shell corrections are $\propto\Gamma/m$. A priori this is not clear. The error as function of Γ/m could behave like $(\Gamma/m)^\kappa$ with $0<\kappa<1$ and then it would not be possible to make a series expansion around $\Gamma/m=0$. In particular, the decay calculation seems not to make any sense if we set $\Gamma=0$ because in the NWA calculation, the on-shell-produced intermediate particle would never decay if its width were zero. For the proof we need additional conditions as assuming a small ratio Γ/m seems not to

be enough. This way we also get an idea where the NWA should be applicable and where it may cause problems. The off-shell cross section can be written as

$$\sigma_{ofs} = \int_{a^2}^{b^2} \frac{dq^2}{2\pi} \frac{\tilde{\sigma}(q^2)}{(q^2-m^2)^2+m^2\Gamma^2} \tag{2.59}$$

where a^2 and b^2 are the kinematical limits for the process and $\tilde{\sigma}(q^2)$ denotes the integrand up to the squared denominator of the propagator. That is, $\tilde{\sigma}$ is the squared product of production matrix element, the numerator of the propagator and the decay matrix element, integrated over $d\Phi_p$ and $d\Phi_d$ including prefactors like $\frac{1}{2M}$. The NWA cross section is given by

$$\sigma_{NWA} = \sigma_p(m^2)\ \frac{1}{\Gamma}\ \Gamma_d(m^2) \tag{2.60}$$

where σ_p and Γ_d are the production cross section and partial decay width, respectively. Now we use the integral

$$\int_{a^2}^{b^2} dq^2 \frac{1}{(q^2-m^2)^2+m^2\Gamma^2} = \frac{1}{m\Gamma}\left(\arctan\frac{m^2-a^2}{m\Gamma} - \arctan\frac{m^2-b^2}{m\Gamma}\right) \tag{2.61}$$

to rewrite

$$\begin{aligned}
\sigma_{ofs}-\sigma_{NWA} &= \int_{a^2}^{b^2} \frac{dq^2}{2\pi} \frac{\tilde{\sigma}(q^2)}{(q^2-m^2)^2+m^2\Gamma^2} - \frac{\sigma_p(m^2)\Gamma_d(m^2)}{\Gamma} && (2.62)\\
&= \int_{a^2}^{b^2} \frac{dq^2}{2\pi} \frac{\tilde{\sigma}(q^2)-\sigma_p(m^2)2m\Gamma_d(m^2)}{(q^2-m^2)^2+m^2\Gamma^2} - \alpha\frac{\sigma_p(m^2)\Gamma_d(m^2)}{\Gamma} && (2.63)\\
&= \int_{a^2}^{b^2} \frac{dq^2}{2\pi} \frac{\tilde{\sigma}(q^2)-\tilde{\sigma}(m^2)}{(q^2-m^2)^2+m^2\Gamma^2} - \alpha\frac{\sigma_p(m^2)\Gamma_d(m^2)}{\Gamma} && (2.64)
\end{aligned}$$

with

$$\alpha = 1 - 2m\Gamma \int_{a^2}^{b^2} \frac{dq^2}{2\pi} \frac{1}{(q^2-m^2)^2+m^2\Gamma^2}. \tag{2.65}$$

In (2.64) we have used the on-shell factorization of the cross section. For the relative deviation R we get

$$\begin{aligned}
|R| &= \left|\frac{\sigma_{ofs}-\sigma_{NWA}}{\sigma_{NWA}}\right| && (2.66)\\
&= \frac{1}{\sigma_{NWA}}\left|\int_{a^2}^{b^2} \frac{dq^2}{2\pi} \frac{\tilde{\sigma}(q^2)-\tilde{\sigma}(m^2)}{(q^2-m^2)^2+m^2\Gamma^2} - \alpha\frac{\sigma_p(m^2)\Gamma_d(m^2)}{\Gamma}\right| && (2.67)\\
&= \left|\int_{a^2}^{b^2} \frac{dq^2}{2\pi} \frac{\tilde{\sigma}(q^2)-\tilde{\sigma}(m^2)}{\sigma_p(m^2)\Gamma_d(m^2)} \frac{\Gamma}{(q^2-m^2)^2+m^2\Gamma^2} - \alpha\right| && (2.68)\\
&\leq \left|\int_{a^2}^{b^2} \frac{dq^2}{2\pi} \frac{\tilde{\sigma}(q^2)-\tilde{\sigma}(m^2)}{\sigma_p(m^2)\Gamma_d(m^2)} \frac{\Gamma}{(q^2-m^2)^2+m^2\Gamma^2}\right| + |\alpha|. && (2.69)
\end{aligned}$$

Assume now, that $\tilde{\sigma}(q^2)$ is twice continuously differentiable in the allowed phasespace. Furthermore, assume that $\sigma_p(q^2)\Gamma_d(q^2) = 0 \Leftrightarrow q^2 \in \{a^2, b^2\}$, i.e. the product of production cross section and decay width vanishes as we approach the kinematical limits but is non-zero in the allowed phasespace. Then, the function

$$g_m(q^2) := \frac{\tilde{\sigma}(q^2)}{\sigma_p(m^2)\Gamma_d(m^2)} \tag{2.70}$$

is twice continuously differentiable with respect to q^2 for all $q^2 \in [a^2, b^2]$ and m^2 in (a^2, b^2). As we focus on resonant decays here, $m^2 \in (a^2, b^2)$ is assumed in the following. By second order Taylor expansion we then get

$$g_m(q^2) = g_m(m^2) + g'_m(m^2) \cdot (q^2 - m^2) + \frac{1}{2} g''_m(\kappa^2) \cdot (q^2 - m^2)^2 \tag{2.71}$$

with $\kappa^2 \in [a^2, b^2]$. Note that κ^2 depends on q^2. The functions g'_m and g''_m as continuous functions on the compact set $[a^2, b^2]$ are then bounded and we can find $L_1 > 0$ and $L_2 > 0$ with

$$|g'_m(q^2)| \leq L_1 \quad \text{and} \quad |g''_m(q^2)| \leq L_2 \quad \forall q^2 \in [a^2, b^2]. \tag{2.72}$$

We can now further evaluate $|R|$ to obtain

$$\begin{aligned}
|R| &\leq \left| \int_{a^2}^{b^2} \frac{dq^2}{2\pi} \frac{\tilde{\sigma}(q^2) - \tilde{\sigma}(m^2)}{\sigma_p(m^2)\Gamma_d(m^2)} \frac{\Gamma}{(q^2 - m^2)^2 + m^2\Gamma^2} \right| + |\alpha| && (2.73)\\
&= \left| \int_{a^2}^{b^2} \frac{dq^2}{2\pi} \left(g_m(q^2) - g_m(m^2)\right) \frac{\Gamma}{(q^2 - m^2)^2 + m^2\Gamma^2} \right| + |\alpha| && (2.74)\\
&= \frac{\Gamma}{2\pi} \left| \int_{a^2}^{b^2} dq^2 \frac{g'_m(m^2) \cdot (q^2 - m^2) + \frac{1}{2} g''_m(\kappa^2) \cdot (q^2 - m^2)^2}{(q^2 - m^2)^2 + m^2\Gamma^2} \right| + |\alpha| && (2.75)\\
&\leq \frac{\Gamma L_1}{2\pi} \left| \int_{a^2}^{b^2} dq^2 \frac{q^2 - m^2}{(q^2 - m^2)^2 + m^2\Gamma^2} \right| && (2.76)\\
&\quad + \frac{\Gamma L_2}{4\pi} \left| \int_{a^2}^{b^2} dq^2 \frac{(q^2 - m^2)^2}{(q^2 - m^2)^2 + m^2\Gamma^2} \right| + |\alpha| && (2.77)\\
&= \frac{\Gamma L_1}{4\pi} \left| \log \frac{(b^2 - m^2)^2 + m^2\Gamma^2}{(a^2 - m^2)^2 + m^2\Gamma^2} \right| + |\alpha| && (2.78)\\
&\quad + \frac{\Gamma L_2}{4\pi} \left(b^2 + m\Gamma \arctan \frac{m^2 - b^2}{m\Gamma} - a^2 - m\Gamma \arctan \frac{m^2 - a^2}{m\Gamma} \right). && (2.79)
\end{aligned}$$

Now we want to develop the log factor for small Γ/m. Using the Taylor expansion for x around $x_0 = 0$ which is given by

$$\log \frac{k + x^2}{l + x^2} = \log \frac{k}{l} + (\frac{1}{k} - \frac{1}{l})x^2 + \mathcal{O}(x^3) \tag{2.80}$$

we get

$$\log\frac{(b^2-m^2)^2+m^2\Gamma^2}{(a^2-m^2)^2+m^2\Gamma^2} = \log\frac{(b^2-m^2)^2/m^4+(\Gamma/m)^2}{(m^2-a^2)^2/m^4+(\Gamma/m)^2} \tag{2.81}$$

$$= \log\frac{(b^2-m^2)^2}{(a^2-m^2)^2}+\mathcal{O}\big((\Gamma/m)^2\big). \tag{2.82}$$

Using this expansion in (2.78) we find that

$$R \leq \frac{\Gamma}{m}\frac{mL_1}{4\pi}\left|\log\frac{(b^2-m^2)^2}{(a^2-m^2)^2}\right|+\mathcal{O}\big((\Gamma/m)^2\big)+|\alpha| \tag{2.83}$$

$$+\frac{\Gamma L_2}{4\pi}\left(b^2+m\Gamma\arctan\frac{m^2-b^2}{m\Gamma}-a^2-m\Gamma\arctan\frac{m^2-a^2}{m\Gamma}\right). \tag{2.84}$$

With the Taylor expansion of $\arctan\frac{k}{x}$ for small positive x

$$\arctan\frac{k}{x}=\operatorname{sign}(k)\frac{\pi}{2}-\frac{x}{k}+\mathcal{O}(x^3) \tag{2.85}$$

we obtain

$$\arctan\frac{m^2-b^2}{m\Gamma} = \arctan\frac{1-b^2/m^2}{\Gamma/m} \tag{2.86}$$

$$= \operatorname{sign}(m^2-b^2)\frac{\pi}{2}-\frac{m\Gamma}{m^2-b^2}+\mathcal{O}\big((\Gamma/m)^3\big) \tag{2.87}$$

and an analog expansion for $\arctan\frac{m^2-a^2}{m\Gamma}$. This way we get

$$R \leq \frac{\Gamma}{m}\frac{mL_1}{4\pi}\left|\log\frac{(b^2-m^2)^2}{(m^2-a^2)^2}\right|+\mathcal{O}\big((\Gamma/m)^2\big)+|\alpha| \tag{2.88}$$

$$+\frac{\Gamma}{m}\frac{mL_2}{4\pi}\left(b^2-a^2-\pi m\Gamma\right)+\mathcal{O}\big((\Gamma/m)^3\big). \tag{2.89}$$

Now we come back to calculating α. We have

$$\alpha = 1-2m\Gamma\int_{a^2}^{b^2}\frac{dq^2}{2\pi}\frac{1}{(q^2-m^2)^2+m^2\Gamma^2} \tag{2.90}$$

$$= 1-2m\Gamma\frac{1}{2\pi m\Gamma}\left(\arctan\frac{m^2-a^2}{m\Gamma}-\arctan\frac{m^2-a^2}{m\Gamma}\right) \tag{2.91}$$

$$= 1-\frac{1}{\pi}\left(\arctan\frac{m^2-a^2}{m\Gamma}-\arctan\frac{m^2-b^2}{m\Gamma}\right). \tag{2.92}$$

Using the expansion of (2.87) and the analog expansion for $\arctan\frac{m^2-a^2}{m\Gamma}$ in (2.92) and using $m^2\in(a^2,b^2)$ for a resonant decay, we get

$$\alpha = 1-\frac{1}{\pi}\left(\frac{\pi}{2}+\frac{\Gamma}{m}\frac{1}{1-b^2/m^2}+\frac{\pi}{2}-\frac{\Gamma}{m}\frac{1}{1-a^2/m^2}+\mathcal{O}\big((\Gamma/m)^3\big)\right) \tag{2.93}$$

$$= \frac{\Gamma}{m}\frac{m^2(a^2-b^2)}{\pi(m^2-a^2)(m^2-b^2)} + \mathcal{O}\big((\Gamma/m)^3\big). \tag{2.94}$$

The final result for R becomes

$$|R| \leq \frac{\Gamma}{m}\frac{mL_1}{4\pi}\left|\log\frac{(b^2-m^2)^2}{(a^2-m^2)^2}\right| + \frac{\Gamma}{m}\frac{mL_2}{4\pi}\left(b^2-a^2\right) \tag{2.95}$$

$$+\frac{\Gamma}{m}\frac{m^2(a^2-b^2)}{\pi(m^2-a^2)(m^2-b^2)} + \mathcal{O}\big((\Gamma/m)^2\big) \tag{2.96}$$

with the Γ-independent constants L_1, L_2 with mass dimension -1 and -3, respectively. We have shown that R is indeed of $\mathcal{O}(\Gamma/m)$ for m in the interior of the kinematically allowed region. However, R of $\mathcal{O}(\Gamma/m)$ just means that for $\Gamma \to 0$, the limit of $R/(\Gamma/m)$ is finite. This is a stronger result than $\sigma_{NWA} \simeq \sigma_{ofs}$ which we obtained in Section 2.4, but it does not prove that the prefactor of Γ/m is small – in particular, it does not mean $R \approx \Gamma/m$. The right-hand side may become arbitrarily large as m^2 approaches the kinematical limits which is not only due to the obvious prefactors of Γ/m but also due to L_1, L_2 potentially becoming very large as m^2 approaches a^2 or b^2. These large factors do not depend on Γ and therefore do not affect the asymptotic behavior. However, for practical calculations we would like the factor multiplying Γ/m to be small. While 'small' in this case is not well defined, a necessary condition is that m is sufficiently far away from the kinematical bounds.

3 NWA in the MSSM

In the previous section we have proven that the NWA error is of $\mathcal{O}(\Gamma/m)$, which, however, does not mean that the error is approximately Γ/m. There are potentially large prefactors and thus, the NWA has to be checked in BSM scenarios. In this section we perform a systematic analysis of the NWA behavior in the MSSM. It is of course not possible to compare for all processes of interest the NWA calculation with the off-shell result – if this were feasible, the NWA would be superfluous. We therefore choose the smallest diagram which contains production and decay of an unstable particle and on the other hand frequently occurs in decay chains of supersymmetric particles. These are the $1 \to 3$ decays, which can be checked systematically for SM extensions. Although we use the Feynman rules of the MSSM for this analysis, in particular the general analysis of Section 3.2 is not specific to supersymmetry and can also be used in other extensions of the SM.

3.1. General considerations

For the NWA calculation of the process in Figure 3.1 the $1 \to 3$ decay is split into two successive $1 \to 2$ decays. The intermediate particle is treated as on-shell final state

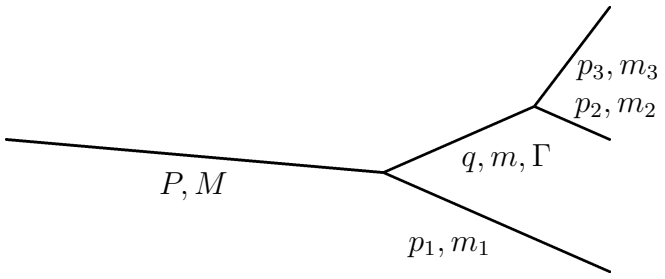

Figure 3.1.: Kinematics of the $1 \to 3$ decay.

vertex	coding	structure	vertex	coding	structure
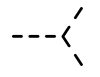	sss	λ	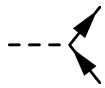	sff	$\alpha P_L + \beta P_R$
	vsv	$\lambda g^{\mu\nu}$	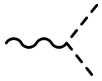	vss	$\lambda(p-k)^\mu$
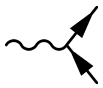	vff	$\gamma^\mu(\alpha P_L + \beta P_R)$		vvv	$\lambda(g^{\nu\lambda}(k_1-k_2)^\mu + g^{\lambda\mu}(k_2-k_3)^\nu + g^{\mu\nu}(k_3-k_1)^\lambda)$

Table 3.1.: The general vertices of the MSSM with the corresponding Feynman rules. Momentum flow is chosen towards the vertex. For the vss vertex, p and k denote the momenta of the scalar particles.

with no spin/polarization correlations between its production and decay to obtain the decay width factorized as

$$\Gamma_{NWA} = \Gamma_p \times \frac{\Gamma_d}{\Gamma} =: \Gamma_p \times BR. \tag{3.1}$$

In this section we perform a systematic analysis of this NWA factorization compared to the full off-shell calculation.

3.2. Resonant $1 \longrightarrow 3$ decays in the MSSM

In the MSSM there are six classes of 3-particle vertices, which are given in Table 3.1 together with the structure of the corresponding vertex-function (see [32] for the complete MSSM Feynman rules). We wrote a program to build up the possible classes of diagrams with these 6 vertex-classes and the result are 48 classes of diagrams, shown in Appendix A. Diagrams which only differ in exchange of the particles with momenta p_2 and p_3 are physically equivalent and counted only once. The other particles (e.g. P and p_1) can not be exchanged since this would change the kinematics. To check the performance of the NWA for these diagrams, the decay width for each process is calculated on-shell as well as off-shell analytically except for the final q^2-integration for Γ_{ofs}. These calculations are performed in Mathematica with FeynCalc [33] used for polarization and spin sums, the trace evaluations and general simplifications. The one-dimensional q^2-integration can not be done analytically for most of the processes or at least not for all masses kept non-zero. But since numerical integration in one dimension is very fast, the evaluation for large numbers of parameter-space points is no problem. The analytical off-shell calculations of the matrix elements and the full widths have been checked for each process as explained in Section 3.6.

3.2.1. Program

In order to compare the different processes, we want to find the maxima and minima of $R = (\Gamma_{ofs}/\Gamma_{NWA} - 1) \,/\, (\Gamma/m)$ depending on $m,\ \Gamma,\ m_1,\ m_2,\ m_3$ and the coupling parameters. M is used as an overall normalization for the other masses. As R has a lot of local maxima and minima, the fast methods for numerical optimization find – depending on the starting point in the at least five dimensional parameter space – one of these local extrema. But as we have to find the global maximum and minimum, we decided to evaluate R on a lattice of about 10^6 points in parameter space and determine the maximum and minimum on this lattice. To be more specific, the lattice consists of 20 equally-distributed values for the four masses (m, m_1, m_2, m_3), four different couplings for each fermionic vertex $(\alpha, \beta) \in \{(1,1),(1,0),(0,1),(1,-1)\}$ and 3 different widths $\Gamma/m \in \{0.1\%, 1\%, 10\%\}$. The couplings for the other types of vertices as well as other overall factors cancel in $\Gamma_{ofs}/\Gamma_{NWA}$.
The 20 values for m_1 are set after m is determined and afterwards the 20 values for m_2 and then m_3 are set. This way we only generate points in the parameter space which fulfill all kinematical and other limitations. The maxima and minima of R as well as the mean value and the standard deviation can then be compared for the 48 processes.
Some care is needed in the determination of the limits we set in the parameter space. When the mass of the intermediate particle approaches the kinematical limits, we find two competing errors - as we have seen in Section 2.3, the propagator is integrated out in the NWA by shifting the integration bounds to infinity which means that we integrate the full Breit-Wigner. For finite bounds the result is smaller since parts of the Breit-Wigner are cut out by the kinematical limits, which makes the NWA result too large, especially when considerable parts are outside the integration region, i.e. when m is in the Γ-vicinity of the kinematical limits. On the other hand we have vanishing phasespace factors in the NWA calculation since the phasespaces in the $1 \to 2$ decays vanish as the sum of the daughter masses approaches the parent mass, whereas for the full $1 \to 3$ decay, the phasespace is finite for $M > m_1 + m_2 + m_3$, so the decay can also be non-resonant with m larger than $M - m_1$ or smaller than $m_2 + m_3$. This forces $\Gamma_{NWA} \to 0$ while $\Gamma_{ofs} > 0$ and therefore we can get large errors for all processes. To generate meaningfull results, we modify the limits $m_2 + m_3 \leq m$ and $m + m_1 \leq M$ to $m_2 + m_3 \leq (1-p)m$ and $m + m_1 \leq (1-p)M$, where p is chosen appropriately. For the different processes we find different sensitivities of R to $m - (m_2 + m_3)$ and $M - (m + m_1)$ and we therefore use $p \in \{5\%, 10\%, 20\%\}$ for all calculations. This way we obtain conservative results with the $p = 20\%$ restriction and can also make predictions for BSM models, which often contain decay chains where the sum of the daughter-particles' masses is close to the parent-particle's mass.
For performance reasons the calculations are implemented in C/C++.
The polarization sums for massive vector bosons are calculated in unitary gauge $\sum_{\lambda_1\lambda_2} \epsilon_\mu^{\star\lambda_1}(k)\epsilon_\nu^{\lambda_2}(k) = -g_{\mu\nu} + \frac{k_\mu k\nu}{m^2}$ and to keep this expression finite we introduce lower bounds for all the masses. We use $m_1, m \geq p\,M$ and $m_2, m_3 \geq p\,m$.

3.2.2. Discussion

The results for the 48 classes are listed in Tables 3.2 and 3.3, where we have chosen $\Gamma/m = 0.01$. In the left-hand columns max_x and min_x are shown, which are the maximum and minimum values of R for $p = x\%$. The last two columns contain the mean value and standard deviation of R for $p = 5\%$. The table is ordered by decreasing maximum of $|R|$ for $p = 10\%$ and the results are given with two significant digits. We do not expect large errors caused by the phasespace factors or off-shell effects due to the propagator, since with p at least 5% in comparison to $\Gamma/m = 1\%$, we should be sufficiently far away from the regions with $(M - m_1)^2 - m^2 \lesssim m\Gamma$ or $m^2 - (m_2 + m_3)^2 \lesssim m\Gamma$ where we expect bad NWA results. Indeed, the all-scalar sss-sss process shows relatively good NWA performance with a maximal error of about 9%. Generally, for $p = 20\%$ the error is in the range of $\frac{\Gamma}{m}$, the largest enhancement factors are about 16 for sss-ssv. In the $p = 10\%$ region things are quite different, factors of order 10^2 are found quite often where an enhancement factor of 100 for $\Gamma/m = 0.01$ means that the off-shell result is larger by a factor of 2 compared to the NWA result, which clearly is not the desired accuracy. Looking at the table we see that for all ..s-sss processes R is quite small. For these processes the factorization of the amplitude is exact and the second vertex is completely independent of q^2, so the only additional source for deviations between NWA and the full calculation are off-shell effects due to the production matrix element. The situation is quite different for the sss-s.. processes. Even though the amplitude factorization is exact again and now the production matrix element is q^2-independent, some processes show very large deviations (sss-ssv), while others have good NWA performance (sss-sff). It seems that the NWA performance does not have a strong dependence on the first vertex. Further investigation of the second-vertex dependence shows, that if we consider the first 24 processes with larger error and the last 24 processes for which the NWA works relatively well and take a look at the second vertices, we find all the processes with -ssv, -vsv, -ffv, -vvv and -svv in the upper half and all processes with -fsf, -sff, -vff, -vss and -sss in the lower half. We study the deviations in more detail in the next section. The weaker dependence on the first vertex can be understood by means of the involved masses. In the first vertex, we have $M^2 \geq (m_1 + \sqrt{q^2})^2$ for a resonant decay and therefore M is the dominant mass. In particular, M^2-terms dominate terms with strong q^2 dependence. For the second vertex we have $q^2 \geq (m_2 + m_3)^2$ and therefore $\sqrt{q^2}$ as dominant mass. The processes with resonant fermions or vector bosons generally don't show larger deviations than the processes with scalars, which shows that correlation effects don't play a crucial role here. We now come to a detailed discussion of the deviations and where they come from.

process	max_{10}	min_{10}	max_5	min_5	max_{20}	min_{20}	mean	dev
sss-ssv	210	−3.6	14000	−8.1	16	−1.0	37	230
ssv-vsv	210	−4.1	7800	−9.2	9.9	−1.6	29	220
ffs-ssv	160	−6.0	9800	−13	14	−2.0	28	170
fsf-ffv	160	−4.9	5300	−11	12	−2.1	13	94
vsv-vvv	150	−3.5	7800	−8.1	14	−0.79	25	130
ffv-vsv	150	−5.0	5500	−10	7.1	−1.9	18	160
vvs-ssv	130	−4.4	7600	−9.4	12	−1.3	27	160
svs-ssv	110	−6.3	6900	−13	9.0	−2.1	19	120
vss-ssv	110	−6.3	6900	−13	9.0	−2.1	19	120
sss-svv	110	−4.0	7200	−8.8	9.2	−1.0	17	110
vvv-vsv	100	−5.1	4100	−10	4.6	−2.1	18	150
vff-ffv	100	−6.0	3000	−13	9.0	−2.2	8.6	64
svv-vsv	96	−4.4	3800	−9.0	3.7	−1.9	13	110
sff-ffv	91	−6.1	2700	−13	8.0	−2.2	7.6	57
ffs-svv	84	−5.3	5100	−10	7.8	−2.1	13	82
vsv-vsv	80	−4.3	3700	−8.9	2.5	−1.8	12	110
vvv-vvv	73	−6.2	3800	−13	6.4	−2.1	10	63
fvf-ffv	72	−6.3	2000	−13	6.8	−2.4	6.6	49
ffv-vvv	72	−6.1	3500	−13	7.7	−2.2	11	61
vvs-svv	67	−4.4	4000	−8.9	6.8	−1.4	12	76
svs-svv	57	−5.3	3700	−10	5.0	−2.2	8.3	59
vss-svv	57	−5.3	3700	−10	5.0	−2.2	8.3	59
ssv-vvv	55	−6.3	3600	−13	3.8	−2.5	7.8	55
svv-vvv	45	−4.8	2200	−9.7	4.4	−1.5	8.4	44
sff-fsf	34	−6.0	280	−13	3.3	−2.4	−0.31	8.4
fsf-fsf	33	−4.8	690	−11	4.8	−2.2	0.070	7.7
vff-fsf	23	−6.1	540	−13	3.2	−2.3	−0.61	5.9
fvf-fsf	19	−6.3	470	−13	2.6	−2.5	−0.60	5.5
sss-sff	18	−4.3	110	−8.9	3.1	−1.7	0.12	5.2
ffs-sff	16	−6.2	100	−13	2.7	−2.4	−0.26	4.8
ssv-vff	15	−4.7	94	−10.0	2.3	−2.1	0.27	5.1
vvs-sff	15	−4.8	96	−9.8	2.4	−1.9	−0.19	4.8
vsv-vss	14	−4.0	140	−8.6	1.4	−1.5	1.7	8.5
svs-sff	14	−6.4	93	−13	1.9	−2.6	−0.52	4.5

Table 3.2.: NWA comparison of resonant $1 \to 3$ decays in the MSSM. The maxima, minima, mean and standard deviation are shown for the relative NWA deviation normalized to the conventionally expected error Γ/m. The particle code is explained in Table 3.1. Processes are ordered by $\max(|max_{10}|, |min_{10}|)$ and the remaining processes are shown in Table 3.3.

process	max_{10}	min_{10}	max_5	min_5	max_{20}	min_{20}	mean	dev
vss-sff	14	−6.4	93	−13	1.9	−2.6	−0.52	4.5
ffv-vff	13	−5.9	86	−12	1.9	−2.2	−0.81	4.1
vvv-vss	13	−6.4	140	−13	0.48	−2.6	0.84	8.0
ffv-vss	12	−6.2	140	−13	0.55	−2.7	1.1	8.0
vvv-vff	12	−6.3	81	−13	1.7	−2.3	−0.72	4.3
ssv-vss	12	−6.2	140	−13	−0.056	−2.8	2.8	9.0
vsv-vff	12	−4.3	79	−8.9	2.0	−1.8	−0.70	4.0
svv-vff	12	−5.0	79	−9.9	1.3	−2.0	−0.78	3.8
svv-vss	11	−5.1	130	−10	0.0021	−2.2	0.91	7.4
svs-sss	5.7	−4.6	33	−9.5	−0.52	−2.2	−1.3	3.1
vss-sss	5.7	−4.6	33	−9.5	−0.52	−2.2	−1.3	3.1
ffs-sss	2.9	−4.8	17	−9.7	−0.58	−2.2	−1.8	1.7
vvs-sss	1.7	−4.4	11	−9.0	−0.61	−2.0	−1.7	1.8
sss-sss	−0.41	−4.4	0.084	−8.9	−0.56	−1.9	−2.0	1.3

Table 3.3.: NWA comparison for the remaining processes. Details as in Table 3.2.

3.2.3. Problematic decays

We first consider the process sss-ssv which features the largest deviations. Note that all processes with -ssv show very large off-shell effects and are therefore located in the upper part of the table. The reason for the large off-shell effects should be most obvious for sss-ssv due to its simple matrix element. For general masses the final q^2 integration can not be done analytically, so we analyze the squared and polarization-summed matrix element

$$\sum_\lambda |\mathcal{M}|^2 = \sum_\lambda \frac{|(p_2+q)^\mu \epsilon_\mu^{\star\lambda}(p_3)|^2}{(q^2-m^2)^2+m^2\Gamma^2} \tag{3.2}$$

$$= \frac{(p_2+q)^\mu \left(-g_{\mu\nu}+\frac{p_{3\mu}p_{3\nu}}{m_3^2}\right)(p_2+q)^\nu}{(q^2-m^2)^2+m^2\Gamma^2} \tag{3.3}$$

$$= \frac{-(p_2+q)^2+\frac{1}{m_3^2}(q^2-p_2^2)^2}{(q^2-m^2)^2+m^2\Gamma^2} \tag{3.4}$$

$$= \frac{1}{m_3^2}\frac{m_2^4-2(m_3^2+q^2)m_2^2+(m_3^2-q^2)^2}{(q^2-m^2)^2+m^2\Gamma^2}. \tag{3.5}$$

Here and in the following we neglect coupling constants for vertices without fermions since they drop out in the ratio $\Gamma_{ofs}/\Gamma_{NWA}$. The integrand for the final q^2 integration is this squared matrix element multiplied by the phasespace factors. Due to the Breit-Wigner shape of the squared matrix element the integrand should be peaked around

$q^2 = m^2$, justifying that – in the NWA – we evaluate the matrix elements for $q^2 = m^2$ only. But the third term in the numerator $(q^2 - m_3^2)^2$ might grow as fast as $(q^2 - m^2)^2$ grows in the denominator, compensating the suppression of the off-shell parts of the amplitude. To clarify this, we set $m_1 = m_2 = 0$ and obtain

$$\sum_\lambda |\mathcal{M}|^2 = \frac{1}{m_3^2} \frac{(m_3^2 - q^2)^2}{(q^2 - m^2)^2 + m^2\Gamma^2} \tag{3.6}$$

which approaches a constant for large q^2 instead of decreasing like q^{-4}. Another effect is that, for $m_3 \approx m$, the peak is suppressed by the factor $(m_3^2 - m^2)^2$. Therefore, if m^2 is small compared to the upper limit $(M - m_1)^2$ for the q^2-integration and m_3 is large, i.e. of the same magnitude as m, there is a large off-shell contribution and the NWA fails. The righthand side of Equation (3.6) is plotted against q^2 in Figure 3.2(a) for small m and $m_3 \approx m$ to illustrate the deviation from the Breit-Wigner shape and in Figure 3.2(b) R is plotted against (m, m_3). The color code is explained in Table 3.4. The reason for the large deviations in ffs-ssv, vvs-ssv, svs-ssv and vss-ssv is the same,

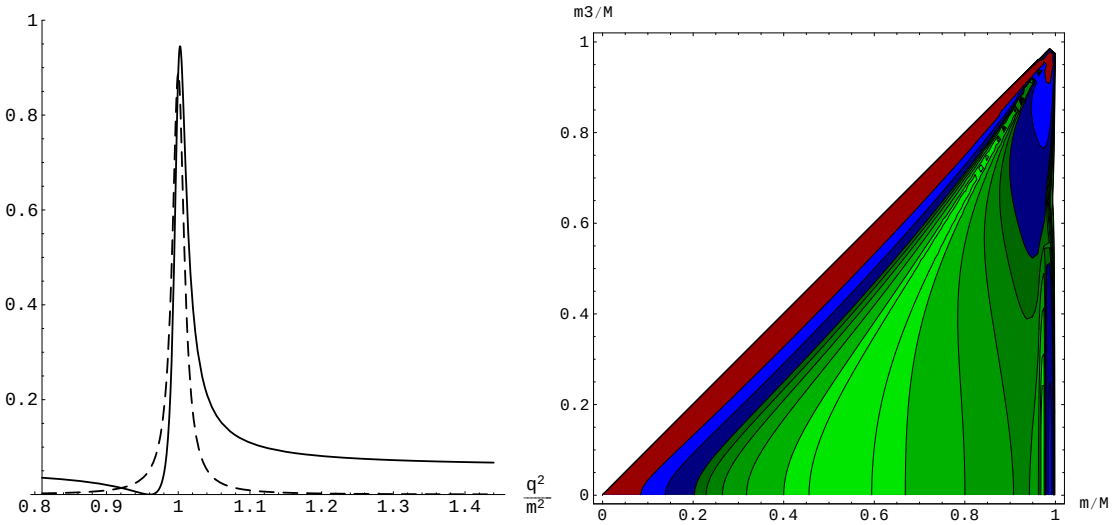

(a) (b)

Figure 3.2.: Plots for sss-ssv. In (a), the squared and polarization summed matrix element of Equation (3.6) is plotted against q^2 as solid line together with a Breit-Wigner shape as dashed line. The parameters are $m/M = 0.1$, $\Gamma/m = 0.01$, $m_1 = m_2 = 0$ and $m_3/m = 0.98$. In (b) a contour plot for R as function of m and m_3 is shown, the color code is explained in Table 3.4 and the remaining parameters are as in (a).

the deviations are smaller because the squared matrix element of the production part

green	$\lvert R\rvert \leq 5$
dark blue	$5 < \lvert R\rvert \leq 10$
light blue	$10 < \lvert R\rvert \leq 25$
dark red	$25 < \lvert R\rvert \leq 50$
light red	$50 < \lvert R\rvert$

Table 3.4.: Color code for the contour plots.

tends to wash out the suppression of the Breit-Wigner peak due to the $(q^2 - m_3^2)^2$ factor. In the MSSM there are a lot of candidates for heavy scalar particles, which have to be identified by their decay products. However, in the SM and the MSSM we do not find a massive vector boson as a stable final state.
The next process of interest is ssv-vsv. An additional feature of this process is the gauge dependence of the off-shell result. In R_ξ gauges, the propagator for the intermediate vector boson depends on the gauge parameter ξ. For $q^2 = m^2$ this dependence drops out, making the NWA calculation gauge-parameter independent. The squared and spin-summed matrix element for this process is

$$|\bar{\mathcal{M}}|^2 = \sum_\lambda |(P + p_1)^\mu \left(-g_{\mu\nu} + (1 - \xi)\frac{q_\mu q_\nu}{q^2 - \xi m^2} \right) \epsilon_\lambda^{\star\nu}(p_3)|^2. \tag{3.7}$$

The problematic part of this amplitude can not be seen that easily, so we calculate the amplitude with the assumption $m_1 = m$ and assume m_3 to be small, i.e. we only keep the terms of lowest order in m_3. In unitary gauge we then get the squared and spin-summed matrix element integrated over the two solid angles Ω_1 and Ω_2

$$\begin{aligned} \int d\Omega_1 d\Omega_2 |\bar{\mathcal{M}}|^2 \;=\; & \frac{4\pi^2}{3m^4 m_3^2 q^4} \frac{\left(m_2^2 - q^2\right)^2}{(q^2 - m^2)^2 + m^2\Gamma^2} \times \\ & \Big(4m^8 - 8\left(M^2 + q^2\right) m^6 + 2\left(2M^4 + 5q^2M^2 + 2q^4\right) m^4 \\ & -6M^2q^2\left(M^2 + q^2\right) m^2 + 3M^4q^4 \Big). \end{aligned} \tag{3.8}$$

Again we have the suppression of the peak for $m_2 \approx m$ due to the factor $\left(m_2^2 - q^2\right)^2$ and the compensation of the q^{-4} decrease of the Breit-Wigner shape, which produces large NWA errors. But now we find a strong dependence of the NWA performance on the gauge parameter ξ. Consider, for example, the parameter set $m/M = m_1/M = 0.05$, $\Gamma/m = 0.01$, $m_2/m = 0.73$ and $m_3/m = 0.05$ which produces $R \approx 1600$ in unitary gauge. In Landau gauge, for $\xi = 0$ which corresponds to replacing m^2 with q^2 in the propagator, this is reduced to $R = 1.4$. The replacement of $1/m^2$ by $1/q^2$ reduces the asymptotic behavior of the matrix element from $\mathcal{O}(q^4)$ to $\mathcal{O}(q^2)$ and this way improves the NWA performance. The ξ dependence of Γ_{ofs} drops out when calculating a gauge-invariant set of diagrams.

For fsf-ffv, the squared and spin-summed matrix element integrated over the two solid angles is

$$\int d\Omega_1 d\Omega_2 |\bar{\mathcal{M}}|^2 = \frac{8\pi^2}{m_3^2 q^2} \frac{\left(m_2^2 - q^2\right)^2}{(q^2 - m^2)^2 + m^2\Gamma^2} \left(\left(M^2 + q^2\right)\left(m^2 + q^2\right) + 4Mq^2 m\right) \quad (3.9)$$

where we have set $m_1 = 0$ and assumed m_3 to be small compared to the other masses. There is the factor $(q^2 - m_2^2)^2$ suppressing the peak and combined factors up to the denominator are of $\mathcal{O}(q^6)$. This not only compensates the q^{-4} decrease of the Breit-Wigner shape, but even produces increasing contributions as q^2 gets larger. The deviations are not larger than for the previously discussed processes because the term $M^2 q^2$ dominates the q^4 term in the last factor.
For vsv-vvv we do not give the full amplitude, since it is quite lengthy. The asymptotic behavior of the numerator is $\propto q^8$, but the leading terms in q^2 are suppressed compared to the other terms. This mitigates the numerator to be effectively $\propto q^6$, which still produces increasing values of the matrix element away from the resonance.
For sss-svv, the squared and spin-summed matrix element is

$$\begin{aligned}
\sum_\lambda |\bar{\mathcal{M}}|^2 &= \sum_\lambda \frac{|\epsilon_\mu^{\star\lambda}(p_2) \cdot \epsilon^{\star\mu\lambda}(p_3)|^2}{(q^2 - m^2)^2 + m^2\Gamma^2} && (3.10)\\
&= \frac{(-g_{\mu\nu} + \frac{p_{2\mu} p_{2\nu}}{m_2^2})(-g^{\mu\nu} + \frac{p_3^\mu p_3^\nu}{m_3^2})}{(q^2 - m^2)^2 + m^2\Gamma^2} && (3.11)\\
&= \frac{2 + \frac{(p_2 \cdot p_3)^2}{m_2^2 m_3^2}}{(q^2 - m^2)^2 + m^2\Gamma^2} && (3.12)\\
&= \frac{2}{(q^2 - m^2)^2 + m^2\Gamma^2} + \frac{1}{4m_2^2 m_3^2} \frac{(q^2 - m_2^2 - m_3^2)^2}{(q^2 - m^2)^2 + m^2\Gamma^2}. && (3.13)
\end{aligned}$$

For one of the masses m_2, m_3 very small, the second term dominates the first one and there we find an asymptotic behavior $\propto q^4$, compensating the q^{-4} decrease. For $m_2^2 + m_3^2 \approx m^2$ we then get a suppression of the peak relative to the off-shell parts.

We have now seen the reasons for the deviations that occur for the processes in the first half of the table. There is the suppression of the peak due to factors in the numerator imitating the behavior of $(q^2 - m^2)^2$ and the (over)compensation of the q^{-4} decrease in the Breit-Wigner shape due to terms $\propto q^n$ with $n \geq 4$. Either one or both of these reasons produce the deviations we have seen in the first half. The processes in the second half either do not show such behavior, like the processes ..s-sff for which we take sss-sff as representative and calculate the squared and spin-summed matrix element to be

$$|\bar{\mathcal{M}}|^2 = 32\pi^2 \frac{(m_2 + m_3)^2 - q^2}{(q^2 - m^2)^2 + m^2\Gamma^2} \quad (3.14)$$

which has a numerator of $\mathcal{O}(q^2)$ and only a weak peak-suppressing factor. Or this behavior occurs only in part of the amplitude and is dominated by other contributions, which can be found for example in ssv-vss. For the processes of the second half we can still find very large max_5 values even though m is not in the Γ-vicinity of the kinematical bounds for $\Gamma/m = 1\%$ and $p = 5\%$.

3.2.4. Spin/polarization effects

In Section 2.5 we have seen that there are no spin/polarization effects in the on-shell case for total decay rates. However, generally there are correlation effects when the intermediate particle is off-shell. To check the result of Section 2.5, we first compare the NWA calculation with the on-shell calculation where the full matrix element is kept. That is, we assume that the intermediate particle is produced on-shell but do not factorize the decay rate into production and decay parts. The relative differences in the two calculations are of $\mathcal{O}(10^{-13})$ for all 48 processes confirming that there are no on-shell correlations.
We then examine correlation effects in the off-shell calculation, i.e. we compare the calculation with the full matrix element integrated over q^2 with the product of the matrix elements of the production and decay part, integrated over q^2. This way we keep the off-shell effects but drop spin/polarization correlations. To be precise, we compare $\int \frac{dq^2}{2\pi} \frac{|\mathcal{M}_p|^2 \, |\mathcal{M}_d|^2}{(q^2-m^2)^2+m^2\Gamma^2}$ with $\int \frac{dq^2}{2\pi} |\mathcal{M}_{full}|^2$. The results for $p = 10\%$ are given in Table 3.5 together with the previously obtained errors of the NWA calculation. For some processes, like ssv-vsv or ffv-vsv, the largest errors and mean deviation are almost the same as for the NWA calculation, showing that for these processes the correlation effects are the main source of NWA deviation. For fsf-fsf the largest errors are even larger than in the NWA calculation, suggesting that the errors due to correlation effects and those due to off-shell contributions partly cancel. On the other hand we find processes like vsv-vvv for which the deviations almost vanish when keeping off-shell contributions. These processes give bad NWA results due to large off-shell contributions.

	off-shell without correlation				on-shell without correlation (NWA)			
process	max_{10}	min_{10}	mean	dev	max_{10}	min_{10}	mean	dev
ssv-vsv	210	0.055	29	210	210	−4.1	29	220
ffv-vsv	150	0	19	140	150	−5.0	18	160
vvv-vsv	100	0	19	140	100	−5.1	18	150
svv-vsv	94	0	14	110	96	−4.4	13	110
vsv-vsv	75	0	12	100	80	−4.3	12	110
fsf-ffv	28	−55	−2.3	9.3	160	−4.9	13	94
vff-ffv	0.90	−43	−2.5	7.3	100	−6.0	8.6	64
fsf-fsf	41	−14	−0.12	4.1	33	−4.8	0.070	7.7
sff-ffv	1.0	−40	−2.4	6.9	91	−6.1	7.6	57
fvf-ffv	1.5	−35	−2.2	6.6	72	−6.3	6.6	49
ssv-vvv	17	0	1.8	9.4	55	−6.3	7.8	55
ssv-vff	12	0	1.4	2.8	15	−4.7	0.27	5.1
ffv-vvv	11	0	0.90	4.9	72	−6.1	11	61
ffv-vff	10	0	0.61	2.1	13	−5.9	−0.81	4.1
ssv-vss	8.8	0	3.2	6.2	12	−6.2	2.8	9.0
svv-vff	8.6	0	0.54	1.8	12	−5.0	−0.78	3.8
vvv-vff	8.4	0	0.62	2.1	12	−6.3	−0.72	4.3
svv-vvv	7.7	0	0.73	4.2	45	−4.8	8.4	44
sff-fsf	7.6	−7.7	−0.20	1.4	34	−6.0	−0.31	8.4
vvv-vvv	7.5	0	0.94	4.9	73	−6.2	10	63
vff-fsf	6.2	−7.1	−0.42	1.5	23	−6.1	−0.61	5.9
vsv-vff	6.9	0	0.35	1.6	12	−4.3	−0.70	4.0
fvf-fsf	5.2	−5.4	−0.31	1.4	19	−6.3	−0.60	5.5
ffv-vss	5.0	0	0.97	2.7	12	−6.2	1.1	8.0
svv-vss	4.7	0	0.87	2.5	11	−5.1	0.91	7.4
vvv-vss	4.7	0	1.0	2.8	13	−6.4	0.84	8.0
vsv-vss	3.7	0	0.44	1.8	14	−4.0	1.7	8.5
vsv-vvv	3.5	0	0.31	1.5	150	−3.5	25	130

Table 3.5.: Deviation R of off-shell calculation without correlations relative to off-shell calculation with correlations in the left-hand columns compared to the deviation of the NWA calculation relative to the off-shell calculation with correlations in the right-hand columns. The predictions of the on-shell calculation with and without correlations are identical. Details as in Table 3.2.

3.3. Resonant decays in specific MSSM scenarios

To check whether there are large deviations between NWA and full calculation in the MSSM, we calculate all resonant $1 \to 3$ processes at the SPS points off-shell and in NWA to compare the resulting decay widths. The SPS points represent only a very small subset of the possible MSSM parameter space, but as a full scan is not possible and phenomenological analyses should be carried out for these points, we focus on them here. Of course, one has to keep in mind that even if there are no large deviations with impact on phenomenology for the SPS points, this might not be true for the general parameter space.
There are some classes of diagrams discussed in the previous section, that do not occur as resonant decays in the MSSM. For example all decays of the forms vss-, vvs-, vsv-, -vss, -vsv can not be resonant since the vector particles of the MSSM are the same as in the SM and the lightest scalar is heavier than the W and Z bosons. This means that of the five vertices for decay processes which were found to produce large deviations in the last section (see Tables 3.2 and 3.3), two do not occur in the MSSM. Considering the list of the last section, where the processes are ordered by the NWA deviations, 10 of the first half of the processes can not occur as resonant decays.

3.3.1. Program

The mass spectra for the ten SPS points are generated with SoftSusy 2.05 [34] and we wrote a program that reads in the masses and total widths of the particles and determines all possible resonant $1 \to 3$ decays. For the sff and vff vertices, specific values for α and β in the coupling $\alpha P_L + \beta P_R$ are needed while for all other vertices the coupling constants drop out in the quotient $\Gamma_{ofs}/\Gamma_{NWA}$. Even for the fermionic vertices we have seen from the generic calculations and plots that the dependence on α and β is quite weak for most of the processes. For some of them however, there is a strong dependence and therefore we use the routines in Madgraph to read in a param_card.dat file (Les-Houches like) for each SPS point and calculate all the coupling parameters which are then used to scan the SPS points for large R-values. The program then interfaces with the program described in Section 3.2 to calculate R for the specific processes. The result is many processes for each SPS point with quite different behavior concerning NWA performance. We filter out the processes with stable particles in the final state and $|R| > 5$. The calculations are done once with the masses of the light quarks and leptons set to zero and once with the PDG masses [30]. The results are the same.

3.3.2. Results

The results are listed in Table 3.6, where the u- and d-type quarks and squarks are representative for the first two generations of quarks and squarks, respectively. Note

process	at SPS	R	Γ/m in %	$(m+m_1)/M$	$(m_2+m_3)/m$
$\tilde{g} \to d\bar{d}\tilde{L}^\star \to d\bar{d}\tilde{\chi}_1^0$	$1a$	9.54	0.935	0.935	0.170
.	$1b$	9.72	0.935	0.936	0.184
.	3	5.18	0.926	0.920	0.187
.	5	11.4	0.956	0.940	0.176
.	6	9.69	0.938	0.939	0.281
$\tilde{g} \to u\tilde{u}_L^\star \to u\bar{u}\tilde{\chi}_1^0$	$1a$	5.98	0.976	0.923	0.172
.	$1b$	7.35	0.952	0.929	0.186
.	5	9.46	0.975	0.935	0.177
.	6	6.57	0.967	0.930	0.284
$\tilde{\chi}_1^+ \to \tilde{\chi}_1^0 W^+ \to \tilde{\chi}_1^0 u\bar{d}$	$1a$	5.21	2.49	0.975	≈ 0
$\tilde{\chi}_1^+ \to \tilde{\chi}_1^0 W^+ \to \chi_1^0 e^+\nu_e$	$1a$	5.21	2.49	0.975	≈ 0
$\tilde{\chi}_1^+ \to \nu_e\tilde{e}_L^\star \to \nu_e e^+\tilde{\chi}_1^0$	3	6.99	0.0550	0.945	0.555
$\tilde{\chi}_2^0 \to e^+\tilde{e}_L \to e^+e^-\tilde{\chi}_1^0$	3	10.0	0.0550	0.951	0.555
$\tilde{\chi}_3^0 \to e^+\tilde{e}_R \to e^+e^-\tilde{\chi}_1^0$	3	9.76	0.0223	0.343	0.889
$\tilde{\chi}_4^0 \to e^+\tilde{e}_R \to e^+e^-\tilde{\chi}_1^0$	3	10.1	0.0223	0.333	0.889
$\tilde{g} \to \bar{b}\tilde{b}_2 \to \bar{b}b\tilde{\chi}_1^0$	4	6.43	1.11	0.934	0.183
$\tilde{g} \to \bar{u}\tilde{u}_L \to \bar{u}d\tilde{\chi}_1^+$	9	114	1.19	0.980	0.157
$\tilde{g} \to d\tilde{d}_L^\star \to d\bar{u}\tilde{\chi}_1^+$	9	209	1.19	0.985	0.156

Table 3.6.: Problematic decays in specific MSSM scenarios, namely the SPS points. Shown are the resonant $1 \to 3$ decays with stable final states and $|R| \geq 5$.

that the deviation for processes with different charge assignments, like $\tilde{g} \to \bar{d}\tilde{d}_L \to \bar{d}d\tilde{\chi}_1^0$ and $\tilde{g} \to d\tilde{d}_L^\star \to d\bar{d}\tilde{\chi}_1^0$, is the same. In this section, only processes with stable final states are examined, that is, only the LSP and the stable SM particles are allowed as decay products. Processes with unstable particles in the 'final state' are examined in the next section.
We now check the processes of Table 3.6 for contributions from other diagrams (non-resonant contributions and diagrams with $|R| < 5$ which are not listed in the table). If we find other large contributions to the decays, these might wash out the NWA error. The numerical results can be found in Appendix B.

SPS 1*a* The processes with large deviations for SPS $1a$ are $\tilde{g} \to d\bar{d}\tilde{\chi}_1^0$, the similar process with up-type quarks $\tilde{g} \to u\bar{u}\tilde{\chi}_1^0$ and the chargino decays $\tilde{\chi}_1^+ \to \tilde{\chi}_1^0 u\bar{d}$ and $\tilde{\chi}_1^+ \to \tilde{\chi}_1^0 e^+\bar{\nu}_e$. The involved masses are $m_{\tilde{g}} = 608\,\text{GeV}$, $m_{\tilde{\chi}_1^0} = 96.7\,\text{GeV}$, $m_{\tilde{d}_R} = 545\,\text{GeV}$, $m_{\tilde{d}_L} = 568\,\text{GeV}$, $m_{\tilde{u}_L} = 561\,\text{GeV}$ and $m_{\tilde{u}_R} = 549\,\text{GeV}$. We first consider $\tilde{g} \to d\bar{d}\tilde{\chi}_1^0$, where we have to coherently sum up the contributing amplitudes shown in Figure 3.3. As can be seen in Table 3.6, for the $\tilde{d}_L$ process $R \approx 10$ at SPS $1a$ while $R \approx 2$ for the $\tilde{d}_R$ process which is not listed in the table. Calculation of the $\tilde{d}_R$ and $\tilde{d}_L$ processes

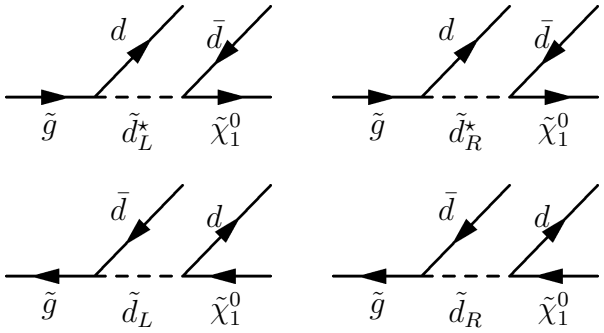

Figure 3.3.: Contributing diagrams for $\tilde{g} \to d\bar{d}\tilde{\chi}_1^0$.

separately gives an about two orders of magnitude larger partial width for the $\tilde{d}_R$ process, for which R is relatively small and $\Gamma_{\tilde{d}_R}/m_{\tilde{d}_R}$ is only about 0.05% rather than about 0.9% for $\tilde{d}_L$. The calculation of the NWA widths has been checked against SDecay [35] and the full widths of the processes against SMadgraph [36] and we used $\alpha_S(M_Z)$ which cancels in the quotient $\Gamma_{ofs}/\Gamma_{NWA}$. So, for the main contribution the NWA works well and only the small $\tilde{d}_L$ contribution has large off-shell effects.
The dominant corrections therefore are expected to be interference effects which could be estimated as follows. We have $\Gamma^{part}_{\tilde{d}_R}/\Gamma^{part}_{\tilde{d}_L} \approx 100$ for the NWA calculation. Thus, we have $|\mathcal{M}_{\tilde{d}_R}|/|\mathcal{M}_{\tilde{d}_L}| \approx 10$ where each matrix element is evaluated on-shell. The resonances are far away from each other $m_{\tilde{d}_L} - m_{\tilde{d}_R} \gg \Gamma_{\tilde{d}_L} + \Gamma_{\tilde{d}_R}$ and therefore $|\mathcal{M}_{\tilde{d}_L}(m^2_{\tilde{d}_R})| \ll |\mathcal{M}_{\tilde{d}_L}(m^2_{\tilde{d}_L})| \approx \frac{1}{10}|\mathcal{M}_{\tilde{d}_R}(m^2_{\tilde{d}_R})|$. If evaluating both matrix elements for the dominant contribution at $q^2 \approx m^2_{\tilde{d}_R}$, we get for the interference effects

$$|\mathcal{M}_{\tilde{d}_L} + \mathcal{M}_{\tilde{d}_R}|^2 - |\mathcal{M}_{\tilde{d}_L}|^2 - |\mathcal{M}_{\tilde{d}_R}|^2 = 2\mathrm{Re}\left(\mathcal{M}^\dagger_{\tilde{d}_L}\mathcal{M}_{\tilde{d}_R}\right) \tag{3.15}$$

$$\ll \frac{2}{10}|\mathcal{M}_{\tilde{d}_R}|^2 \tag{3.16}$$

and thus we expect the errors due to interference to be very small compared to 20%. We calculate the total decay rate for the process by implementing the full amplitude generated by SMadgraph in the Monte Carlo integrator described in Section 3.6 and compare it to the NWA calculation for $\Gamma^{part}_{\tilde{d}_R}$. The relative deviation is about 1.2%.
The situation for the $\tilde{g} \to u\bar{u}\tilde{\chi}_1^0$ process is quite similar. Again the contribution of the $\tilde{u}_R$ process is much larger than the $\tilde{u}_L$ contribution and for the right-handed up-squark we have good NWA performance. The relative error of the NWA calculation for $\tilde{u}_R$ compared to the full calculation is about 1.1%.

For SPS 1a there are two more processes which produce large deviations – the $\tilde{\chi}_1^+$ decays into $\tilde{\chi}_1^0 e^+\nu_e$ and $\tilde{\chi}_1^0 u\bar{d}$ with a W boson as intermediate particle. R is about 5 for these processes but as Γ/m is relatively large for W, the absolute deviation is about 10%.

For $\tilde{\chi}_1^+ \to \tilde{\chi}_1^0 e^+ \nu_e$ there are non-resonant contributions by diagrams with $\tilde{e}_L$ and $\tilde{\nu}_e$ as intermediate particles, shown in Figure 3.4. The main contribution is from the reso-

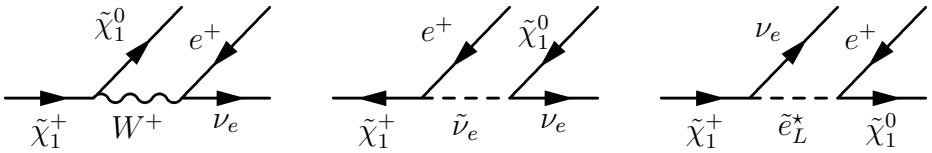

Figure 3.4.: Contributing diagrams for $\tilde{\chi}_1^+ \to \tilde{\chi}_1^0 e^+ \nu_e$.

nant W diagram. The contribution from the $\tilde{e}_L$ diagram is very small because $\tilde{e}_L$ is far from being resonant (in terms of its width $\Gamma_{\tilde{e}_L} = 0.214\,\text{GeV}$, $m_{\tilde{e}_L} = 203\,\text{GeV}$ is much larger than the parent particle mass $m_{\tilde{\chi}_1^\pm} = 182\,\text{GeV}$) and thus its contribution is suppressed, while $\tilde{\nu}_e$ is much closer to being resonant ($\Gamma_{\tilde{\nu}_e} = 0.150\,\text{GeV}$, $m_{\tilde{\nu}_e} = 185\,\text{GeV}$) and the partial width for this diagram is about 20% of the partial width of the W diagram. Due to this 20% non-resonant contribution we can not apply the NWA to this process. The error of the NWA width for the W diagram compared to the full calculation turns out to be even larger than 30% due to additional interference effects. For $\tilde{\chi}_1^+ \to \tilde{\chi}_1^0 u\bar{d}$ there are non-resonant contributions as well, they are shown in Figure 3.5. But in contrast to $\tilde{\chi}_1^+ \to \tilde{\chi}_1^0 e^+ \nu_e$ the non-resonant contributions are very small,

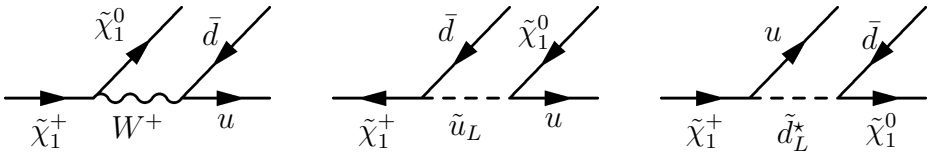

Figure 3.5.: Contributing diagrams for $\tilde{\chi}_1^+ \to \tilde{\chi}_1^0 u\bar{d}$.

since $m_{\tilde{u}_L}, m_{\tilde{d}_L} \gg m_{\tilde{\chi}_1^+}$, thus making the NWA applicable. An off-shell calculation of the three isolated processes gives a more than four orders of magnitude larger partial width for the resonant W process compared to the other two processes. Comparing the NWA result for the W process with the full calculation we find a deviation of about 11%. This large error is particularly important for this process, as there are no non-factorizing higher-order QCD corrections for the resonant diagram, since the chargino and the neutralino do not participate in the strong interaction. Thus, we do not expect large corrections at next-to-leading order since the electroweak corrections are expected to be smaller than 10% due to the small coupling constant.
A problem is ensuring gauge invariance of this decay width, as the introduction of the constant finite width can break gauge invariance, as described in the introduction and we want to drop two of the contributing diagrams. Here one could apply the gauge-preserving constant factor scheme, i.e. multiply the matrix element for all the three processes by the factor $\frac{q^2-m^2}{q^2-m^2+im\Gamma}$. This way, we multiply a gauge-invariant amplitute with a gauge-independent factor, maintaining gauge invariance at the price of an

ad-hoc factor for the non-resonant contributions. However, as the non-resonant contributions are very small, this ad-hoc factor is harmless. To check for gauge dependence, we implemented the calculation with the gauge-dependent propagator $\frac{-g_{\mu\nu}+(1-\xi)\frac{q_\mu q_\nu}{q^2-\xi m^2}}{q^2-m^2+im\Gamma}$ to check the dependence on the gauge parameter ξ. Up to the numerical uncertainty in the integration, we found a constant cross section.
At a collider the $u\bar{d}$ final state can not be distinguished from an $s\bar{c}$ final state since all four quarks hadronize. But as the couplings and masses are nearly identical in the first two quark and squark generations, there is nothing new for this process and as there is no interference between the processes with different final states, the relative NWA error is very similar for the sum of both processes.
The contribution of the decays $\tilde{\chi}_1^+ \to \tilde{\chi}_1^0 u\bar{d}$ and $\tilde{\chi}_1^+ \to \tilde{\chi}_1^0 s\bar{c}$ to the total width of $\tilde{\chi}_1^+$ is only about 5%. For the NWA calculation this can be understood as result of the small phasespace for $\tilde{\chi}_1^+ \to \tilde{\chi}_1^0 W^+$, as the sum of $m_{\tilde{\chi}_1^0}$ and m_W already is about 97.5% of $m_{\tilde{\chi}_1^\pm}$. The dominant chargino decays at SPS 1a are $\tilde{\chi}_1^+ \to \tilde{\tau}_1^+ \tilde{\nu}_\tau \to \cdots$. The smallness of the NWA-problematic widths is a general feature as large errors occur mainly for mass configurations which produce small phasespaces.
For most of the processes, the coupling parameters don't play an important role, but for the processes $\tilde{\chi}_1^+ \to \tilde{\chi}_1^0 W^+ \to \chi_1^0 u\bar{d}$ and $\tilde{\chi}_1^+ \to \tilde{\chi}_1^0 W^+ \to \chi_1^0 e^+ \nu_e$ we found a strong dependence on the first coupling which is shown in Figure 3.6.
More generally, the coupling is important for ffs vertices, which have large off-shell contributions. R depends only on the ratio α/β, which is obvious from the calculations, since overall scaling factors drop out in the ratio $\Gamma_{ofs}/\Gamma_{NWA}$. Furthermore, R is symmetric under exchange of α and β because in the squared amplitudes either $(\alpha^2+\beta^2)$ or $\alpha \cdot \beta$ appear.

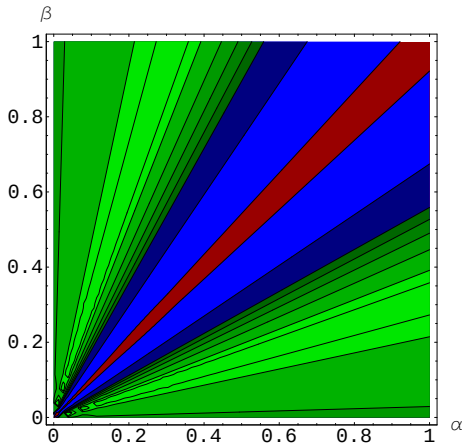

Figure 3.6.: Dependence of the relative error R on the coupling $\alpha P_L + \beta P_R$ for ffv-vff. The color code is explained in Table 3.4.

SPS 1b, 4, 5, 6 For SPS 1b, 5 and 6, we have only the two processes already discussed for SPS 1a and since the discussion is very similar, it is not repeated here in detail. For $\tilde{g} \to q\bar{q}\tilde{\chi}_1^0$ with $q = d, s$, the error of Γ_{NWA} for the $\tilde{q}_R$ process compared to the off-shell calculation including all diagrams is about 0.89% at SPS 6, about 0.71% at SPS 5 and 0.65% at SPS 1b, which is much larger than Γ/m but still small in absolute terms due to the very small ratio Γ/m. For $\tilde{g} \to q\bar{q}\tilde{\chi}_1^0$ with $q = u, c$, the errors are 0.87%, 0.95%, 2.3% for SPS 1b, 5, 6, respectively.
At SPS 4 we have the process $\tilde{g} \to \bar{b}b\tilde{\chi}_1^0$ to which diagrams with resonant $\tilde{b}_1$ and $\tilde{b}_2$ contribute. These resonances are sufficiently separated to apply the argument already used at SPS 1a to neglect interference effects. For the $\tilde{b}_1$ processes the NWA works very well ($R = -0.659$, $\Gamma/m = 1.11\%$) and their partial widths are about a factor 100 larger than the contributions of the $\tilde{b}_2$ processes. The overall error is about 2%.

SPS 3 Again, the previously discussed process $\tilde{g} \to d\bar{d}\tilde{\chi}_1^0$ appears for this benchmark point, but with even smaller error and therefore we focus on the other processes.
The other processes appearing in the table are $\tilde{\chi}_1^+ \to \nu_e \tilde{e}_L^\star \to \nu_e e^+ \tilde{\chi}_1^0$ and $\tilde{\chi}_2^0 \to e^+ \tilde{e}_L \to e^+ e^- \tilde{\chi}_1^0$. The first one is part of the $\tilde{\chi}_1^+ \to \nu_e e^+ \tilde{\chi}_1^0$ process already discussed for SPS 1a. The diagrams are shown in Figure 3.4, but now all three diagrams are resonant, since the masses are $m_{\tilde{\chi}_1^\pm} = 306\,\text{GeV}$, $m_W = 80.4\,\text{GeV}$, $m_{\tilde{e}_L} = 289\,\text{GeV}$ and $m_{\tilde{\nu}_e} = 275\,\text{GeV}$, $m_{\tilde{\chi}_1^0} = 161\,\text{GeV}$. The dominant part is the $\tilde{\nu}_e$ process with a partial width about a factor 3 larger than the width of the $\tilde{e}_L$ process. The decay through the W boson can be neglected. Again, the resonances $m^2_{\tilde{e}_L}$ and $m^2_{\tilde{e}_R}$ are far away from each other in terms of their total widths and thus we do not expect large interference effects. Due to the very small ratio of $\Gamma_{\tilde{e}_L}/m_{\tilde{e}_L}$ of about 0.06%, the large value of R does not produce a large deviation in absolute terms. The deviation of the NWA calculation is about 0.9% which is larger than the values expected by the estimate Γ/m but still the NWA is a good approximation.
For $\tilde{\chi}_2^0 \to e^+ e^- \tilde{\chi}_1^0$, there are 5 contributing processes which are shown in Figure 3.7. The intermediate particles $\tilde{e}_L$, $\tilde{e}_R$ and Z are all resonant with the resonances

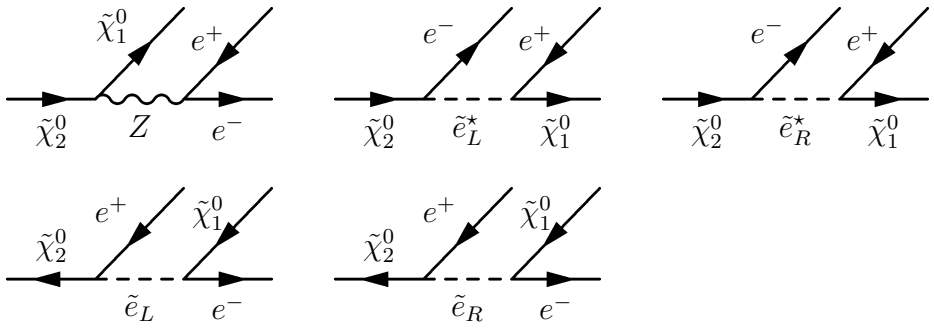

Figure 3.7.: Contributing diagrams for $\tilde{\chi}_2^0 \to \tilde{\chi}_1^0\, e^+\, e^-$.

sufficiently far away from each other to not expect large interference effects. The

dominant contribution is due to the $\tilde{e}_L$ diagram for which we found the large R-value. Comparing the sum of the NWA widths for the three processes with the full result, we find an error of about 2.4%. For the $\tilde{\chi}_3^0$ and $\tilde{\chi}_4^0$ decays we also find parts of the processes with large off-shell contributions. The ratio Γ/m for these processes is even smaller and there are again additional contributions for which the NWA works well. As the discussion is quite similar to the $\tilde{\chi}_2^0$ decay, it is not repeated here.

SPS 9 For SPS 9 the process $\tilde{g} \to \bar{u}d\tilde{\chi}_1^+$, to which the two diagrams shown in Figure 3.8 contribute, gets very large off-shell contributions. Both of the contributing

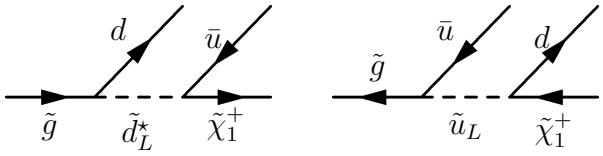

Figure 3.8.: Contributing diagrams for $\tilde{g} \to \tilde{\chi}_1^+ \bar{u}d$.

diagrams are listed in the table with R of order 10^2, while Γ/m is about 1% giving an absolute deviation of at least a factor two. The $\tilde{d}_L$ and $\tilde{u}_L$ resonances are separated by about 7 GeV which is small compared to their widths of about 15 GeV. Thus we expect large interference effects which produce an additional large error. The conventional Γ/m error estimate which would give an error of 1% is completely wrong for this decay, for which the sum of the NWA widths is too small by roughly a factor of 3. However, the total width of 0.09 GeV for the gluino decaying into $ud\tilde{\chi}_1^0$ is small compared to its total width of 14.3 GeV and keeping in mind its large mass of $m_{\tilde{g}} = 1286$ GeV, it is not very likely to play an important role at the LHC.

3.4. Parts of longer decay chains in specific MSSM scenarios

In the preceding discussion we focussed on decays with stable final states, that is on the ends of decay chains. As one would like to apply the NWA also in the inner parts of decay chains (e.g. for the processes in the Section 3.5), the results for unstable particles which further decay in the 'final states' are of interest as well. To address this, we also calculate the relative NWA deviation for resonant processes with one unstable 'final state' particle at the SPS points. The results are given in Appendix C. Of course, these results are only meant to give hints on where to be careful, as additional scales come into play in complex processes, which might introduce additional effects.

3.5. Phenomenologically interesting decay modes

In this section we check the NWA performance for the processes used in the analyses of [37], where SPS 1a is considered. The first kind of process is $\tilde{\chi}_2^0 \to l^{\pm}\tilde{l}_R^{\mp} \to l^+l^-\tilde{\chi}_1^0$, where l and $\tilde{l}_R$ denote (s)leptons of the first two generations. This process is of interest because the two leptons in the final state provide a natural trigger and it is part of $\tilde{q}_L \to q\tilde{\chi}_2^0 \to ql^{\pm}\tilde{l}_R^{\mp} \to ql^+l^-\tilde{\chi}_1^0$, which can be used to extract various invariant masses of particle subsets from kinematical edges and thresholds. Since the width of $\tilde{\chi}_2^0$ is only about 0.01% of its mass, the factorization of the decay chain at this point does not introduce large errors and we consider the part $\tilde{\chi}_2^0 \to l^{\pm}\tilde{l}_R^{\mp} \to l^+l^-\tilde{\chi}_1^0$. The widths of the righthanded sleptons $\tilde{l}_R$ are about 0.15% of their masses and we therefore expect the error due to the $\tilde{l}_R$ factorization to dominate.
Also of interest is $\tilde{\chi}_2^0 \to \tau^{\pm}\tilde{\tau}_1^{\mp} \to \tau^+\tau^-\tilde{\chi}_1^0$ which is used to measure the $\tilde{\tau}_1$ mass. The Γ/m ratio for the $\tilde{\tau}_1$ is about 0.1%. The results for comparison of NWA and off-shell-calculation for these processes are shown in Table 3.7. The R-factors are about 3, which is only slightly larger than Γ/m and as Γ/m is very small, the overall error is small and the NWA is a very good approximation here.
Another set of important processes are the gluino decays, since a large number of them could be produced at the LHC. In particular the decays $\tilde{g} \to \bar{b}\tilde{b}_1 \to \bar{b}b\tilde{\chi}_i^0$ as well as $\tilde{g} \to \bar{t}\tilde{t}_1 \to \bar{t}b\tilde{\chi}_j^+$ and $\tilde{g} \to \bar{b}\tilde{b}_i \to \bar{b}t\tilde{\chi}_j^-$ are of interest for studies of the stop and sbottom sector. There are additional processes of interest for the stop and sbottom sector and in Table 3.7, we show the relative deviation of the NWA and off-shell results for all resonant gluino decays into third generation quarks at SPS 1a. As can be seen, R is not very large for these processes, but together with Γ/m ratios of $\mathcal{O}(1\%)$, errors of about 3% occur.

process	SPS	R	Γ/m in %	$(m+m_1)/M$	$(m_2+m_3)/m$
$\tilde{\chi}_2^0 \to e^+\tilde{e}_R \to e^+e^-\tilde{\chi}_1^0$	$1a$	-2.84	0.150	0.796	0.671
$\tilde{\chi}_2^0 \to \mu^+\tilde{\mu}_R \to \mu^+\mu^-\tilde{\chi}_1^0$	$1a$	-2.84	0.150	0.796	0.672
$\tilde{\chi}_2^0 \to \tau^+\tilde{\tau}_1 \to \tau^+\tau^-\tilde{\chi}_1^0$	$1a$	-2.67	0.110	0.752	0.732
$\tilde{g} \to \tilde{t}_1\bar{t} \to \tilde{t}_1\bar{b}W^-$	$1a$	-1.77	0.893	0.946	0.483
$\tilde{g} \to \bar{b}\tilde{b}_1 \to \bar{b}\tilde{t}_1W^-$	$1a$	-4.43	0.728	0.851	0.936
$\tilde{g} \to \bar{b}\tilde{b}_1 \to \bar{b}b\tilde{\chi}_1^0$	$1a$	-0.448	0.728	0.851	0.197
$\tilde{g} \to \bar{b}\tilde{b}_1 \to \bar{b}b\tilde{\chi}_2^0$	$1a$	-0.974	0.728	0.851	0.361
$\tilde{g} \to \bar{b}\tilde{b}_1 \to \bar{b}b\tilde{\chi}_3^0$	$1a$	-3.32	0.728	0.851	0.717
$\tilde{g} \to \bar{b}\tilde{b}_1 \to \bar{b}b\tilde{\chi}_4^0$	$1a$	-3.66	0.728	0.851	0.752
$\tilde{g} \to \bar{b}\tilde{b}_1 \to \bar{b}t\tilde{\chi}_1^-$	$1a$	-2.46	0.728	0.851	0.695
$\tilde{g} \to \bar{b}\tilde{b}_2 \to \bar{b}\tilde{t}_1W^-$	$1a$	-6.81	0.147	0.902	0.883
$\tilde{g} \to \bar{b}\tilde{b}_2 \to \bar{b}b\tilde{\chi}_1^0$	$1a$	1.79	0.147	0.902	0.186
$\tilde{g} \to \bar{b}\tilde{b}_2 \to \bar{b}b\tilde{\chi}_2^0$	$1a$	0.950	0.147	0.902	0.341
$\tilde{g} \to \bar{b}\tilde{b}_2 \to \bar{b}b\tilde{\chi}_3^0$	$1a$	-2.45	0.147	0.902	0.677
$\tilde{g} \to \bar{b}\tilde{b}_2 \to \bar{b}b\tilde{\chi}_4^0$	$1a$	-2.97	0.147	0.902	0.710
$\tilde{g} \to \bar{b}\tilde{b}_2 \to \bar{b}t\tilde{\chi}_1^-$	$1a$	-1.37	0.147	0.902	0.656
$\tilde{g} \to \bar{t}\tilde{t}_1 \to \bar{t}b\tilde{\chi}_1^+$	$1a$	-1.46	0.506	0.946	0.465
$\tilde{g} \to \bar{t}\tilde{t}_1 \to \bar{t}b\tilde{\chi}_2^+$	$1a$	-6.54	0.506	0.946	0.961
$\tilde{g} \to \bar{t}\tilde{t}_1 \to \bar{t}t\tilde{\chi}_1^0$	$1a$	-2.21	0.506	0.946	0.680
$\tilde{g} \to \bar{t}\tilde{t}_1 \to \bar{t}t\tilde{\chi}_2^0$	$1a$	-5.56	0.506	0.946	0.891

Table 3.7.: $\tilde{\chi}_2^0$ and gluino decays at SPS 1a.

3.6. Checking the calculations with Monte Carlo integration

In order to check the analytic calculations of the amplitudes and phasespace factors we implement a simple Monte Carlo integration. To be prepared for other processes the program should be kept as general as possible. So we use the matrix-element generator SMadgraph to give us a fortran routine calculating the squared and spin-summed Feynman amplitude for a given process and given point in phasespace. To generate appropriate points we use the phasespace factorization discussed in Section 2.1, that is, we generate a properly distributed q^2 and the angles Ω_1 of p_1 in the restframe of the decaying particle and the angle of p_2 in the restframe of the intermediate particle equally distributed. We generate q^2 distributed as a Breit-Wigner resonance around the intermediate mass m, which is realized by

$$q^2 = m^2 + m\Gamma \tan(x) \tag{3.17}$$

with a linear mapping for x

$$x = (x_{max} - x_{min})r + x_{min} \tag{3.18}$$

where $x_{max/min} = \arctan \frac{q^2_{max/min} - m^2}{m\Gamma}$ and r is equally-distributed in $[0, 1]$. The phasespace factor then becomes

$$\frac{dq^2}{2\pi} = dr \frac{x_{max} - x_{min}}{2\pi} \frac{(q^2 - m^2)^2 + (m\Gamma)^2}{m\Gamma} \tag{3.19}$$

which cancels the denominator of the propagator and thus reduces the variance of the integrand (as described in the introduction) to speed up the Monte Carlo integration. The benefit of this parameterization is that the angles are equally distributed and most of the q^2-values are centered around m^2 which makes the Monte Carlo integration converge faster. To determine the bounds for q^2 we use evaluations of q^2 once in the restframe of the parent particle and once in the restframe of the intermediate particle

$$\begin{aligned} q^2 &= (P - p_1)^2 = M^2 - 2Pp_1 + m_1^2 = M^2 - 2M\sqrt{m_1^2 + \vec{p}_1^{\,2}} + m_1^2 \\ &\leq (M - m_1)^2 \end{aligned}$$

and

$$\begin{aligned} q^2 &= (p_2 + p_3)^2 = m_2^2 + 2\sqrt{m_2^2 + \vec{p}_2^{\,2}}\sqrt{m_3^2 + \vec{p}_3^{\,2}} - 2\vec{p}_2 \cdot \vec{p}_3 + m_3^2 \\ &= m_2^2 + 2\sqrt{m_2^2 + \vec{p}_2^{\,2}}\sqrt{m_3^2 + \vec{p}_2^{\,2}} + 2\vec{p}_2^{\,2} + m_3^2 \\ &\geq (m_2 + m_3)^2 \end{aligned}$$

to obtain

$$(m_2 + m_3)^2 \leq q^2 \leq (M - m_1)^2. \tag{3.20}$$

We also implement a check for energy-momentum conservation on the generated phasespace points. Now, p_1 can easily be calculated in the restframe of P while p_2 and p_3 are calculated in the restframe of q. After boosting p_2 and p_3 back into the restframe of P, we have generated an appropriate point in phasespace for which SMadgraph returns the squared and spin-summed matrix element. The integration can be carried out by multiplying the squared amplitude with the phasespace factors and the Jacobi determinant and summing up the results.
The analytical calculations for each process have been checked against the Monte Carlo integrated matrix element. The check for each process has been performed for 3 points in parameter space, where we compared the amplitudes for three phasespace points and the total decay widths. The agreement between analytical and numerical results is at least 8 significant digits for the amplitudes and 5 significant digits for the total decay widths.

Improving the NWA performance

4

For almost all of the processes with large deviations, the sum of the daughter masses is not too far away from the parent mass in one of the $1 \to 2$ decays. This suggests that at least part of the deviations can be traced back to the vanishing phasespace factors near the kinematical limits, forcing $\Gamma_{NWA} \to 0$ while Γ_{ofs} stays finite. Therefore, we now want to find improvements of the simple $\Gamma_{NWA} = \Gamma_{prod} \times \mathrm{BR}$ factorization which better take into account the phasespace properties and on the other hand maintain as much simplification of the NWA formula as possible.

4.1. Effective-mass NWA

As mentioned before, at least some deviation can be traced back to the vanishing phasespace in the NWA calculations with the daughter masses approaching the parent mass. Since we want to maintain the general simplifications of the NWA, we can not rely on special properties of the matrix elements to find improvements. The first thing to do therefore is to improve the NWA for the all-scalar process, where the matrix elements do not play any role at all. In Figure 4.1 the obtained total widths in NWA and off-shell are plotted in some arbitrary normalization as functions of the intermediate-particle mass m. As can be seen there, with m approaching the kinematical limits, the NWA width starts to fall stronger than the off-shell width. We now want to find a better description with improved threshold behavior. Recalling from the previous sections that – neglecting spin correlation – we made the replacement

$$\int \frac{dq^2}{2\pi} \Gamma_p(q^2) \frac{2m}{(q^2-m^2)^2+m^2\Gamma^2} \Gamma_d(q^2) \to \Gamma_p(m^2) \frac{1}{\Gamma} \Gamma_d(m^2),$$

the NWA could also be obtained by inserting a factor $\pi m \Gamma \delta(q^2 - m^2)$ into the integral, giving

$$\int dq^2 \Gamma_p(q^2) \frac{m^2\Gamma}{(q^2-m^2)^2+m^2\Gamma^2} \Gamma_d(q^2) \delta(q^2-m^2). \tag{4.1}$$

The factor $\pi m \Gamma$ is a normalization factor introduced to obtain the correct NWA formula. Taking a look at the integrand, which is strongly peaked around $q^2 = m^2$,

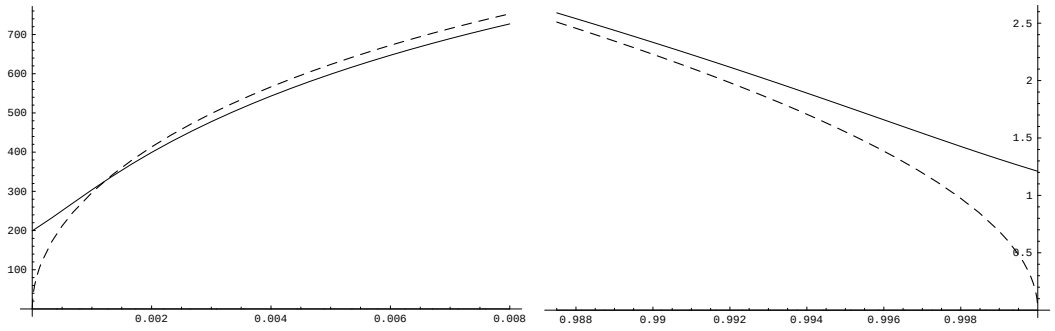

Figure 4.1.: Threshold behavior of NWA decay rate (dashed line) compared to off-shell decay rate (solid line) for $\Gamma/m = 0.01$. On the lefthand side the behavior for $m \to m_1 + m_2$ is shown, on the righthand side for $m \to M - m_1$.

this corresponds to taking the value of the integrand at its maximum and multiply it with a factor proportional to the width of the peak, basically $m\Gamma$. The problem now can be reformulated as follows. For $q^2 = m^2$ the squared denominator of the propagator has its maximum – it is not necessarily the maximum of the full integrand because Γ_p and Γ_d, in particular the phasespaces, are functions of q^2 as well. Especially as we approach the kinematic limits in one of the decays, these phasespace factors vanish and the maximum is shifted considerably. To take this into account while not being too much process-specific, we want to determine the maximum of the product of the phasespace factors and the squared denominator $\frac{PS(q^2)}{(q^2-m^2)+m^2\Gamma^2}$ and consider it as an effective mass m^2_{eff}. This effective mass does not depend on any process-specific information and is given as a function of the general kind of process, e.g. $1 \to 3$ or $2 \to 4$ and the masses of the external particles. The determination of the correct maximum might be too complicated for arbitrary phasespaces, but as we expect the maximum not to shift too much, we use a series expansion of the phasespacefactor in q^2 up to the second order. The maximum of the integrand

$$I(q^2) := \frac{PS(m^2) + \frac{dPS}{dq^2}(m^2)(q^2 - m^2) + \frac{1}{2}\frac{d^2PS}{d(q^2)^2}(m^2)(q^2 - m^2)^2}{(q^2 - m^2)^2 + m^2\Gamma^2} \tag{4.2}$$

can then be determined analytically by solving $\frac{d}{dq^2}I(q^2) = 0$. The solution, with $a = PS(m^2)$, $b = \frac{d}{dq^2}PS(m^2)$ and $c = \frac{d^2}{d(q^2)^2}PS(m^2)$, is

$$m^2_{eff} = m^2 + \frac{1}{b}\left(-a + cm^2\Gamma^2 \pm \sqrt{a^2 - 2cm^2\Gamma^2 a + c^2m^4\Gamma^4 + b^2m^2\Gamma^2}\right). \tag{4.3}$$

Only the positive-sign solution is relevant, since for $\Gamma \to 0$, the effective mass should fulfill $m^2_{eff} \to m^2$. With this effective mass, the NWA formula is the same as before with m^2 replaced by m^2_{eff}

$$\Gamma_{NWA_{eff}} = \Gamma_p(m^2_{eff})\frac{1}{\Gamma}\Gamma_d(m^2_{eff}). \tag{4.4}$$

With $m_{eff}^2 \to m^2$ for $\Gamma \to 0$, we maintain the property that $\Gamma_{ofs}/\Gamma_{NWA_{eff}} \to 1$ for $\Gamma \to 0$ which was discussed for the NWA in Section 2.4. For the $1 \to 3$ decays the phasespace factor is

$$PS(q^2) = \frac{1}{16^2\pi^4} \frac{|\vec{p}_1(q^2)||\vec{p}_2(q^2)|}{M\sqrt{q^2}} \tag{4.5}$$

and in Figure 4.2 the widths calculated off-shell as well as with NWA are compared to the new method. The modified NWA reproduces the usual NWA widths for m^2 far away from the kinematical bounds but produces much better results as m^2 approaches these bounds in one of the decays. There is only a small region for $m \to m_2 + m_3$, where the too strong decrease in the NWA width compensates the slightly too large NWA width for larger values of m. There the usual NWA produces slightly better results. Since in the calculation we only use a series expansion of the phasespace factor, which can be obtained for any kind of phasespace, this procedure can be applied to arbitrary processes. The expansion up to second order in q^2 is a compromise to keep the calculation as simple as possible while achieving a satisfactory precision. This choice is not critical – expansion linear in q^2 could be chosen as well, simplifying the expression for m_{eff}^2. This modified NWA should produce the same results for the

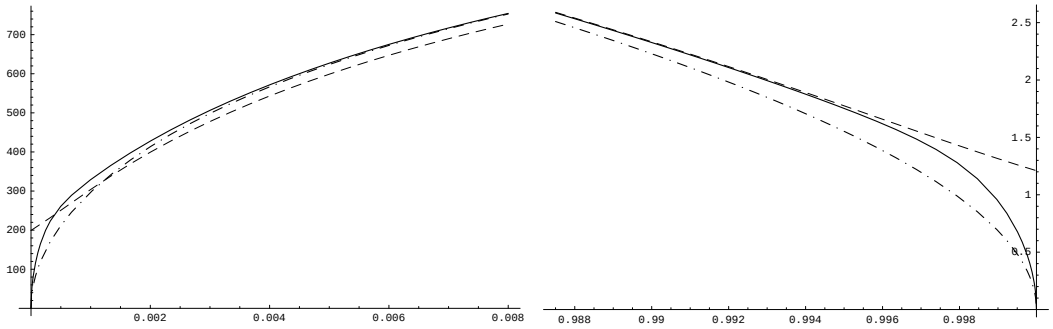

Figure 4.2.: Threshold behavior of the modified NWA formula in comparison to the ordinary NWA and off-shell calculation. The lefthand side shows $m \to m_1 + m_2$, the righthand side $m \to M - m_1$ for $\Gamma/m = 0.01$. The dashed line is the off-shell calculation, the dot-dashed line the NWA result and the solid one is obtained with the effective-mass NWA.

scans in Section 3.2, since m-values near the kinematic bounds are excluded there. For the analysis in Sections 3.3 and 3.4 slight improvements are expected. Therefore the program is rerun with the modified NWA. For the decays with stable final state particles, the new results are listed in Table 4.1. Again all resonant decays with stable final state particles are listed and the first and second generation quarks are represented by u and d. Only for the decays at SPS 3 the deviation is almost the same as before, while we see a slight decrease of the relative error for all other processes. We note that the total widths of the resonant particles at SPS 3 are very small and that

process	at SPS	R'	R	Γ/m in %
$\tilde{g} \to d\tilde{d}_L^\star \to d\bar{d}\tilde{\chi}_1^0$	$1a$	9.03	9.54	0.935
.	$1b$	9.20	9.72	0.935
.	3	4.88	5.18	0.926
.	5	10.8	11.4	0.956
.	6	9.13	9.69	0.938
$\tilde{g} \to u\tilde{u}_L^\star \to u\bar{u}\tilde{\chi}_1^0$	$1a$	5.62	5.98	0.976
.	$1b$	6.93	7.35	0.952
.	5	8.93	9.46	0.975
.	6	6.15	6.57	0.967
$\tilde{\chi}_1^+ \to \tilde{\chi}_1^0 W^+ \to \tilde{\chi}_1^0 u\bar{d}$	$1a$	4.61	5.21	2.49
$\tilde{\chi}_1^+ \to \tilde{\chi}_1^0 W^+ \to \chi_1^0 e^+\nu_e$	$1a$	4.61	5.21	2.49
$\tilde{\chi}_1^+ \to \nu_e \tilde{e}_L^\star \to \nu_e e^+ \tilde{\chi}_1^0$	3	6.96	6.99	0.0550
$\tilde{\chi}_2^0 \to e^+\tilde{e}_L \to e^+e^-\tilde{\chi}_1^0$	3	9.99	10.0	0.0550
$\tilde{\chi}_3^0 \to e^+\tilde{e}_R \to e^+e^-\tilde{\chi}_1^0$	3	9.75	9.76	0.0223
$\tilde{\chi}_4^0 \to e^+\tilde{e}_R \to e^+e^-\tilde{\chi}_1^0$	3	10.1	10.1	0.0223
$\tilde{g} \to \bar{b}\tilde{b}_2 \to \bar{b}b\tilde{\chi}_1^0$	4	5.98	6.43	1.11
$\tilde{g} \to \bar{u}\tilde{u}_L \to \bar{u}d\tilde{\chi}_1^+$	9	98.8	114	1.19
$\tilde{g} \to d\tilde{d}_L^\star \to d\bar{u}\tilde{\chi}_1^+$	9	169	209	1.19

Table 4.1.: Specific processes in the MSSM for the ten SPS points. R' is the relative error normalized to Γ/m, obtained with the modified NWA formula of Equation (4.4). For comparison we also list the relative deviation R, obtained with the original NWA formula.

m is not close to the kinematical bounds. Therefore we do not find an improvement of the NWA for these decays.

4.2. Correct treatment of integration bounds

As we have seen in Section 2.3, the NWA can be obtained by shifting the integration bounds for q^2 to infinity and this way integrating the full Breit-Wigner form. This is a good approximation if the resonance is sufficiently centered in the kinematically allowed region, making the contributions from the kinematically forbidden region small. If on the other hand, the resonance is near one of the bounds, considerable parts of the Breit-Wigner are kinematically forbidden and shifting the integration bounds is not a good approximation anymore. Since the integral

$$\int_{a^2}^{b^2} \frac{dq^2}{2\pi} \frac{1}{(q^2-m^2)^2+m^2\Gamma^2}$$

can be calculated analytically, we can also use the NWA without the shift of the integration bounds. This way we obtain

$$\begin{aligned}
\Gamma'_{NWA} &= \Gamma_p \times \int_{q^2_{min}}^{q^2_{max}} \frac{dq^2}{2\pi} \frac{2m}{(q^2-m^2)^2+(m\Gamma)^2} \times \Gamma_d && (4.6)\\
&= \Gamma_p \times \int_{(m_2+m_3)^2}^{(M-m_1)^2} \frac{dq^2}{2\pi} \frac{2m}{(q^2-m^2)^2+(m\Gamma)^2} \times \Gamma_d && (4.7)\\
&= \Gamma_p \times \int_{(m_2+m_3)^2-m^2}^{(M-m_1)^2-m^2} \frac{dx}{2\pi} \frac{2m}{x^2+(m\Gamma)^2} \times \Gamma_d && (4.8)\\
&= \frac{\Gamma_p\Gamma_d}{\Gamma} \times \\
&\quad \frac{1}{\pi}\left[\arctan\left(\frac{(M-m_1)^2-m^2}{m\Gamma}\right) - \arctan\left(\frac{(m_2+m_3)^2-m^2}{m\Gamma}\right)\right]. && (4.9)
\end{aligned}$$

Now, this formula can be used for the factorized calculation. With this NWA formula, the proof that the error is of $\mathcal{O}(\Gamma/m)$ would even be shortened since the term α which we get in the proof in Section 2.6 does not occur. However, we find that this modified formula produces even larger errors than the ordinary NWA. This can be understood by considering that all the decays with bad NWA behavior have a large positive R due to the fact that the NWA cross section is too small for these decays. This smallness of the NWA result can be attributed to correlation effects, off-shell contributions or vanishing phasespace factors. But anyway, the corrections due to the correct integration bounds only further reduce the NWA decay rate, thus increasing the error. In fact the error due to the integration of the full Breit-Wigner partly compensates the error due to the vanishing phasespace when approaching the kinematical bounds.

5 Summary

Good narrow-width approximation (NWA) performance is a necessary precondition to obtain accurate predictions, in particular with beyond-leading-order calculations, for complicated scattering processes such as production and decay of supersymmetric particles. The purpose of this work was to systematically check the NWA for BSM physics.

We first developed and proved general properties of the NWA. We gave a formal way of obtaining the NWA from the full calculation by using certain assumptions and showed that the NWA becomes exact with vanishing width of the intermediate particle. Then we considered correlation effects and showed that they have no impact on total decay rates once we assume the intermediate particle to be on the mass-shell. The main result of our general investigation is that the NWA error is of $\mathcal{O}(\Gamma/m)$ which we have proven under certain weak assumptions.

We then focussed on the MSSM as a specific BSM model and chose the $1 \to 3$ decays for a systematic analysis. These processes frequently occur as parts of decay chains and on the other hand are simple enough to be checked for all particle combinations and large numbers of parameter configurations. We generally found good NWA performance for resonances in the very interior of the kinematically allowed region but process-specific, problematic behavior near the kinematical bounds. After giving a ranking of the different processes with respect to NWA performance, we discussed the relevant decays and how the deviations arise. The two main conditions that have to be fulfilled for the NWA to break down are a large hierarchy between the mass of the parent particle and the masses of the decay products, and the mass of the unstable particle has to be near the kinematical bounds.

The third part was the application of the analysis done so far to specific scenarios of the MSSM. For that purpose we used the SPS benchmark points to generate and check all possible resonant $1 \to 3$ decays for these specific low-energy scenarios. We filtered out the processes with stable final states and large deviations and for these considered all sub- and non-resonant contributions as well as interference effects. For the first eight SPS points we found only the process $\tilde{\chi}_1^+ \to \tilde{\chi}_1^0 u\bar{d}$ with bad NWA performance which is not remedied by other contributions. For this process we have

an error of about 11% and after arguing on a very general footing that interference effects are small, the NWA is still a good approximation for all other processes. At SPS 9 we again found two processes giving very bad NWA results which are too small by more than a factor 2 even though the interval $[m - \Gamma, m + \Gamma]$ is completely inside the kinematically allowed region. However, these are very few problematic decays and keeping them in mind the NWA should very well be applicable for the $1 \to 3$ decays with stable final states at the SPS points. For processes with unstable particles in the 'final state' we found a lot of decays with bad NWA performance. For one unstable and two stable particles as decay products the results are given in the appendix.
In the last part of this work we again considered the assumptions and approximations that are necessary to formally obtain the NWA and developed improvements of the simple $\sigma_p \times \mathrm{BR}$ formula. These modifications preserve the simplifications due to the NWA not only for loop calculations but also for tree-level processes. We improved the treatment of the phasespace by taking into account the strongly varying phasespace factors near the kinematical bounds and the resulting modified NWA formula is as simple as the original one up to the replacement of the intermediate-particle mass by an effective mass, which depends on the numbers of incoming and outgoing particles and their respective masses. We then applied this modified NWA formula to the decays obtained for the SPS points and generally found a slight decrease of the NWA error.

Feynman diagrams and amplitudes

In Tables A.1-A.3 we show the 48 processes with the corresponding amplitudes. Since we will sum/average over the spins and polarizations we do not write the indices explicitly.

diagram	process	amplitude
	ffs-sff	$\bar{u}(p_1)C_1u(P) \times \bar{u}(p_3)C_2v(p_2)$
	ffs-sss	$\bar{u}(p_1)C_1u(P)\lambda_2$
	ffs-ssv	$\bar{u}(p_1)C_1u(P) \times \lambda_2(q+p_2)\cdot\epsilon^\star(p_3)$
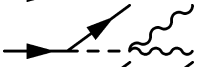	ffs-svv	$\bar{u}(p_1)C_1u(P) \times \lambda_2\epsilon^\star(p_2)\cdot\epsilon^\star(p_3)$
	ffv-vff	$\bar{u}(p_1)\gamma_\mu C_1u(P) \times (-g_{\mu\nu}+\frac{q_\mu q_\nu}{m^2}) \times \bar{u}(p_3)\gamma_\mu C_2v(p_2)$
	ffv-vss	$\bar{u}(p_1)\gamma_\mu C_1u(P) \times (-g_{\mu\nu}+\frac{q_\mu q_\nu}{m^2}) \times \lambda_2(p_2-p_3)_\nu$
	ffv-vsv	$\bar{u}(p_1)\gamma_\mu C_1u(P) \times (-g_{\mu\nu}+\frac{q_\mu q_\nu}{m^2}) \times \lambda_2\epsilon^\star_\nu(p_3)$
	ffv-vvv	$\bar{u}(p_1)\gamma_\mu C_1u(P) \times (-g_{\mu\nu}+\frac{q_\mu q_\nu}{m^2}) \times i\lambda_2\epsilon^\star_\rho(p_2)\epsilon^\star_\sigma(p_3)$ $(g^{\nu\sigma}(q+p_3)^\rho + g^{\sigma\rho}(p_2-p_3)^\nu - g^{\rho\nu}(p_2+q)^\sigma)$
	fsf-ffv	$\bar{u}(p_2)\gamma^\nu C_2\epsilon^\star_\nu(p_3) \times (\not{q}+m) \times C_1u(P)$

Table A.1.: Diagrams and amplitudes for the resonant $1 \to 3$ decays. The amplitudes are given with $C_i = \alpha_i P_L + \beta_i P_R$. The factor $\frac{i}{q^2-m^2+im\Gamma}$ is suppressed and spin/polarization indices are not written explicitly.

diagram	process	amplitude
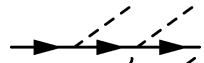	fsf-fsf	$\bar{u}(p_3)C_2 \times (\not{q} + m) \times C_1 u(P)$
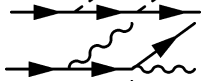	fvf-ffv	$\bar{u}(p_2)\gamma^\nu C_2 \epsilon_\nu^\star(p_3) \times (\not{q} + m) \times \gamma^\mu C_1 \epsilon_\mu^\star(p_1) u(P)$
	fvf-fsf	$\bar{u}(p_3)C_2 \times (\not{q} + m) \times \gamma^\mu C_1 \epsilon_\mu^\star(p_1) u(P)$
	sff-ffs	$\bar{u}(p_2)C_2 \times (\not{q} + m) \times C_1 v(p_1)$
	sff-ffv	$\bar{u}(p_2)\gamma^\nu C_2 \epsilon_\nu^\star(p_3) \times (\not{q} + m) \times C_1 v(p_1)$
	sss-sff	$\lambda_1 \bar{u}(p_3) C_2 v(p_2)$
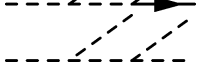	sss-sss	$\lambda_1 \lambda_2$
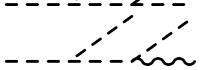	sss-ssv	$\lambda_1 \lambda_2 (q + p_2) \cdot \epsilon^\star(p_3)$
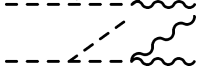	sss-svv	$\lambda_1 \lambda_2 \epsilon^\star(p_2) \cdot \epsilon^\star(p_3)$
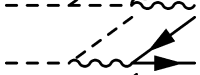	ssv-vff	$\lambda_1 (P+q)^\mu \times (-g_{\mu\nu} + \frac{q_\mu q_\nu}{m^2}) \times \bar{u}(p_3)\gamma_\mu C_2 v(p_2)$
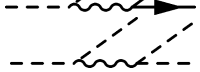	ssv-vss	$\lambda_1 (P+q)^\mu \times (-g_{\mu\nu} + \frac{q_\mu q_\nu}{m^2}) \times \lambda_2 (p_2 - p_3)_\nu$
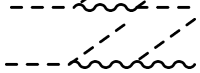	ssv-vsv	$\lambda_1 (P+q)^\mu \times (-g_{\mu\nu} + \frac{q_\mu q_\nu}{m^2}) \times \lambda_2 \epsilon_\nu^\star(p_3)$
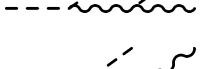	ssv-vvv	$\lambda_1 (P+q)^\mu \times (-g_{\mu\nu} + \frac{q_\mu q_\nu}{m^2}) \times i\lambda_2 \epsilon_\rho^\star(p_2) \epsilon_\sigma^\star(p_3)$ $(g^{\nu\sigma}(q+p_3)^\rho + g^{\sigma\rho}(p_2-p_3)^\nu - g^{\rho\nu}(p_2+q)^\sigma)$
	svs-sff	$\lambda_1 (P+q) \cdot \epsilon^\star(p_1) \times \bar{u}(p_3) C_2 v(p_2)$
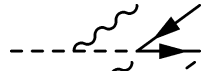	svs-sss	$\lambda_1 (P+q) \cdot \epsilon^\star(p_1) \lambda_2$
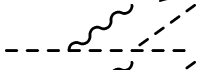	svs-ssv	$\lambda_1 (P+q) \cdot \epsilon^\star(p_1) \times \lambda_2 (q+p_2) \cdot \epsilon^\star(p_3)$
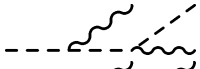	svs-svv	$\lambda_1 (P+q) \cdot \epsilon^\star(p_1) \times \lambda_2 \epsilon^\star(p_2) \cdot \epsilon^\star(p_3)$
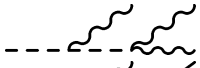	svv-vff	$\lambda_1 \epsilon_\mu^\star(p_1) \times (-g_{\mu\nu} + \frac{q_\mu q_\nu}{m^2}) \times \bar{u}(p_3)\gamma_\mu C_2 v(p_2)$
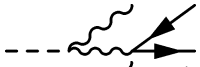	svv-vss	$\lambda_1 \epsilon_\mu^\star(p_1) \times (-g_{\mu\nu} + \frac{q_\mu q_\nu}{m^2}) \times \lambda_2 (p_2 - p_3)_\nu$
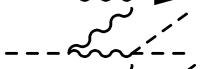	svv-vsv	$\lambda_1 \epsilon_\mu^\star(p_1) \times (-g_{\mu\nu} + \frac{q_\mu q_\nu}{m^2}) \times \lambda_2 \epsilon_\nu^\star(p_3)$

Table A.2.: Diagrams and amplitudes for the resonant $1 \to 3$ decays. Details as in Table A.1.

diagram	process	amplitude
	svv-vvv	$\lambda_1\epsilon^\star_\mu(p_1) \times (-g_{\mu\nu} + \frac{q_\mu q_\nu}{m^2}) \times i\lambda_2\epsilon^\star_\rho(p_2)\epsilon^\star_\sigma(p_3)$ $(g^{\nu\sigma}(q+p_3)^\rho + g^{\sigma\rho}(p_2-p_3)^\nu - g^{\rho\nu}(p_2+q)^\sigma)$
	vff-ffv	$\bar{u}(p_2)\gamma^\mu C_2\epsilon^\star_\mu(p_3) \times (\not{q} + m) \times \gamma^\nu C_1 v(p_1)\epsilon_\nu(P)$
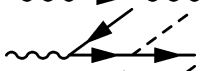	vff-fsf	$\bar{u}(p_3)C_2 \times (\not{q} + m) \times \gamma^\mu C_1\epsilon_\mu(P)v(p_1)$
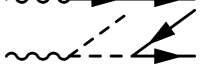	vss-sff	$\lambda_1(p_1-q)\cdot\epsilon(P) \times \bar{u}(p_3)C_2 v(p_2)$
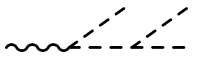	vss-sss	$\lambda_1(p_1-q)\cdot\epsilon(P)\lambda_2$
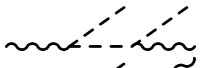	vss-ssv	$\lambda_1(p_1-q)\cdot\epsilon(P) \times \lambda_2(q+p_2)\cdot\epsilon^\star(p_3)$
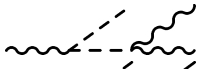	vss-svv	$\lambda_1(p_1-q)\cdot\epsilon(P) \times \lambda_2\epsilon^\star(p_2)\cdot\epsilon^\star(p_3)$
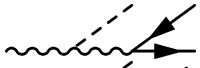	vsv-vff	$\lambda_1\epsilon_\mu(P) \times (-g_{\mu\nu} + \frac{q_\mu q_\nu}{m^2}) \times \bar{u}(p_3)\gamma_\nu C_2 v(p_2)$
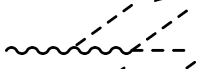	vsv-vss	$\lambda_1\epsilon_\mu(P) \times (-g_{\mu\nu} + \frac{q_\mu q_\nu}{m^2}) \times \lambda_2(p_2-p_3)_\nu$
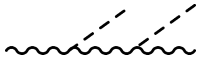	vsv-vsv	$\lambda_1\epsilon_\mu(P) \times (-g_{\mu\nu} + \frac{q_\mu q_\nu}{m^2}) \times \lambda_2\epsilon^\star_\nu(p_3)$
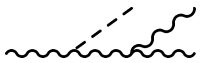	vsv-vvv	$\lambda_1\epsilon_\mu(P) \times (-g_{\mu\nu} + \frac{q_\mu q_\nu}{m^2}) \times i\lambda_2\epsilon^\star_\rho(p_2)\epsilon^\star_\sigma(p_3)$ $\lambda_2(g^{\nu\sigma}(q+p_3)^\rho + g^{\sigma\rho}(p_2-p_3)^\nu - g^{\rho\nu}(p_2+q)^\sigma)$
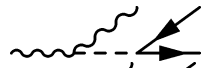	vvs-sff	$\lambda_1\epsilon(P)\cdot\epsilon^\star(p_1) \times \bar{u}(p_3)C_2 v(p_2)$
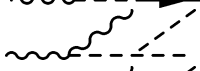	vvs-sss	$\lambda_1\epsilon(P)\cdot\epsilon^\star(p_1)\lambda_2$
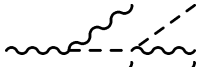	vvs-ssv	$\lambda_1\epsilon(P)\cdot\epsilon^\star(p_1) \times \lambda_2(q+p_2)\cdot\epsilon^\star(p_3)$
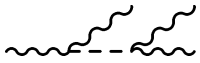	vvs-svv	$\lambda_1\epsilon(P)\cdot\epsilon^\star(p_1) \times \lambda_2\epsilon^\star(p_2)\cdot\epsilon^\star(p_3)$
	vvv-vff	$\lambda_1(g^{\kappa\mu}(P+q)^\lambda + g^{\mu\lambda}(p_1-q)^\kappa - g^{\lambda\kappa}(p_1+P)^\mu)$ $i\epsilon_\kappa(P)\epsilon^\star_\lambda(p_1) \times (-g_{\mu\nu} + \frac{q_\mu q_\nu}{m^2}) \times \bar{u}(p_3)\gamma_\mu C_2 v(p_2)$
	vvv-vss	$\lambda_1(g^{\kappa\mu}(P+q)^\lambda + g^{\mu\lambda}(p_1-q)^\kappa - g^{\lambda\kappa}(p_1+P)^\mu)$ $i\epsilon_\kappa(P)\epsilon^\star_\lambda(p_1) \times (-g_{\mu\nu} + \frac{q_\mu q_\nu}{m^2}) \times \lambda_2(p_2-p_3)_\nu$
	vvv-vsv	$\lambda_1(g^{\kappa\mu}(P+q)^\lambda + g^{\mu\lambda}(p_1-q)^\kappa - g^{\lambda\kappa}(p_1+P)^\mu)$ $i\epsilon_\kappa(P)\epsilon^\star_\lambda(p_1) \times (-g_{\mu\nu} + \frac{q_\mu q_\nu}{m^2}) \times \lambda_2\epsilon^\star_\nu(p_3)$
	vvv-vvv	$(g^{\kappa\mu}(P+q)^\lambda + g^{\mu\lambda}(p_1-q)^\kappa - g^{\lambda\kappa}(p_1+P)^\mu)$ $i\epsilon_\kappa(P)\epsilon^\star_\lambda(p_1) \times (-g_{\mu\nu} + \frac{q_\mu q_\nu}{m^2}) \times i\epsilon^\star_\rho(p_2)\epsilon^\star_\sigma(p_3)$ $\lambda_2(g^{\nu\sigma}(q+p_3)^\rho + g^{\sigma\rho}(p_2-p_3)^\nu - g^{\rho\nu}(p_2+q)^\sigma)$

Table A.3.: Diagrams and amplitudes for the resonant $1 \to 3$ decays. Details as in Table A.1.

Decay widths at SPS points

B

process	Γ_{ofs}/GeV	Γ_{NWA}/GeV	Γ_{sdecay}/GeV	Γ_{mg}/GeV
$\tilde{g} \to d\tilde{d}_L \to dd\tilde{\chi}_1^0$	0.003548	0.003258	0.003296	0.003556
$\tilde{g} \to d\tilde{d}_R \to dd\tilde{\chi}_1^0$	0.3369	0.3365	0.3404	0.3369
$\tilde{g} \to dd\tilde{\chi}_1^0$	$\sum \Gamma_{NWA} = 0.6795\,\text{GeV}$			0.6808
$\tilde{g} \to u\tilde{u}_L \to uu\tilde{\chi}_1^0$	0.001372	0.001297	0.001306	0.001370
$\tilde{g} \to u\tilde{u}_R \to uu\tilde{\chi}_1^0$	0.2983	0.2965	0.3000	0.2983
$\tilde{g} \to uu\tilde{\chi}_1^0$	$\sum \Gamma_{NWA} = 0.5955\,\text{GeV}$			0.5993
$\tilde{\chi}_1^+ \to \tilde{\chi}_1^0 W^+ \to \tilde{\chi}_1^0 ud$	$4.713 \cdot 10^{-4}$	$4.252 \cdot 10^{-4}$	$4.251 \cdot 10^{-4}$	$4.713 \cdot 10^{-4}$
$\tilde{\chi}_1^+ \to d\tilde{u}_L \to d\tilde{\chi}_1^0 u$	$6.138 \cdot 10^{-9}$	-	-	$6.144 \cdot 10^{-9}$
$\tilde{\chi}_1^+ \to u\tilde{d}_L \to u\tilde{\chi}_1^0 u$	$1.723 \cdot 10^{-8}$	-	-	$1.725 \cdot 10^{-8}$
$\tilde{\chi}_1^+ \to \tilde{\chi}_1^0 ud$	$\Gamma_{NWA} = 4.252 \cdot 10^{-4}\,\text{GeV}$			$4.731 \cdot 10^{-4}$
$\tilde{\chi}_1^+ \to \tilde{\chi}_1^0 W^+ \to \tilde{\chi}_1^0 e^+ \nu_e$	$1.571 \cdot 10^{-4}$	$1.417 \cdot 10^{-4}$	$1.371 \cdot 10^{-4}$	$1.571 \cdot 10^{-4}$
$\tilde{\chi}_1^+ \to e^+ \tilde{\nu}_e \to e^+ \tilde{\chi}_1^0 \nu_e$	$3.149 \cdot 10^{-5}$	-	-	$3.159 \cdot 10^{-5}$
$\tilde{\chi}_1^+ \to \nu_e \tilde{e}_L \to \nu_e \tilde{\chi}_1^0 e^+$	$6.184 \cdot 10^{-6}$	-	-	$6.188 \cdot 10^{-6}$
$\tilde{\chi}_1^+ \to \chi_1^0 e^+ \nu_e$	$\Gamma_{NWA} = 1.417 \cdot 10^{-4}\,\text{GeV}$			$1.935 \cdot 10^{-4}$

Table B.1.: Results for SPS 1a. SMadgraph results (Γ_{mg}) with $2 \cdot 10^7$ points and Monte Carlo error $\approx 0.1\%$. The matrix elements of Madgraph and off-shell are equal to at least 8 digits. The remaining deviations are due to the Monte Carlo integration. For SM particle branching ratios, values from the PDG have been used in SDecay results.

process	Γ_{ofs}/GeV	Γ_{NWA}/GeV	Γ_{sdecay}/GeV	Γ_{mg}/GeV
SPS 3				
$\tilde{\chi}_1^+ \to \tilde{\chi}_1^0 W^+ \to \tilde{\chi}_1^0 e^+ \nu_e$	0.001444	0.001465	0.001419	0.001446
$\tilde{\chi}_1^+ \to e^+ \tilde{\nu}_e \to e^+ \tilde{\chi}_1^0 \nu_e$	0.04288	0.04290	0.04290	0.04181
$\tilde{\chi}_1^+ \to \nu_e \tilde{e}_L \to \nu_e \tilde{\chi}_1^0 e^+$	0.01310	0.01305	0.01305	0.01304
$\tilde{\chi}_1^+ \to \chi_1^0 e^+ \nu_e$	$\sum \Gamma_{NWA} = 0.05742\,\text{GeV}$			0.05691
$\tilde{\chi}_2^0 \to \tilde{\chi}_1^0 Z \to \tilde{\chi}_1^0 e^+ e^-$	$3.946 \cdot 10^{-5}$	$4.022 \cdot 10^{-5}$	$3.915 \cdot 10^{-5}$	$3.951 \cdot 10^{-5}$
$\tilde{\chi}_2^0 \to e^- \tilde{e}_L \to e^- e^+ \tilde{\chi}_1^0$	0.005645	0.005614	0.005614	0.005644
$\tilde{\chi}_2^0 \to e^- \tilde{e}_R \to e^- e^+ \tilde{\chi}_1^0$	$8.508 \cdot 10^{-4}$	$8.504 \cdot 10^{-4}$	$8.328 \cdot 10^{-4}$	$8.457 \cdot 10^{-4}$
$\tilde{\chi}_2^0 \to \tilde{\chi}_1^0 e^+ e^-$	$\sum \Gamma_{NWA} = 0.01269\,\text{GeV}$			0.01300
SPS 9				
$\tilde{g} \to d \tilde{d}_L \to d u \tilde{\chi}_1^0$	0.03679	0.01057	0.01065	0.03718
$\tilde{g} \to u \tilde{u}_L \to u d \tilde{\chi}_1^0$	0.04694	0.01989	0.01998	0.04692
$\tilde{g} \to u d \tilde{\chi}_1^0$	$\sum \Gamma_{NWA} = 0.03046\,\text{GeV}$			0.08906

Table B.2.: Results for SPS 3 and SPS 9. Details as in Table B.1.

Decay fragments at SPS points

C

process	SPS	R	Γ/m in %	$(m+m_1)/M$	$(m_2+m_3)/m$
$H^\pm \to \tilde{\chi}_1^0 \tilde{\chi}_1^\pm \to \tilde{\chi}_1^0 \tilde{\chi}_1^0 W$	$1a$	28.0	0.009	0.683	0.975
$\tilde{\chi}_2^\pm \to e\tilde{\nu}_e \to ee\tilde{\chi}_1^\pm$	$1a$	180.1	0.081	0.488	0.981
$\tilde{\chi}_2^\pm \to e\tilde{\nu}_e \to e\nu_e\tilde{\chi}_2^0$	$1a$	133.7	0.081	0.488	0.977
$\tilde{\chi}_3^0 \to \nu_e\tilde{\nu}_e \to \nu_e e\tilde{\chi}_1^\pm$	$1a$	167.8	0.081	0.509	0.981
$\tilde{\chi}_3^0 \to \nu_e\tilde{\nu}_e \to \nu_e\nu_e\tilde{\chi}_2^0$	$1a$	124.6	0.081	0.509	0.977
$\tilde{\chi}_4^0 \to \nu_e\tilde{\nu}_e \to \nu_e e\tilde{\chi}_1^\pm$	$1a$	181.4	0.081	0.485	0.981
$\tilde{\chi}_4^0 \to \nu_e\tilde{\nu}_e \to \nu_e\nu_e\tilde{\chi}_2^0$	$1a$	134.7	0.081	0.485	0.977
$\tilde{\nu}_e \to e\tilde{\chi}_1^\pm \to e\tilde{\chi}_1^0 W$	$1a$	-22.5	0.009	0.981	0.975
$\tilde{\nu}_e \to \nu_e\tilde{\chi}_2^0 \to \nu_e\tilde{e}_R e$	$1a$	40.5	0.011	0.977	0.796
$\tilde{c}_L \to s\tilde{\chi}_1^\pm \to s\tilde{\chi}_1^0 W$	$1a$	39.2	0.009	0.326	0.975
$\tilde{d}_L \to u\tilde{\chi}_1^\pm \to u\tilde{\chi}_1^0 W$	$1a$	39.9	0.009	0.320	0.975
$\tilde{e}_L \to \nu_e\tilde{\chi}_1^\pm \to \nu_e\tilde{\chi}_1^0 W$	$1a$	-10.2	0.009	0.895	0.975
$\tilde{s}_L \to c\tilde{\chi}_1^\pm \to c\tilde{\chi}_1^0 W$	$1a$	39.9	0.009	0.322	0.975
$\tilde{t}_1 \to b\tilde{\chi}_1^\pm \to b\tilde{\chi}_1^0 W$	$1a$	23.7	0.009	0.465	0.975
$\tilde{t}_1 \to b\tilde{\chi}_2^\pm \to b\tilde{\chi}_1^0 W$	$1a$	15.5	0.655	0.961	0.466
$\tilde{t}_1 \to b\tilde{\chi}_2^\pm \to b\tilde{\nu}_e e$	$1a$	28.1	0.655	0.961	0.488
$\tilde{t}_1 \to b\tilde{\chi}_2^\pm \to b\tilde{e}_L\nu_e$	$1a$	25.4	0.655	0.961	0.534
$\tilde{t}_2 \to b\tilde{\chi}_1^\pm \to b\tilde{\chi}_1^0 W$	$1a$	41.7	0.009	0.317	0.975
$\tilde{u}_L \to d\tilde{\chi}_1^\pm \to d\tilde{\chi}_1^0 W$	$1a$	39.2	0.009	0.324	0.975
$\tilde{\chi}_2^\pm \to e\tilde{\nu}_e \to e\tilde{\chi}_1^\pm$	$1b$	11.9	0.093	0.618	0.942
$\tilde{\chi}_3^0 \to \nu_e\tilde{\nu}_e \to \nu_e\tilde{\chi}_1^\pm$	$1b$	11.0	0.093	0.631	0.942
$\tilde{\chi}_4^0 \to \nu_e\tilde{\nu}_e \to \nu_e\tilde{\chi}_1^\pm$	$1b$	12.1	0.093	0.616	0.942

Table C.1.: Specific processes in the MSSM at SPS points 1a and 1b. Here we show the processes with one unstable and two stable particels in the 'final state' and with $|R| > 5$. The charge assignments are not written explicitly except of the charged Higgs and Charginos to distinguish them from the neutral particles.

process	SPS	R	Γ/m in %	$(m+m_1)/M$	$(m_2+m_3)/m$
$H^\pm \to \tilde{\chi}_1^0\tilde{\chi}_1^\pm \to \tilde{\chi}_1^0\tilde{\chi}_1^0 W$	2	23.6	0.003	0.238	0.856
$\tilde{\nu}_e \to e\tilde{\chi}_1^\pm \to e\tilde{\chi}_1^0 W$	2	12.5	0.003	0.163	0.856
$\tilde{c}_L \to s\tilde{\chi}_1^\pm \to s\tilde{\chi}_1^0 W$	2	13.8	0.003	0.153	0.856
$\tilde{d}_L \to u\tilde{\chi}_1^\pm \to u\tilde{\chi}_1^0 W$	2	13.8	0.003	0.152	0.856
$\tilde{e}_L \to \nu_e\tilde{\chi}_1^\pm \to \nu_e\tilde{\chi}_1^0 W$	2	12.5	0.003	0.163	0.856
$\tilde{s}_L \to c\tilde{\chi}_1^\pm \to c\tilde{\chi}_1^0 W$	2	13.8	0.003	0.153	0.856
$\tilde{t}_2 \to b\tilde{\chi}_1^\pm \to b\tilde{\chi}_1^0 W$	2	10.5	0.003	0.186	0.856
$\tilde{u}_L \to d\tilde{\chi}_1^\pm \to d\tilde{\chi}_1^0 W$	2	13.8	0.003	0.153	0.856
$H^0 \to \tilde{e}_R\tilde{e}_R \to \tilde{e}_R e\tilde{\chi}_1^0$	3	10.8	0.022	0.614	0.889
$\tilde{\nu}_e \to \nu_e\tilde{\chi}_4^0 \to \nu_e h^0\tilde{\chi}_1^0$	4	15.3	0.499	0.944	0.560
$\tilde{c}_L \to c\tilde{g} \to c\tilde{b}_1 b$	4	14.7	0.287	0.967	0.840
$\tilde{c}_R \to c\tilde{g} \to c\tilde{b}_1 b$	4	14.5	0.287	0.982	0.840
$\tilde{c}_R \to c\tilde{g} \to c\tilde{b}_2 b$	4	10.4	0.287	0.982	0.934
$\tilde{d}_R \to d\tilde{g} \to d\tilde{b}_1 b$	4	42.8	0.287	0.987	0.840
$\tilde{d}_R \to d\tilde{g} \to d\tilde{b}_2 b$	4	34.8	0.287	0.987	0.934
$\tilde{e}_R \to e\tilde{\chi}_3^0 \to e\tilde{\chi}_1^0 Z$	4	22.2	0.508	0.961	0.528
$\tilde{e}_R \to e\tilde{\chi}_3^0 \to eh^0\tilde{\chi}_1^0$	4	32.4	0.508	0.961	0.582
$\tilde{e}_R \to e\tilde{\chi}_4^0 \to e\tilde{\chi}_1^0 Z$	4	4936.4	0.499	0.998	0.508
$\tilde{e}_R \to e\tilde{\chi}_4^0 \to eh^0\tilde{\chi}_1^0$	4	6739.9	0.499	0.998	0.560
$\tilde{s}_R \to s\tilde{g} \to s\tilde{b}_1 b$	4	43.0	0.287	0.988	0.840
$\tilde{s}_R \to s\tilde{g} \to s\tilde{b}_2 b$	4	35.1	0.287	0.988	0.934
$\tilde{t}_2 \to \tilde{b}_1 W \to \tilde{b}_1 cs$	4	32.8	2.491	0.996	0.027
$\tilde{t}_2 \to \tilde{b}_1 W \to \tilde{b}_1 e\nu_e$	4	32.8	2.491	0.996	≈ 0
$\tilde{t}_2 \to \tilde{b}_1 W \to \tilde{b}_1 ud$	4	32.8	2.491	0.996	≈ 0
$\tilde{t}_2 \to W\tilde{b}_1 \to Wb\tilde{\chi}_1^0$	4	756.9	1.018	0.996	0.204
$\tilde{u}_L \to u\tilde{g} \to u\tilde{b}_1 b$	4	14.6	0.287	0.965	0.840
$\tilde{u}_R \to u\tilde{g} \to u\tilde{b}_1 b$	4	14.4	0.287	0.981	0.840
$\tilde{u}_R \to u\tilde{g} \to u\tilde{b}_2 b$	4	10.3	0.287	0.981	0.934

Table C.2.: Specific processes in the MSSM at SPS points 2, 3 and 4. Details as in Table C.1.

process	SPS	R	Γ/m in %	$(m+m_1)/M$	$(m_2+m_3)/m$
$\tilde{\chi}_2^\pm \to e\tilde{\nu}_e \to ee\tilde{\chi}_1^\pm$	5	29.9	0.097	0.383	0.941
$\tilde{\chi}_2^\pm \to e\tilde{\nu}_e \to e\nu_e\tilde{\chi}_2^0$	5	30.4	0.097	0.383	0.941
$\tilde{\chi}_2^\pm \to \nu_e\tilde{e}_L \to \nu_e e\tilde{\chi}_2^0$	5	10.2	0.112	0.400	0.902
$\tilde{\chi}_2^\pm \to \nu_e\tilde{e}_L \to \nu_e\nu_e\tilde{\chi}_1^\pm$	5	10.1	0.112	0.400	0.902
$\tilde{\chi}_3^0 \to e\tilde{e}_L \to ee\tilde{\chi}_2^0$	5	10.2	0.112	0.400	0.902
$\tilde{\chi}_3^0 \to e\tilde{e}_L \to e\nu_e\tilde{\chi}_1^\pm$	5	10.1	0.112	0.400	0.902
$\tilde{\chi}_3^0 \to \nu_e\tilde{\nu}_e \to \nu_e e\tilde{\chi}_1^\pm$	5	29.8	0.097	0.384	0.941
$\tilde{\chi}_3^0 \to \nu_e\tilde{\nu}_e \to \nu_e\nu_e\tilde{\chi}_2^0$	5	30.3	0.097	0.384	0.941
$\tilde{\chi}_4^0 \to e\tilde{e}_L \to ee\tilde{\chi}_2^0$	5	10.4	0.112	0.394	0.902
$\tilde{\chi}_4^0 \to e\tilde{e}_L \to e\nu_e\tilde{\chi}_1^\pm$	5	10.3	0.112	0.394	0.902
$\tilde{\chi}_4^0 \to \nu_e\tilde{\nu}_e \to \nu_e e\tilde{\chi}_1^\pm$	5	30.4	0.097	0.378	0.941
$\tilde{\chi}_4^0 \to \nu_e\tilde{\nu}_e \to \nu_e\nu_e\tilde{\chi}_2^0$	5	30.9	0.097	0.378	0.941
$\tilde{b}_2 \to b\tilde{\chi}_3^0 \to b\tilde{\chi}_1^0 Z$	5	290.9	1.556	0.995	0.329
$\tilde{b}_2 \to b\tilde{\chi}_3^0 \to b\tilde{\nu}_e\nu_e$	5	527.2	1.556	0.995	0.384
$\tilde{b}_2 \to b\tilde{\chi}_3^0 \to b\tilde{b}_1 b$	5	85.1	1.556	0.995	0.879
$\tilde{b}_2 \to b\tilde{\chi}_3^0 \to b\tilde{e}_L e$	5	514.5	1.556	0.995	0.400
$\tilde{b}_2 \to b\tilde{\chi}_3^0 \to b\tilde{e}_R e$	5	363.5	1.556	0.995	0.301
$\tilde{b}_2 \to b\tilde{\chi}_3^0 \to bh^0\tilde{\chi}_1^0$	5	469.6	1.556	0.995	0.365
$\tilde{c}_L \to c\tilde{\chi}_3^0 \to c\tilde{\chi}_1^0 Z$	5	12.5	1.556	0.951	0.329
$\tilde{c}_L \to c\tilde{\chi}_3^0 \to c\tilde{\nu}_e\nu_e$	5	28.3	1.556	0.951	0.384
$\tilde{c}_L \to c\tilde{\chi}_3^0 \to c\tilde{e}_L e$	5	27.6	1.556	0.951	0.400
$\tilde{c}_L \to c\tilde{\chi}_3^0 \to c\tilde{e}_R e$	5	16.7	1.556	0.951	0.301
$\tilde{c}_L \to c\tilde{\chi}_3^0 \to ch^0\tilde{\chi}_1^0$	5	24.0	1.556	0.951	0.365
$\tilde{c}_L \to c\tilde{\chi}_4^0 \to c\tilde{\chi}_1^0 Z$	5	26.0	2.921	0.965	0.324
$\tilde{c}_L \to c\tilde{\chi}_4^0 \to c\tilde{\nu}_e\nu_e$	5	54.0	2.921	0.965	0.378
$\tilde{c}_L \to c\tilde{\chi}_4^0 \to c\tilde{e}_L e$	5	52.7	2.921	0.965	0.394
$\tilde{c}_L \to c\tilde{\chi}_4^0 \to c\tilde{e}_R e$	5	33.2	2.921	0.965	0.297
$\tilde{c}_L \to c\tilde{\chi}_4^0 \to ch^0\tilde{\chi}_1^0$	5	46.2	2.921	0.965	0.360
$\tilde{c}_L \to s\tilde{\chi}_2^\pm \to s\tilde{\chi}_1^0 W$	5	15.3	1.924	0.952	0.312
$\tilde{c}_L \to s\tilde{\chi}_2^\pm \to s\tilde{\nu}_e e$	5	29.6	1.924	0.952	0.383
$\tilde{c}_L \to s\tilde{\chi}_2^\pm \to s\tilde{e}_L\nu_e$	5	28.9	1.924	0.952	0.400
$\tilde{c}_L \to s\tilde{\chi}_2^\pm \to s\tilde{t}_1 b$	5	28.2	1.924	0.952	0.416
$\tilde{c}_R \to c\tilde{\chi}_3^0 \to c\tilde{\chi}_1^0 Z$	5	56.6	1.556	0.976	0.329
$\tilde{c}_R \to c\tilde{\chi}_3^0 \to c\tilde{\nu}_e\nu_e$	5	66.9	1.556	0.976	0.384
$\tilde{c}_R \to c\tilde{\chi}_3^0 \to c\tilde{b}_1 b$	5	16.9	1.556	0.976	0.879
$\tilde{c}_R \to c\tilde{\chi}_3^0 \to c\tilde{e}_L e$	5	66.1	1.556	0.976	0.400
$\tilde{c}_R \to c\tilde{\chi}_3^0 \to c\tilde{e}_R e$	5	120.1	1.556	0.976	0.301

Table C.3.: Specific processes in the MSSM at SPS point 5. Details as in Table C.1.

process	SPS	R	Γ/m in %	$(m+m_1)/M$	$(m_2+m_3)/m$
$\tilde{c}_R \to c\tilde{\chi}_3^0 \to ch^0\tilde{\chi}_1^0$	5	94.2	1.556	0.976	0.365
$\tilde{c}_R \to c\tilde{\chi}_4^0 \to c\tilde{\chi}_1^0 Z$	5	306.4	2.921	0.991	0.324
$\tilde{c}_R \to c\tilde{\chi}_4^0 \to c\tilde{\nu}_e\nu_e$	5	359.6	2.921	0.991	0.378
$\tilde{c}_R \to c\tilde{\chi}_4^0 \to c\tilde{b}_1 b$	5	69.1	2.921	0.991	0.866
$\tilde{c}_R \to c\tilde{\chi}_4^0 \to c\tilde{e}_L e$	5	355.2	2.921	0.991	0.394
$\tilde{c}_R \to c\tilde{\chi}_4^0 \to c\tilde{e}_R e$	5	655.3	2.921	0.991	0.297
$\tilde{c}_R \to c\tilde{\chi}_4^0 \to ch^0\tilde{\chi}_1^0$	5	510.6	2.921	0.991	0.360
$\tilde{d}_L \to d\tilde{\chi}_3^0 \to d\tilde{\nu}_e\nu_e$	5	23.6	1.556	0.944	0.384
$\tilde{d}_L \to d\tilde{\chi}_3^0 \to d\tilde{e}_L e$	5	23.0	1.556	0.944	0.400
$\tilde{d}_L \to d\tilde{\chi}_3^0 \to d\tilde{e}_R e$	5	13.6	1.556	0.944	0.301
$\tilde{d}_L \to d\tilde{\chi}_3^0 \to dh^0\tilde{\chi}_1^0$	5	19.9	1.556	0.944	0.365
$\tilde{d}_L \to d\tilde{\chi}_4^0 \to d\tilde{\chi}_1^0 Z$	5	19.8	2.921	0.959	0.324
$\tilde{d}_L \to d\tilde{\chi}_4^0 \to d\tilde{\nu}_e\nu_e$	5	42.3	2.921	0.959	0.378
$\tilde{d}_L \to d\tilde{\chi}_4^0 \to d\tilde{e}_L e$	5	41.3	2.921	0.959	0.394
$\tilde{d}_L \to d\tilde{\chi}_4^0 \to d\tilde{e}_R e$	5	25.6	2.921	0.959	0.297
$\tilde{d}_L \to d\tilde{\chi}_4^0 \to dh^0\tilde{\chi}_1^0$	5	36.1	2.921	0.959	0.360
$\tilde{d}_L \to u\tilde{\chi}_2^\pm \to u\tilde{\chi}_1^0 W$	5	12.3	1.924	0.945	0.312
$\tilde{d}_L \to u\tilde{\chi}_2^\pm \to u\tilde{\nu}_e e$	5	24.7	1.924	0.945	0.383
$\tilde{d}_L \to u\tilde{\chi}_2^\pm \to u\tilde{e}_L\nu_e$	5	24.0	1.924	0.945	0.400
$\tilde{d}_L \to u\tilde{\chi}_2^\pm \to u\tilde{t}_1 b$	5	23.5	1.924	0.945	0.416
$\tilde{d}_R \to d\tilde{\chi}_3^0 \to d\tilde{\chi}_1^0 Z$	5	123.5	1.556	0.983	0.329
$\tilde{d}_R \to d\tilde{\chi}_3^0 \to d\tilde{\nu}_e\nu_e$	5	144.2	1.556	0.983	0.384
$\tilde{d}_R \to d\tilde{\chi}_3^0 \to d\tilde{b}_1 b$	5	42.9	1.556	0.983	0.879
$\tilde{d}_R \to d\tilde{\chi}_3^0 \to d\tilde{e}_L e$	5	142.5	1.556	0.983	0.400
$\tilde{d}_R \to d\tilde{\chi}_3^0 \to d\tilde{e}_R e$	5	255.8	1.556	0.983	0.301
$\tilde{d}_R \to d\tilde{\chi}_3^0 \to dh^0\tilde{\chi}_1^0$	5	201.4	1.556	0.983	0.365
$\tilde{d}_R \to d\tilde{\chi}_4^0 \to d\tilde{\chi}_1^0 Z$	5	8279.6	2.921	0.998	0.324
$\tilde{d}_R \to d\tilde{\chi}_4^0 \to d\tilde{\nu}_e\nu_e$	5	9764.7	2.921	0.998	0.378
$\tilde{d}_R \to d\tilde{\chi}_4^0 \to d\tilde{b}_1 b$	5	1832.3	2.921	0.998	0.866
$\tilde{d}_R \to d\tilde{\chi}_4^0 \to d\tilde{e}_L e$	5	9638.2	2.921	0.998	0.394
$\tilde{d}_R \to d\tilde{\chi}_4^0 \to d\tilde{e}_R e$	5	18328	2.921	0.998	0.297
$\tilde{d}_R \to d\tilde{\chi}_4^0 \to dh^0\tilde{\chi}_1^0$	5	14121.2	2.921	0.998	0.360
$\tilde{g} \to b\tilde{b}_2 \to bb\tilde{\chi}_3^0$	5	60.4	0.102	0.903	0.995
$\tilde{g} \to c\tilde{c}_L \to cc\tilde{\chi}_3^0$	5	−12.6	0.975	0.937	0.951

Table C.4.: Specific processes in the MSSM at SPS point 5. Details as in Table C.1.

process	SPS	R	Γ/m in %	$(m+m_1)/M$	$(m_2+m_3)/m$
$\tilde{g} \to c\tilde{c}_L \to cc\tilde{\chi}_4^0$	5	-12.8	0.975	0.937	0.965
$\tilde{g} \to c\tilde{c}_L \to cs\tilde{\chi}_2^\pm$	5	-12.6	0.975	0.937	0.952
$\tilde{g} \to c\tilde{c}_R \to cc\tilde{\chi}_4^0$	5	56.2	0.211	0.913	0.991
$\tilde{g} \to d\tilde{d}_L \to dd\tilde{\chi}_3^0$	5	-12.9	0.956	0.940	0.944
$\tilde{g} \to d\tilde{d}_L \to dd\tilde{\chi}_4^0$	5	-13.8	0.956	0.940	0.959
$\tilde{g} \to d\tilde{d}_L \to du\tilde{\chi}_2^\pm$	5	-13.0	0.956	0.940	0.945
$\tilde{g} \to d\tilde{d}_R \to dd\tilde{\chi}_3^0$	5	15.2	0.053	0.903	0.983
$\tilde{g} \to d\tilde{d}_R \to dd\tilde{\chi}_4^0$	5	1992.0	0.053	0.903	0.998
$\tilde{g} \to s\tilde{s}_L \to sc\tilde{\chi}_2^\pm$	5	-13.0	0.956	0.941	0.947
$\tilde{g} \to s\tilde{s}_L \to ss\tilde{\chi}_3^0$	5	-12.9	0.956	0.941	0.945
$\tilde{g} \to s\tilde{s}_L \to ss\tilde{\chi}_4^0$	5	-13.8	0.956	0.941	0.960
$\tilde{g} \to s\tilde{s}_R \to ss\tilde{\chi}_3^0$	5	15.3	0.053	0.904	0.984
$\tilde{g} \to s\tilde{s}_R \to ss\tilde{\chi}_4^0$	5	3284.3	0.053	0.904	≈ 1
$\tilde{g} \to u\tilde{u}_L \to ud\tilde{\chi}_2^\pm$	5	-12.6	0.975	0.935	0.950
$\tilde{g} \to u\tilde{u}_L \to uu\tilde{\chi}_3^0$	5	-12.5	0.975	0.935	0.949
$\tilde{g} \to u\tilde{u}_L \to uu\tilde{\chi}_4^0$	5	-12.8	0.975	0.935	0.964
$\tilde{g} \to u\tilde{u}_R \to uu\tilde{\chi}_4^0$	5	54.9	0.211	0.911	0.990
$\tilde{s}_L \to c\tilde{\chi}_2^\pm \to c\tilde{\chi}_1^0 W$	5	12.3	1.924	0.947	0.312
$\tilde{s}_L \to c\tilde{\chi}_2^\pm \to c\tilde{\nu}_e e$	5	24.7	1.924	0.947	0.383
$\tilde{s}_L \to c\tilde{\chi}_2^\pm \to c\tilde{e}_L \nu_e$	5	24.1	1.924	0.947	0.400
$\tilde{s}_L \to c\tilde{\chi}_2^\pm \to c\tilde{t}_1 b$	5	23.5	1.924	0.947	0.416
$\tilde{s}_L \to s\tilde{\chi}_3^0 \to s\tilde{\chi}_1^0 Z$	5	10.0	1.556	0.945	0.329
$\tilde{s}_L \to s\tilde{\chi}_3^0 \to s\tilde{\nu}_e \nu_e$	5	23.7	1.556	0.945	0.384
$\tilde{s}_L \to s\tilde{\chi}_3^0 \to s\tilde{e}_L e$	5	23.1	1.556	0.945	0.400
$\tilde{s}_L \to s\tilde{\chi}_3^0 \to s\tilde{e}_R e$	5	13.6	1.556	0.945	0.301
$\tilde{s}_L \to s\tilde{\chi}_3^0 \to sh^0\tilde{\chi}_1^0$	5	19.9	1.556	0.945	0.365
$\tilde{s}_L \to s\tilde{\chi}_4^0 \to s\tilde{\chi}_1^0 Z$	5	19.8	2.921	0.960	0.324
$\tilde{s}_L \to s\tilde{\chi}_4^0 \to s\tilde{\nu}_e \nu_e$	5	42.3	2.921	0.960	0.378
$\tilde{s}_L \to s\tilde{\chi}_4^0 \to s\tilde{e}_L e$	5	41.3	2.921	0.960	0.394
$\tilde{s}_L \to s\tilde{\chi}_4^0 \to s\tilde{e}_R e$	5	25.6	2.921	0.960	0.297
$\tilde{s}_L \to s\tilde{\chi}_4^0 \to sh^0\tilde{\chi}_1^0$	5	36.1	2.921	0.960	0.360
$\tilde{s}_R \to s\tilde{\chi}_3^0 \to s\tilde{\chi}_1^0 Z$	5	124.0	1.556	0.984	0.329
$\tilde{s}_R \to s\tilde{\chi}_3^0 \to s\tilde{\nu}_e \nu_e$	5	144.7	1.556	0.984	0.384
$\tilde{s}_R \to s\tilde{\chi}_3^0 \to s\tilde{b}_1 b$	5	43.1	1.556	0.984	0.879
$\tilde{s}_R \to s\tilde{\chi}_3^0 \to s\tilde{e}_L e$	5	143.0	1.556	0.984	0.400
$\tilde{s}_R \to s\tilde{\chi}_3^0 \to s\tilde{e}_R e$	5	256.8	1.556	0.984	0.301
$\tilde{s}_R \to s\tilde{\chi}_3^0 \to sh^0\tilde{\chi}_1^0$	5	202.2	1.556	0.984	0.365

Table C.5.: Specific processes in the MSSM at SPS point 5. Details as in Table C.1.

process	SPS	R	Γ/m in %	$(m+m_1)/M$	$(m_2+m_3)/m$
$\tilde{s}_R \to s\tilde{\chi}_4^0 \to s\tilde{\chi}_1^0 Z$	5	13356.5	2.921	≈ 1	0.324
$\tilde{s}_R \to s\tilde{\chi}_4^0 \to s\tilde{\nu}_e\nu_e$	5	15749.8	2.921	≈ 1	0.378
$\tilde{s}_R \to s\tilde{\chi}_4^0 \to s\tilde{b}_1 b$	5	2967.1	2.921	≈ 1	0.866
$\tilde{s}_R \to s\tilde{\chi}_4^0 \to s\tilde{e}_L e$	5	15545.9	2.921	≈ 1	0.394
$\tilde{s}_R \to s\tilde{\chi}_4^0 \to s\tilde{e}_R e$	5	29550.1	2.921	≈ 1	0.297
$\tilde{s}_R \to s\tilde{\chi}_4^0 \to sh^0\tilde{\chi}_1^0$	5	22770.6	2.921	≈ 1	0.360
$\tilde{t}_2 \to b\tilde{\chi}_2^\pm \to b\tilde{\chi}_1^0 W$	5	215.5	1.924	0.993	0.312
$\tilde{t}_2 \to b\tilde{\chi}_2^\pm \to b\tilde{\nu}_e e$	5	364.5	1.924	0.993	0.383
$\tilde{t}_2 \to b\tilde{\chi}_2^\pm \to b\tilde{e}_L\nu_e$	5	355.6	1.924	0.993	0.400
$\tilde{t}_2 \to b\tilde{\chi}_2^\pm \to b\tilde{t}_1 b$	5	347.9	1.924	0.993	0.416
$\tilde{t}_2 \to W\tilde{b}_1 \to Wb\tilde{\chi}_1^0$	5	62.4	2.807	0.983	0.221
$\tilde{u}_L \to d\tilde{\chi}_2^\pm \to d\tilde{\chi}_1^0 W$	5	15.3	1.924	0.950	0.312
$\tilde{u}_L \to d\tilde{\chi}_2^\pm \to d\tilde{\nu}_e e$	5	29.6	1.924	0.950	0.383
$\tilde{u}_L \to d\tilde{\chi}_2^\pm \to d\tilde{e}_L\nu_e$	5	28.9	1.924	0.950	0.400
$\tilde{u}_L \to d\tilde{\chi}_2^\pm \to d\tilde{t}_1 b$	5	28.2	1.924	0.950	0.416
$\tilde{u}_L \to u\tilde{\chi}_3^0 \to u\tilde{\chi}_1^0 Z$	5	12.5	1.556	0.949	0.329
$\tilde{u}_L \to u\tilde{\chi}_3^0 \to u\tilde{\nu}_e\nu_e$	5	28.3	1.556	0.949	0.384
$\tilde{u}_L \to u\tilde{\chi}_3^0 \to u\tilde{e}_L e$	5	27.6	1.556	0.949	0.400
$\tilde{u}_L \to u\tilde{\chi}_3^0 \to u\tilde{e}_R e$	5	16.7	1.556	0.949	0.301
$\tilde{u}_L \to u\tilde{\chi}_3^0 \to uh^0\tilde{\chi}_1^0$	5	24.0	1.556	0.949	0.365
$\tilde{u}_L \to u\tilde{\chi}_4^0 \to u\tilde{\chi}_1^0 Z$	5	26.0	2.921	0.964	0.324
$\tilde{u}_L \to u\tilde{\chi}_4^0 \to u\tilde{\nu}_e\nu_e$	5	53.9	2.921	0.964	0.378
$\tilde{u}_L \to u\tilde{\chi}_4^0 \to u\tilde{e}_L e$	5	52.6	2.921	0.964	0.394
$\tilde{u}_L \to u\tilde{\chi}_4^0 \to u\tilde{e}_R e$	5	33.1	2.921	0.964	0.297
$\tilde{u}_L \to u\tilde{\chi}_4^0 \to uh^0\tilde{\chi}_1^0$	5	46.1	2.921	0.964	0.360
$\tilde{u}_R \to u\tilde{\chi}_3^0 \to u\tilde{\chi}_1^0 Z$	5	56.5	1.556	0.974	0.329
$\tilde{u}_R \to u\tilde{\chi}_3^0 \to u\tilde{\nu}_e\nu_e$	5	66.6	1.556	0.974	0.384
$\tilde{u}_R \to u\tilde{\chi}_3^0 \to u\tilde{b}_1 b$	5	16.9	1.556	0.974	0.879
$\tilde{u}_R \to u\tilde{\chi}_3^0 \to u\tilde{e}_L e$	5	65.9	1.556	0.974	0.400
$\tilde{u}_R \to u\tilde{\chi}_3^0 \to u\tilde{e}_R e$	5	119.7	1.556	0.974	0.301
$\tilde{u}_R \to u\tilde{\chi}_3^0 \to uh^0\tilde{\chi}_1^0$	5	94.0	1.556	0.974	0.365
$\tilde{u}_R \to u\tilde{\chi}_4^0 \to u\tilde{\chi}_1^0 Z$	5	301.0	2.921	0.990	0.324
$\tilde{u}_R \to u\tilde{\chi}_4^0 \to u\tilde{\nu}_e\nu_e$	5	353.3	2.921	0.990	0.378
$\tilde{u}_R \to u\tilde{\chi}_4^0 \to u\tilde{b}_1 b$	5	67.7	2.921	0.990	0.866
$\tilde{u}_R \to u\tilde{\chi}_4^0 \to u\tilde{e}_L e$	5	349.1	2.921	0.990	0.394
$\tilde{u}_R \to u\tilde{\chi}_4^0 \to u\tilde{e}_R e$	5	644.0	2.921	0.990	0.297
$\tilde{u}_R \to u\tilde{\chi}_4^0 \to uh^0\tilde{\chi}_1^0$	5	501.8	2.921	0.990	0.360

Table C.6.: Specific processes in the MSSM at SPS point 5. Details as in Table C.1.

process	SPS	R	Γ/m in %	$(m+m_1)/M$	$(m_2+m_3)/m$
$\tilde{\chi}_3^0 \to e\tilde{e}_R \to ee\tilde{\chi}_2^0$	6	23.5	0.062	0.556	0.951
$\tilde{\chi}_4^0 \to e\tilde{e}_R \to ee\tilde{\chi}_2^0$	6	25.6	0.062	0.534	0.951
$A^0 \to \tilde{\tau}_1\tilde{\tau}_2 \to \tilde{\tau}_1\tilde{\tau}_1 Z$	7	-16.7	0.062	0.992	0.808
$A^0 \to \tilde{\tau}_1\tilde{\tau}_2 \to \tilde{\tau}_1 h^0\tilde{\tau}_1$	7	-13.1	0.062	0.992	0.886
$H^0 \to \tilde{\tau}_1\tilde{\tau}_2 \to \tilde{\tau}_1\tilde{\tau}_1 Z$	7	-15.8	0.062	0.991	0.808
$H^0 \to \tilde{\tau}_1\tilde{\tau}_2 \to \tilde{\tau}_1 h^0\tilde{\tau}_1$	7	-12.5	0.062	0.991	0.886
$\tilde{\chi}_1^\pm \to \nu_e\tilde{e}_L \to \nu_e e\tilde{\chi}_1^0$	7	58.1	0.036	0.979	0.620
$\tilde{\chi}_2^0 \to e\tilde{e}_L \to ee\tilde{\chi}_1^0$	7	21.7	0.036	0.967	0.62
$\tilde{\chi}_4^0 \to h^0\tilde{\chi}_2^0 \to h^0\tilde{e}_R e$	7	-11.8	0.080	0.995	0.477
$\tilde{g} \to c\tilde{c}_L \to cc\tilde{\chi}_1^0$	7	12.9	0.944	0.944	0.184
$\tilde{g} \to c\tilde{c}_L \to cc\tilde{\chi}_2^0$	7	11.3	0.944	0.944	0.305
$\tilde{g} \to c\tilde{c}_L \to cc\tilde{\chi}_3^0$	7	10.4	0.944	0.944	0.358
$\tilde{g} \to c\tilde{c}_L \to cs\tilde{\chi}_1^\pm$	7	11.3	0.944	0.944	0.301
$\tilde{g} \to d\tilde{d}_L \to dd\tilde{\chi}_1^0$	7	18.5	0.926	0.951	0.181
$\tilde{g} \to d\tilde{d}_L \to dd\tilde{\chi}_2^0$	7	16.4	0.926	0.951	0.301
$\tilde{g} \to d\tilde{d}_L \to dd\tilde{\chi}_3^0$	7	15.3	0.926	0.951	0.353
$\tilde{g} \to d\tilde{d}_L \to dd\tilde{\chi}_4^0$	7	13.4	0.926	0.951	0.427
$\tilde{g} \to d\tilde{d}_L \to du\tilde{\chi}_1^\pm$	7	16.5	0.926	0.951	0.298
$\tilde{g} \to d\tilde{d}_L \to du\tilde{\chi}_2^\pm$	7	13.4	0.926	0.951	0.427
$\tilde{g} \to s\tilde{s}_L \to sc\tilde{\chi}_1^\pm$	7	16.5	0.926	0.952	0.299
$\tilde{g} \to s\tilde{s}_L \to sc\tilde{\chi}_2^\pm$	7	13.4	0.926	0.952	0.428
$\tilde{g} \to s\tilde{s}_L \to ss\tilde{\chi}_1^0$	7	18.5	0.926	0.952	0.182
$\tilde{g} \to s\tilde{s}_L \to ss\tilde{\chi}_2^0$	7	16.4	0.926	0.952	0.302
$\tilde{g} \to s\tilde{s}_L \to ss\tilde{\chi}_3^0$	7	15.3	0.926	0.952	0.354
$\tilde{g} \to s\tilde{s}_L \to ss\tilde{\chi}_4^0$	7	13.4	0.926	0.952	0.428
$\tilde{g} \to u\tilde{u}_L \to ud\tilde{\chi}_1^\pm$	7	11.3	0.944	0.943	0.300
$\tilde{g} \to u\tilde{u}_L \to uu\tilde{\chi}_1^0$	7	12.9	0.944	0.943	0.182
$\tilde{g} \to u\tilde{u}_L \to uu\tilde{\chi}_2^0$	7	11.3	0.944	0.943	0.304
$\tilde{g} \to u\tilde{u}_L \to uu\tilde{\chi}_3^0$	7	10.4	0.944	0.943	0.356
$\tilde{t}_2 \to b\tilde{\chi}_1^\pm \to b\tilde{e}_L\nu_e$	7	11.3	0.049	0.306	0.979

Table C.7.: Specific processes in the MSSM at SPS points 6 and 7. Details as in Table C.1.

process	SPS	R	Γ/m in %	$(m+m_1)/M$	$(m_2+m_3)/m$
$\tilde{b}_1 \to \tilde{t}_1 W \to \tilde{t}_1 cs$	8	95.1	2.491	0.999	0.027
$\tilde{b}_1 \to \tilde{t}_1 W \to \tilde{t}_1 e\nu_e$	8	95.1	2.491	0.999	≈ 0
$\tilde{b}_1 \to \tilde{t}_1 W \to \tilde{t}_1 ud$	8	95.1	2.491	0.999	≈ 0
$\tilde{b}_1 \to b\tilde{\chi}_3^0 \to b\tilde{e}_R e$	9	17.4	0.704	0.936	0.306
$\tilde{b}_1 \to b\tilde{\chi}_4^0 \to b\tilde{\nu}_e \nu_e$	9	10.5	0.712	0.939	0.307
$\tilde{b}_1 \to b\tilde{\chi}_4^0 \to b\tilde{e}_L e$	9	10.4	0.712	0.939	0.321
$\tilde{b}_1 \to b\tilde{\chi}_4^0 \to b\tilde{e}_R e$	9	18.5	0.712	0.939	0.304
$\tilde{b}_2 \to W\tilde{t}_2 \to Wb\tilde{\chi}_1^\pm$	9	50.4	≈ 0	0.971	0.178
$\tilde{g} \to b\tilde{b}_2 \to bb\tilde{\chi}_1^0$	9	76.2	0.037	0.978	0.161
$\tilde{g} \to b\tilde{b}_2 \to bb\tilde{\chi}_2^0$	9	57.9	0.037	0.978	0.441
$\tilde{g} \to b\tilde{b}_2 \to bb\tilde{\chi}_3^0$	9	13.7	0.037	0.978	0.821
$\tilde{g} \to b\tilde{b}_2 \to bb\tilde{\chi}_4^0$	9	13.2	0.037	0.978	0.825
$\tilde{g} \to b\tilde{b}_2 \to bt\tilde{\chi}_1^\pm$	9	73.0	0.037	0.978	0.297
$\tilde{g} \to c\tilde{c}_L \to cc\tilde{\chi}_1^0$	9	114.3	1.191	0.981	0.158
$\tilde{g} \to c\tilde{c}_L \to cc\tilde{\chi}_2^0$	9	86.8	1.191	0.981	0.436
$\tilde{g} \to c\tilde{c}_L \to cc\tilde{\chi}_3^0$	9	24.4	1.191	0.981	0.815
$\tilde{g} \to c\tilde{c}_L \to cc\tilde{\chi}_4^0$	9	23.6	1.191	0.981	0.818
$\tilde{g} \to c\tilde{c}_L \to cs\tilde{\chi}_2^\pm$	9	24.8	1.191	0.981	0.812
$\tilde{g} \to c\tilde{c}_R \to cc\tilde{\chi}_1^0$	9	274.9	0.145	0.988	0.157
$\tilde{g} \to c\tilde{c}_R \to cc\tilde{\chi}_2^0$	9	213.2	0.145	0.988	0.433
$\tilde{g} \to c\tilde{c}_R \to cc\tilde{\chi}_3^0$	9	78.6	0.145	0.988	0.809
$\tilde{g} \to c\tilde{c}_R \to cc\tilde{\chi}_4^0$	9	77.1	0.145	0.988	0.812
$\tilde{g} \to d\tilde{d}_L \to dd\tilde{\chi}_1^0$	9	209.0	1.188	0.985	0.156
$\tilde{g} \to d\tilde{d}_L \to dd\tilde{\chi}_2^0$	9	159.9	1.188	0.985	0.433

Table C.8.: Specific processes in the MSSM at SPS points 8 and 9. Details as in Table C.1.

process	SPS	R	Γ/m in %	$(m+m_1)/M$	$(m_2+m_3)/m$
$\tilde{g} \to d\tilde{d}_L \to d d \tilde{\chi}_3^0$	9	52.8	1.188	0.985	0.809
$\tilde{g} \to d\tilde{d}_L \to d d \tilde{\chi}_4^0$	9	51.6	1.188	0.985	0.813
$\tilde{g} \to d\tilde{d}_L \to d u \tilde{\chi}_2^\pm$	9	53.6	1.188	0.985	0.807
$\tilde{g} \to d\tilde{d}_R \to d d \tilde{\chi}_1^0$	9	302.9	0.034	0.988	0.156
$\tilde{g} \to d\tilde{d}_R \to d d \tilde{\chi}_2^0$	9	235.3	0.034	0.988	0.432
$\tilde{g} \to d\tilde{d}_R \to d d \tilde{\chi}_3^0$	9	88.5	0.034	0.988	0.807
$\tilde{g} \to d\tilde{d}_R \to d d \tilde{\chi}_4^0$	9	86.9	0.034	0.988	0.811
$\tilde{g} \to s\tilde{s}_L \to s c \tilde{\chi}_2^\pm$	9	53.7	1.188	0.986	0.808
$\tilde{g} \to s\tilde{s}_L \to s s \tilde{\chi}_1^0$	9	209.3	1.188	0.986	0.157
$\tilde{g} \to s\tilde{s}_L \to s s \tilde{\chi}_2^0$	9	160.1	1.188	0.986	0.434
$\tilde{g} \to s\tilde{s}_L \to s s \tilde{\chi}_3^0$	9	52.9	1.188	0.986	0.810
$\tilde{g} \to s\tilde{s}_L \to s s \tilde{\chi}_4^0$	9	51.7	1.188	0.986	0.813
$\tilde{g} \to s\tilde{s}_R \to s s \tilde{\chi}_1^0$	9	303.4	0.034	0.988	0.156
$\tilde{g} \to s\tilde{s}_R \to s s \tilde{\chi}_2^0$	9	235.8	0.034	0.988	0.433
$\tilde{g} \to s\tilde{s}_R \to s s \tilde{\chi}_3^0$	9	88.7	0.034	0.988	0.808
$\tilde{g} \to s\tilde{s}_R \to s s \tilde{\chi}_4^0$	9	87.0	0.034	0.988	0.812
$\tilde{g} \to u\tilde{u}_L \to u d \tilde{\chi}_2^\pm$	9	24.8	1.191	0.980	0.812
$\tilde{g} \to u\tilde{u}_L \to u u \tilde{\chi}_1^0$	9	114.1	1.191	0.980	0.157
$\tilde{g} \to u\tilde{u}_L \to u u \tilde{\chi}_2^0$	9	86.7	1.191	0.980	0.435
$\tilde{g} \to u\tilde{u}_L \to u u \tilde{\chi}_3^0$	9	24.3	1.191	0.980	0.814
$\tilde{g} \to u\tilde{u}_L \to u u \tilde{\chi}_4^0$	9	23.6	1.191	0.980	0.817
$\tilde{g} \to u\tilde{u}_R \to u u \tilde{\chi}_1^0$	9	274.1	0.145	0.987	0.156
$\tilde{g} \to u\tilde{u}_R \to u u \tilde{\chi}_2^0$	9	212.6	0.145	0.987	0.432
$\tilde{g} \to u\tilde{u}_R \to u u \tilde{\chi}_3^0$	9	78.4	0.145	0.987	0.808
$\tilde{g} \to u\tilde{u}_R \to u u \tilde{\chi}_4^0$	9	76.8	0.145	0.987	0.811

Table C.9.: Specific processes in the MSSM at SPS point 9. Details as in Table C.1.

Bibliography

[1] A. Denner, S. Dittmaier, M. Roth, and L. H. Wieders, Phys. Lett. **B612**, 223 (2005), hep-ph/0502063.

[2] J. Wess and J. Bagger, *Supersymmetry and Supergravity* (Princeton University Press, 1992).

[3] S. P. Martin, (1997), hep-ph/9709356.

[4] S. R. Coleman and J. Mandula, Phys. Rev. **159**, 1251 (1967).

[5] J. Wess and B. Zumino, Nucl. Phys. **B78**, 1 (1974).

[6] P. Fayet and J. Iliopoulos, Phys. Lett. **B51**, 461 (1974).

[7] L. O'Raifeartaigh, Nucl. Phys. **B96**, 331 (1975).

[8] A. H. Chamseddine, R. Arnowitt, and P. Nath, Phys. Rev. Lett. **49**, 970 (1982).

[9] R. Barbieri, S. Ferrara, and C. A. Savoy, Phys. Lett. **B119**, 343 (1982).

[10] M. Dine and A. E. Nelson, Phys. Rev. **D48**, 1277 (1993), hep-ph/9303230.

[11] M. Dine, A. E. Nelson, and Y. Shirman, Phys. Rev. **D51**, 1362 (1995), hep-ph/9408384.

[12] M. Dine, A. E. Nelson, Y. Nir, and Y. Shirman, Phys. Rev. **D53**, 2658 (1996), hep-ph/9507378.

[13] L. Randall and R. Sundrum, Nucl. Phys. **B557**, 79 (1999), hep-th/9810155.

[14] L. Girardello and M. T. Grisaru, Nucl. Phys. **B194**, 65 (1982).

[15] S. L. Adler and W. A. Bardeen, Phys. Rev. **182**, 1517 (1969).

[16] J. S. Bell and R. Jackiw, Nuovo Cim. **A60**, 47 (1969).

[17] G. R. Farrar and P. Fayet, Phys. Lett. **B76**, 575 (1978).

[18] B. C. Allanach *et al.*, (2002), hep-ph/0202233.

[19] N. Ghodbane and H.-U. Martyn, (2002), hep-ph/0201233.

[20] WMAP, D. N. Spergel *et al.*, Astrophys. J. Suppl. **148**, 175 (2003), astro-ph/0302209.

[21] WMAP, C. L. Bennett *et al.*, Astrophys. J. Suppl. **148**, 1 (2003), astro-ph/0302207.

[22] A. Denner, H. Eck, O. Hahn, and J. Kublbeck, Phys. Lett. **B291**, 278 (1992).

[23] C. Schwinn, (2003), hep-ph/0307057.

[24] U. Baur, J. A. M. Vermaseren, and D. Zeppenfeld, Nucl. Phys. **B375**, 3 (1992).

[25] A. Denner, S. Dittmaier, M. Roth, and D. Wackeroth, Nucl. Phys. **B560**, 33 (1999), hep-ph/9904472.

[26] G. Lopez Castro, J. L. Lucio, and J. Pestieau, Mod. Phys. Lett. **A6**, 3679 (1991).

[27] W. Beenakker *et al.*, Nucl. Phys. **B500**, 255 (1997), hep-ph/9612260.

[28] S. Dittmaier and M. Roth, Nucl. Phys. **B642**, 307 (2002), hep-ph/0206070.

[29] W. H. Press, B. P. Flannery, S. A. Teukolsky, and W. T. Vetterling, *Numerical Recipes in C : The Art of Scientific Computing* (Cambridge University Press, 1992).

[30] Particle Data Group, W. M. Yao *et al.*, J. Phys. **G33**, 1 (2006).

[31] E. Byckling and K. Kajantie, *Particle Kinematics* (John Wiley & Sons Ltd., 1973).

[32] J. Rosiek, (1995), hep-ph/9511250.

[33] R. Mertig, M. Bohm, and A. Denner, Comput. Phys. Commun. **64**, 345 (1991).

[34] B. C. Allanach, Comput. Phys. Commun. **143**, 305 (2002), hep-ph/0104145.

[35] M. Muhlleitner, A. Djouadi, and Y. Mambrini, Comput. Phys. Commun. **168**, 46 (2005), hep-ph/0311167.

[36] G. C. Cho *et al.*, Phys. Rev. **D73**, 054002 (2006), hep-ph/0601063.

[37] LHC/LC Study Group, G. Weiglein *et al.*, Phys. Rept. **426**, 47 (2006), hep-ph/0410364.

[38] M. E. Peskin and D. V. Schroeder, *An Introduction to Quantum Field Theory* (Addison-Wesley, 2003).

[39] J. Terning, *Modern Supersymmetry* (Oxford University Press, 2006).

Danksagung

An dieser Stelle möchte ich mich bei all jenen bedanken, die zum Gelingen dieser Arbeit beigetragen haben. Insbesondere gilt mein Dank:

- Dr. Nikolas Kauer für die interessante Themenstellung und die engagierte Betreuung, sowie für viele interessante Diskussionen.
- Professor Dr. Rückl für die Möglichkeit, an seinem Lehrstuhl meinem Interesse an der Teilchenphysik nachzugehen und für die Ermöglichung der Teilnahme an der Herbstschule Maria Laach.
- all denen, die mich während des Studiums begleitet und unterstützt haben, besonders Nadine und meinen Eltern.

Erklärung

Hiermit erkläre ich, dass ich die vorliegende Arbeit selbständig verfasst und keine anderen als die angegebenen Hilfsmittel verwendet habe.

Würzburg, den 32.11.2007

Christoph Uhlemann